TAMPERE UNIVERSITY OF TECHNOLOGY

SAMI RISSANEN

BINDING OF CHOLERA TOXIN TO LIPID BILAYERS OF VARIOUS COMPOSITIONS

Master of Science Thesis

Examiner: Ilpo Vattulainen
Examiner and topic approved in the
Faculty of Natural Sciences council
meeting on April 3rd 2013

ABSTRACT

TAMPERE UNIVERSITY OF TECHNOLOGY
Master's Degree Programme in Science and Engineering
RISSANEN, SAMI: Binding of Cholera Toxin to Lipid Bilayers of Various Compositions
Master of Science Thesis, 81 pages
May 2013
Major: Advanced Engineering Physics
Examiner: Professor Ilpo Vattulainen
Keywords: BODIPY, cholera toxin, fluorescence, GM1, lipid packing, molecular dynamics, protein binding

During the last decades, several cholera pandemics have taken place. Still, cholera currently continues to be a major cause of morbidity and mortality making it a worldwide health problem. The causative agent of the disease is the bacterium *Vibrio cholerae*, and the toxin responsible for the symptoms is called cholera toxin (CT). CT is an AB_5 hexameric enterotoxin consisting of two non-covalently bound parts: A and B subunits. The A subunit is responsible for the toxicity functions of CT while the B-pentamer is responsible for the binding of CT to the plasma membrane (PM) in the intestinal lumen of human body. The B-pentamer has been found to tether to GM1 gangliosides in the lipid rafts in PM. One way to investigate these kinds of events is to use fluorescence spectroscopy, where fluorescent markers, such as BODIPY dyes, are employed.

In this study, we investigate the effect of the composition of lipid bilayers on the binding of CT. For this purpose, we employ atomic-scale molecular dynamics simulations for a total of 2.8 microseconds. We consider two different lipid environments: a bilayer consisting of DOPC (1,2-dioleoyl-*sn*-glycero-3-phosphocholine) in a liquid-disordered phase (l_d) and a bilayer consisting of SSM (N-stearoyl-d-erythro-sphingosylphosphorylcholine) and cholesterol in a liquid-ordered phase (l_o). These membranes are enriched with both the native GM1 and the BODIPY-labeled GM1 resulting in four different lipid environments. In addition to four 500-nanosecond simulations of these membranes in the presence of the protein we also study the same four systems for 200 nanoseconds without the B-pentamer, this case serving as a reference.

The results show that cholera toxin binds rapidly to all simulated membranes. However, membrane properties important to the toxin binding were noticed to be dependent on the composition of the lipid bilayer. Electrostatic potential was observed to change significantly between the l_d and l_o phases. Also the geometry of the head group of GM1, essential for the receptor–ligand fitting, was noticed to change as the composition of the bilayer was altered. The results support the idea of CT binding to the GM1 ganglioside, and the membrane in the l_d phase was noticed to be the most favorable for the toxin binding.

TIIVISTELMÄ

TAMPEREEN TEKNILLINEN YLIOPISTO
Teknis-luonnontieteellinen koulutusohjelma
RISSANEN, SAMI: Koleratoksiinin sitoutuminen erilaisiin lipidikalvoihin
Diplomityo, 81 sivua
Toukokuu 2013
Paaaine: Teknillinen fysiikka
Tarkastaja: Professori Ilpo Vattulainen
Avainsanat: BODIPY, koleratoksiini, fluoresenssi, GM1, lipidien järjestäytyminen, molekyylidynamiikka, proteiinin sitoutuminen

Viimeisten vuosisatojen aikana on esiintynyt useita kolerapandemioita. Silti kolera on edelleen maailmanlaajuinen terveysongelma aiheuttaen runsaasti sairastumisia ja kuolemia vuosittain. Koleran aiheuttaa *Vibrio cholerae* -bakteerin erittämä koleratoksiini. Se on heksameerinen (AB_5) enterotoksiini, joka koostuu ei-kovalenttisesti toisiinsa sitoutuneista A- ja B-alayksiköstä. A-alayksikkö on koleratoksiinin myrkyllinen osa, kun taas B-pentameeri vastaa proteiinin sitoutumisesta solukalvoon ihmisen suolistossa. Kokeissa B-pentameerin on havaittu sitoutuvan solukalvon GM1-reseptoreihin. Näissä mittauksissa fluoresenssispektroskopia on usein käytetty menetelmä, jolloin fluoresoivat merkkiaineet, kuten BODIPY, ovat tarvittavia apuvälineitä.

Tässä työssä tutkittiin kuinka lipidikoostumus ja lipidien järjestäytyminen solukalvossa vaikuttavat koleratoksiinin sitoutumiseen. Tätä varten simuloitiin yhteensä 2.8 mikrosekuntia atomitason molekyylidynamiikkasimulaatioita. Tutkimuksessa rakennettiin kaksi erilaista lipidiympäristöä, joista toinen mallinsi epäjärjestäytynyttä kalvoa koostuen DOPC-lipideistä, ja toinen järjestynyttä kalvoa koostuen SSM-lipideistä ja kolesterolista. Molempiin kalvoihin lisättiin sekä tavallista GM1-molekyyliä että BODIPY:llä muokattua GM1-molekyyliä niin, että yhteensä tutkittavia solukalvoja saatiin neljä kappaletta. Kaikkia kalvoja simuloitiin koleratoksiinin läsnäollessa 500 nanosekuntia, ja referenssisysteemeiksi samoja kalvoja ilman proteiinia 200 nanosekuntia.

Tutkimuksessa havaittiin, että koleratoksiini sitoutui nopeasti kaikkiin tutkittuihin solukalvoihin. Proteiinin sitoutumiselle tärkeiden solukalvon ominaisuuksien huomattiin kuitenkin vaihtelevan lipidikompositiota muutettaessa. Solukalvon elektrostaattisen potentiaalin havaittiin muuttuvan, kun epäjärjestyneestä faasista siirryttiin järjestyneeseen. Tämän lisäksi myös GM1-reseptorin pääryhmän geometrian huomattiin muuttuvan solukalvon kompositiota muutettaessa. Tulokset tukevat aiemmin esitettyä ajatusta siitä, että koleratoksiini sitoutuu GM1-gangliosidiin ja sitoutuminen on suotuisampaa epäjärjestyneeseen kalvoon.

PREFACE

This Master of Science Thesis was carried out in the Biological Physics and Soft Matter (BIO) research group of the Department of Physics of Tampere University of Technology between October 2012 and March 2013. The molecular dynamics simulations were conducted using the computing services of the Finnish IT Centre for Scientific Computing (CSC) and the Tampere Center for Scientific Computing (TCSC).

First of all, I would like to thank my examiner professor Ilpo Vattulainen for giving me the opportunity to carry out this exciting project in a friendly environment of his research group. Without his knowledge on the field and the resources of the group, this Thesis could not have been done.

Special thanks go to Tomasz Róg who adviced and supported me through the various stages of this project. Thanks should be also directed to Matti, Tuomo and Adam for all the help as well as all the pleasant discussions during this Thesis project. I would also like to thank all of my other colleagues for their advice and making my days at work enjoyable.

Last but not least, I want to thank my family and friends for all their company and support during my studies and the writing process of this Thesis.

Tampere, April 2013

Sami Rissanen

CONTENTS

ABREVIATION

k_{B}	Boltzmann constant
$k_{\mathrm{B}}T$	Thermal energy
AC	Adenylate cyclase
Ace	Accessory cholera enterotoxin
ADP	Adenosine diphosphate
ADPR	Adenine diphosphate ribose
ARF6	ADP ribosylation factor 6
cAMP	Cyclic adenosine monophosphate
Chol	Cholesterol
COM	Center of mass
COPI	Coat protein complex I
CT	Cholera toxin
CTA	Cholera toxin A subunit
CTB	Cholera toxin B subunit
DIG	Detergent-insoluble glycosphingolipid
DNA	Deoxyribonucleic acid
Dsb	Disulphide bridge
EE	Early endosome
Eps	Extracellular protein system
ER	Endoplasmic reticulum
ERAD	Endoplasmic reticulum-associated protein degradation
G Protein	Guanine nucleotide-binding protein
Gal	Galactose

GalNac	N-acetylgalactosamine
GDP	Guanosine diphosphate
GFP	Green fluorescent protein
GSL	Glycosphingolipid
GTP	Guanosine triphosphate
KDEL	The amino acid sequence Lys-Asp-Glu-Leu
LJ	Lennard-Jones interactions
LPS	Lipopolysaccharide
LT	Heat-labile enterotoxin
MEE	Multilocus enzyme electrophoresis
MD	Molecular dynamics
NAD	Nicotinamide adenine dinucleotide
NADH	Nicotinamide adenine dinucleotide and hydrogen
NpT	Grand canonical ensemble
NVE	Microcanonical ensemble
NVT	Canonical ensemble
ORS	Oral rehydration solution
PBC	Periodic boundary conditions
PDB	Protein Data Bank
PDI	Protein disulphide isomerase
RE	Recycling endosome
RFLP	Restriction fragment length polymorphism
RMSD	Root mean square deviation
SLT	Shiga-like toxin
T2SS	Type II secretion system
TGN	Trans-golgi network

TDH	Thermostable direct hemolysin
VMD	Visual Molecular Dynamics
WHO	World Health Organization
Zot	Zonula occludens toxin

1. INTRODUCTION

Seven acknowledged cholera pandemics have taken place during the last decades [1]. Cholera still continues to be a major cause of morbidity and mortality making it a worldwide health problem. As many as 3–5 million cases and 120,000 deaths are recorded every year [2]. The disease is contracted through ingestion of contaminated food or water, which makes it a major problem in developing countries, where access to safe food and water and sufficient sanitation cannot be assured for all. Cholera is characterized by profuse diarrhea and vomiting, which leads to a loss of body fluids and dehydration. Without prompt attempt to treat the patient, the disease becomes fatal in most cases.

The causative agent of the disease is the bacterium *Vibrio cholerae*, and the responsible toxin for the symptoms is cholera toxin (CT). CT is a hexameric AB_5 enterotoxin consisting of two amino acid sequences, A and B subunits. The A subunit (CTA) is responsible for the toxicity of CT. It catalyzes adenosine diphosphate (ADP) ribosylation of the α subunit of the guanosine triphosphate (GTP) binding protein. This leads to activation of adenylate cyclase which increases the level of cyclic adenosine monophosphate (cAMP), causing the secretion of ions and water into the intestinal lumen of human body. The B subunit (CTB or B-pentamer) consists of five tightly packed B monomers. The B-pentamer is responsible for the toxin binding and it is considered as a molecular recognition unit and delivery vehicle for the A subunit [3, 4]. It has been noticed that the CTB has a high affinity to GM1 ganglioside receptor, which is found in the outer leaflet of plasma membranes of virtually all cell types [3].

In addition to the research of new drugs against cholera, B-pentamer is also used in other studies such as investigation of membrane properties [5, 6]. In that field, fluorescence spectroscopy is a commonly used method. Furthermore, fluorescent probes are often required in these studies. Lots of different fluorophores are known and the BODIPY fluorophore family is one of them. It has gained popularity because of its excellent properties as a fluorescent probe [7].

In general, the data obtained from experiments is often affected by the perturbation caused by fluctuations in the experiments or the applied methodology itself. Also, the needed resolution to examine interactions and structural properties is often limited. The idea for this study originates from experimental studies which showed

that the affinity of cholera toxins to a membrane varies when the lipid packing is altered. Additionally, it has been suggested that the BODIPY fluorophore used in the experiments as a marker for the GM1 receptor perturbates the toxin binding process.

Due to poor resolution in experiments, the aim of this thesis was to study through atomistic molecular dynamics simulations how the changing of the lipid composition of a protein-free membrane affects the binding of cholera toxin. For this purpose, a total of 8 different systems were simulated. Both the membrane in the liquid-disordered phase (consisting of DOPC) and the membrane in the liquid-ordered phase (consisting of 1:1 SSM and cholesterol) were enriched with the native GM1 and BODIPY-labelled GM1 molecules, resulting in four different membranes. The membranes in the presence of the B-pentamer were simulated for 500 ns, and the membranes in the absence of CTB for 200 ns as a reference.

This thesis is divided into seven chapters. The next chapter focuses on the biological background relevant to this study, describing the nature of the cholera disease. Causative organism of the disease and the most important toxin secreted by the bacterium are discussed in more detail. The third chapter provides basic knowledge about the fluorescence phenomenon and how it can be used in experimental measurements. The fourth chapter concentrates on the principles of the classical molecular dynamics method used in this study, with an emphasis on the force field and the ensembles used to describe the physical conditions. The fifth chapter is dedicated to the simulated systems describing the initial configurations as well as the parameters applied in the simulations. The sixth chapter contains the results obtained from the simulations and discusses their meaning in a biological framework. Finally, the seventh chapter summarizes the results along with an outlook for future research.

2. BIOLOGICAL BACKGROUND

In this chapter the background relevant to this study is discussed. First, the nature of the cholera disease is given with a short history about it. Second, the causative organism of the disease, *Vibrio Cholerae*, is presented. Next, the bacterial toxins are reviewed in general. The chapter is closed with a discussion about the responsible toxin for the symptoms, cholera toxin. The information in this chapter is based on a few books [8–10] and review papers [4, 11, 12].

2.1 Overview of Cholera

Cholera is a disease which begins with a sudden onset of massive diarrhea accompanied by a loss of a large amount of protein-free fluid along with electrolytes and ions. In addition to diarrhea and vomiting, a hypovolemic shock and acidosis are characteristic symptoms of the disease. Without prompt attention to treat the patient, the resulting hydration produces tachycardia, hypotension and vascular collapse. Under such severe conditions the disease becomes fatal in most cases.

2.1.1 History of Cholera

The etymology of the term "cholera" is not totally clear. It was first seen in the works of Hippocrates and believed to have been derived from the Greek words *chole* (bile) and *rein* (to flow), thus meaning the flow of bile [13]. Afterwards, there have been many other suggestions [14–16] to the origin of the name, but a generally accepted understanding of the etymology is still missing.

Cholera often occurs in epidemics. If an epidemic lasts for many years and spreads to many different countries and even across continents, it is usually called a pandemic. It is generally recognized that seven distinct pandemics of cholera have occurred. The first one took place in the 19^{th} century in India and the last one in the mid of the 20^{th} century, beginning in Indonesia [16]. Currently ongoing outbreaks in Zimbabwe and Haiti are included in the seventh pandemic [17].

The purpose of this study is not to review the whole history of the disease, though a few important discoveries made in the 1800's and the early 1900's are worth of emphasizing. In the 1830's, during the second pandemic, O'Shaughnessy first demonstrated that the characteristic rice water stools of patients contained salts and alkali. A few decades later, John Snow made an observation that cholera is

transmitted through water. In the late 1800's during the 5^{th} pandemic, Robert Koch managed to isolate the bacterium from the rice water stools of cholera patients [18]. At the moment, Koch named the bacterium as "comma bacilli" because of the comma shape of the bacterium, nowadays known as *Vibrio cholerae* (*V. cholerae*).

Plenty of different types of the bacterium *V. cholerae* have been found. The serogroup O1 of *V. cholerae* was in charge of all the first five pandemics. During the seventh pandemic, a new biotype, El Tor, was found. Also a totally new serogroup O139 was found in the 1990's. Properties of the bacterium *V. Cholerae* will be discussed in more detail in section 2.2.

2.1.2 Causation and Treatment of the Disease

It is known that the causative agent of cholera is the bacterium *Vibrio cholerae*. Apparently, humans are the only natural hosts for the cholera vibrios. Cholera is acquired through ingestion of water or food contaminated with the feces of an infected human being. Usually, most of the cholera-causing vibrios die in the stomach because of the acidic environment. However, some bacteria may survive into the small intestine where they multiply rapidly and produce toxins. One of the toxins secreted by *V. cholerae* is the cholera toxin. It causes a profuse amount of water and electrolytes to be secreted into the bowels, to be eliminated as watery diarrhea. The loss of a large volume of fluid and electrolytes has to be replaced to prevent kidney failure, coma, and death.

The key to the treatment of cholera lies in preventing the dehydration. This can be taken care of by replacing the fluids and electrolytes lost through diarrhea and vomiting. Rehydration can be accomplished orally [19, 20], which makes the treatment greatly simplified. The method currently being used and recommended by the World Health Organization (WHO) is oral rehydration solution (ORS) containing water, sugar, and salts. However, in the case of severe dehydration, treatment has to be done intravenously. An antibiotic called tetracycline is also used to shorten the duration of the illness and reduce the fluid loss [21].

2.2 Bacterium Vibrio Cholerae

Cells are the basic structural units of all living organisms. Bacteria are the smallest living cells and they have a cytoplasmic membrane surrounded by a cell wall. The wall is rigid because of a unique polymer called peptidoglycan [22]. A simple prokaryotic cell does not include any mitochondria, lysosomes, endoplasmic reticulum, or other organelles typical to eukaryotic cell. In fact, most bacteria are about the size of a mitochondria. Bacteria have no nucleus, but all the chemical elements of nucleic acid and protein synthesis are present due to a single double-stranded deoxyribonucleic

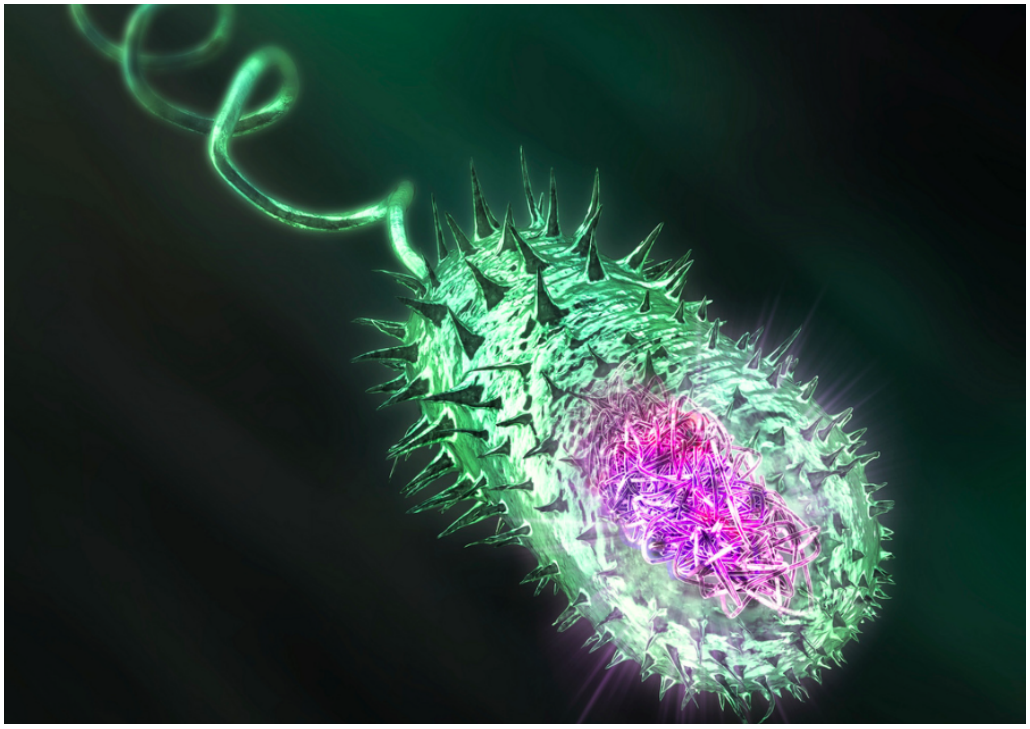

Figure 2.1: Illustration of bacterium *Vibrio cholerae*. The huge flagellum, several pilis, and the nucleoid, which contains the genome of the bacterium can be clearly seen. Picture modified from [23].

acid (DNA) chromosome in the cytoplasm. Although the nutritional requirements vary greatly among the bacteria, most of them are free-living if given an appropriate energy source.

The cholera vibrios are gram-negative, slightly curved and often comma-shaped rods with an average diameter of 0.55 μm and length of 1.8 μm (see Fig. 2.1). A classification of *V. cholerae* is summarized in Table 2.1. The protoplasm of the bacterial cell consists of an electron-transparent central zone, the nucleus, and is surrounded by the electron-dense region of the cytoplasm. The bacterial protoplasm of *V. cholerae* is bounded by the plasma membrane, which exhibits a trilamellar structure with an overall thickness of about 7.5 nm. The outer side of the plasma membrane has a periplasmic space thickness of 5–10 nm. The periplasmic space is covered by another layer of membranous structure, the cell wall, which also has a trilamellar structure with an overall thickness of about 10 nm at the outermost periphery of the cell.

The mobility of the bacterium depends on a single polar flagellum possessed by it. The flagellum has a core covered by a sheath. The diameters of the core and the sheath are about 15 and 30 nm, respectively. The single polar flagellum is attached to a structure called the basal granule, which is about 65 nm in size in the bacterial protoplasm.

Table 2.1: Classification of bacterium *V. cholerae* [10].

Type	Name
Kingdom	Bacteria
Phylum	Proteobacteria
Class	Gamma Proteobacteria
Order	Vibrionales
Family	*Vibrionaceae*
Genus	*Vibrio*
Species	*V. cholerae*
Binomial name	*Vibrio cholerae*

Several different kinds of a hair-like appendage called fimbriae or pili have been found on the surface of the bacterium. The presence of a small number of pili of diameter 6-8 nm was first recorded on El Tor vibrios. Also an other completely different type of pili has been detected and it has been found to be a colonization factor of the *V. cholerae* serogroup O1.

2.2.1 Subtyping

To investigate *V. cholerae* in more detail and categorize it into different species, sophisticated methods are needed. The following methods have proven to be useful for classifying or characterizing the strain of *V. cholerae*, and they can be used either singly or in combination: restriction fragment length polymorphism (RFLP) of *ctx* genes [24, 25], RFLP analysis of ribosomal ribonucleic acid (rRNA) genes [26], deoxyribonucleic acid (DNA) or gene probes [24, 25, 27], and multilocus enzyme electrophoresis (MEE) or zymovar analysis [28].

Different *V. cholerae* species have been divided into different serogroups. The serogrouping is performed on the basis of the heat-stable O-antigen of the bacteria. There are already around 200 serogroups (O1 to O200) identified and more may be found in the future. Serogroups O1 and O139 are the most important ones to be remembered. Previously all major cholera epidemics were caused by the same serogroup O1. In 1992 the serogroup O139 was emerged to cause an epidemic in the Indian subcontinent. The O1 serogroup has been subdivided further into three different serotypes and two different biotypes. Three serotypes are Inaba, Ogawa, and Hikojima, where the names denote their historical origins. DNA sequences of Inaba and Ogawa antigens are nearly identical. The two biotypes of O1 strains are classical and El Tor. Subdivision is based on several tests described by Chatterjee *et al.* [29]. The El Tor biotype was discovered in 1971 as the causative agent of the seventh pandemic of cholera. A summary of different serogroups, serotypes, and biotypes of *V. cholerae* is presented in Table 2.2.

Table 2.2: Classification of *V. cholerae* species [10].

Serogroups	Epidemic spread	Serotypes	Biotypes (names)
O1	High	Inaba,Ogawa,Hikojima	2 (classical, El Tor)
O139	High	Nil	1
Other non-O1	Low	Nil	1

2.2.2 Growth Requirements and Characteristics

The nutritional requirements for cholera vibrios are rather simple. They grow in media containing an inorganic nitrogen source, a utilisable carbohydrate, and appropriate minerals. Vibrios can grow anaerobically, although they reach higher population densities in the presence of aeration. They are sensitive to low pH and therefore their growth is stimulated by the addition of NaCl (1%). Vibrio cultures are usually grown by shaking at 37 °C [30].

The mechanism of division of *V. cholerae* is similar to that of any other gram-negative bacterium: elongation to double the original length and then division through a simple pinch-off process. In a favorable habitat, cholera vibrios grow rapidly with a generation time of less than 30 minutes.

2.3 Bacterial Toxins

Bacterial toxins are usually proteins, encoded by the bacterial chromosomal genes, plasmids, or phages. *Vibrio cholerae* produces several different toxins all of them belonging to the family *Vibrionaceae*. In order to better understand the functions of the bacterium *V. Cholerae* and one of its toxins, cholera toxin, it is useful to get familiar with the basics of bacterial toxins in general. The different types of toxins produced by bacterial cells are broadly classified as endotoxins, exotoxins, and enterotoxins. A few basic properties that differentiate the endotoxins and the exotoxins are listed in Table 2.3. Enterotoxins are a type of exotoxin released by bacteria in the intestine. Cholera toxin is an enterotoxin.

Usually the toxins are liberated from the organism by lysis. However, some are shed along with outer membrane proteins in vesicles. Toxins may damage or alter the functions of the eukaryotic cell membrane. They interact with specific receptors on the surface of the membrane and penetrate through the cell to reach their intracellular target. Many protein toxins have an AB-structure where A denotes an enzyme that is part of the toxin and B binds to the receptor. Toxins are activated either when produced by the bacterium or when bound to the membrane receptor. An enzymatic process common to many toxins is adenosine diphosphate (ADP)–ribosylation of the adenylate cyclase regulatory proteins, leading to an increase in intracellular cyclic

Table 2.3: General properties of typical endotoxins and exotoxins [10].

Property	Endotoxin	Exotoxin
Chemical nature	Lipopolysaccharide	Protein
Relationship to cell	Part of outer membrane	Extracellularly secreted
Denatured by boiling	No	Usually yes
Antigenic	Yes	Yes
Forms toxoid	No	Yes
Potency	Relatively low	Relatively high
Specificity	Low degree	High degree
Enzyme activity	No	Usually yes
Pyrogenicity	Yes	Occasionally

adenosine monophosphate (cAMP). Although many toxin effects caused by bacteria have been described, only a few toxins have been identified and characterized, and only for a few toxins their mode of action has been determined at the molecular level [31].

Some of the toxins excreted by *V. cholerae* are listed below: Cholera enterotoxin or cholera toxin (CT), Zonula occludens toxin (Zot), Accessory cholera enterotoxin (Ace), Hemolysin/cytolysin, Shiga-like toxin (SLT), and thermostable direct hemolysin (TDH).

2.3.1 Bacterial Endotoxins

Endotoxins refer to the lipopolysaccharide (LPS) complex associated with the outer membranes of gram-negative bacteria regardless of whether the organism is a pathogen or not. Most of the endotoxin remains associated with the cell wall until the bacteria disintegrates, which means that these toxins are available for action only after the death and lysis of the bacteria to which they belong. The LPSs are complex amphiphilic molecules with a molecular weight of around 10 kDa. They consist of three regions: a hydrophobic lipid A which anchors LPS to the outer membrane of bacteria, a core polysaccharide comprising inner and outer cores, and an O-specific polysaccharide chain that is mostly responsible for LPS immune recognition. The structure of a bacterial endotoxin is illustrated in Fig. 2.2.

2.3.2 Bacterial Exotoxins

Exotoxins are a group of soluble proteins excreted by a microorganism, including bacteria, algae, fungi, and protozoa. Exotoxins enter host cells and alter the cell physiology. Both gram-negative and gram-positive bacteria can produce exotoxins. Bacterial exotoxins possess an AB structure-function organization, in which the A

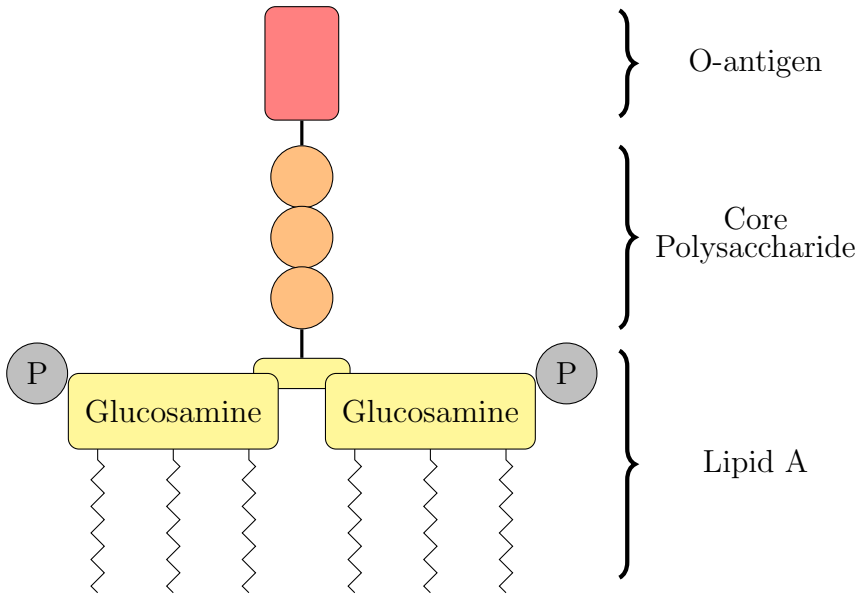

Figure 2.2: A schematic of the structure of bacterial endotoxin.

domain represents the catalytic domain and the B-domain consists of the receptor-binding and translocation domain. Thus, the B-domain is responsible for the transport of the catalytic A domain into the intracellular compartment of the host cell [32].

Exotoxins may be generally classified by taking into account both their sites and their modes of action. Extracellularly acting toxins can be further classified according to their site of action into membrane-damaging toxins like hemolysins and phospholipase, and non-membrane-damaging toxins like lipase and collagenase. On the other hand, intracellularly acting toxins can be classified in accordance to their mode of action. One subgroup consists of nonribosylating toxins like shiga toxin and adenylate cyclase. The other consists of ADP-ribosyl transferases which promote the breakdown of nicotinamide adenine dinucleotide (NAD) into nicotinamide and adenine diphosphate ribose (ADPR). The binding of ADPR to various proteins results in inactivation of the bound protein. Cholera toxin belongs into this group.

2.4 Cholera Toxin

Cholera toxin (CT, sometimes abbreviated to CTX, CTx or Ctx) is secreted by the gram-negative bacterium *Vibrio cholerae* in the intestinal lumen in humans causing the massive secretory diarrhea clinically characteristic of cholera. In 1959, two experiments [33, 34] established that the CT is an exotoxin, and nowadays it is known that CT belongs to the larger family of AB toxins [35]. Besides studies related to the disease cholera, CT can also be fluorescent labelled and used to investigate for example membrane properties [5, 6].

2.4.1 Structure

In the experiments of Finkelstein and LoSpalluto [36, 37], two different factors with different biological activities were indentified via purification. The first one was a toxin termed as choleragen, now known as the cholera toxin. It was noticed to be toxic. The second factor was noncytotoxic and was found to act as a toxoid. It was termed choleragenoid, nowadays known as CTB, the B subunit of CT. Both the CT and CTB were made commercially available, allowing investigators to study cholera toxin in more detail.

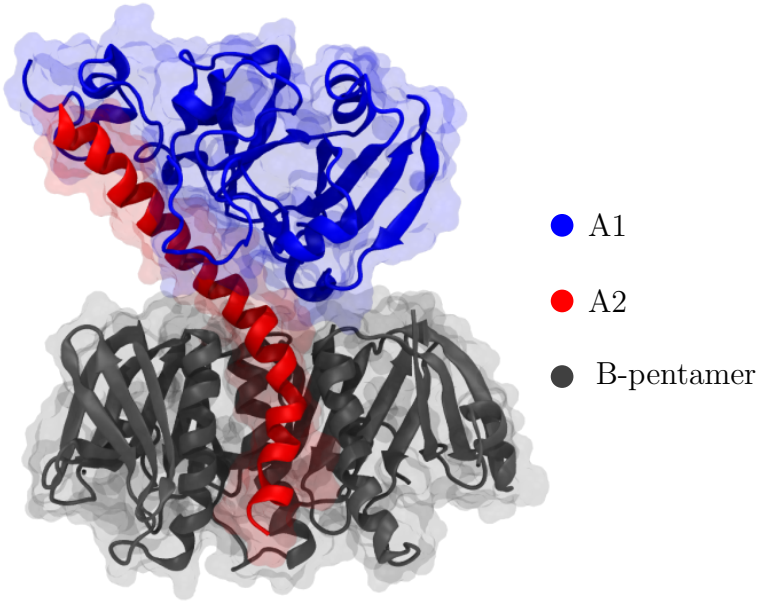

Figure 2.3: Cholera toxin as visualized in Visual Molecular Dynamics (VMD) [38]. Final picture rendered using Tachyon ray tracing library [39]. CT can be found in the Protein Data Bank (PDB) [40] database by its identifier 1XTC [41]. Red color represents the A2 subunit of CT, gray the B-pentamer of CT, and blue the A1 subunit of CT. The A1 and A2 chains are linked by a flexible loop that contains a proteolytic cleavage site subtended by a disulphide bond [42].

A series of experiments involving gel electrophoresis and other techniques revealed the oligomeric structure of the holotoxin CT [43–47]. Crystals of choleragen were grown succesfully from batches of freshly isolated, isoelectrically pure cholera toxin [48], and the three-dimensional structure of CT at 2.5 Å resolution was determined by X-ray crystallography [41]. In addition, the isolated CTB subunit was also crystallized and its structure determined independently by X-ray crystallography at a resolution of 2.4 Å [49]. During extensive experimental measurements, it was noticed that long-term storage in solution at 4 °C or room temperature storage resulted in extensive isoelectric heterogenity [4, 48], and this lead into six different isoelectric species of CT: AB_5, AB_4B', $AB_3B'_2$, $AB_2B'_3$, ABB'_4 and AB'_5.

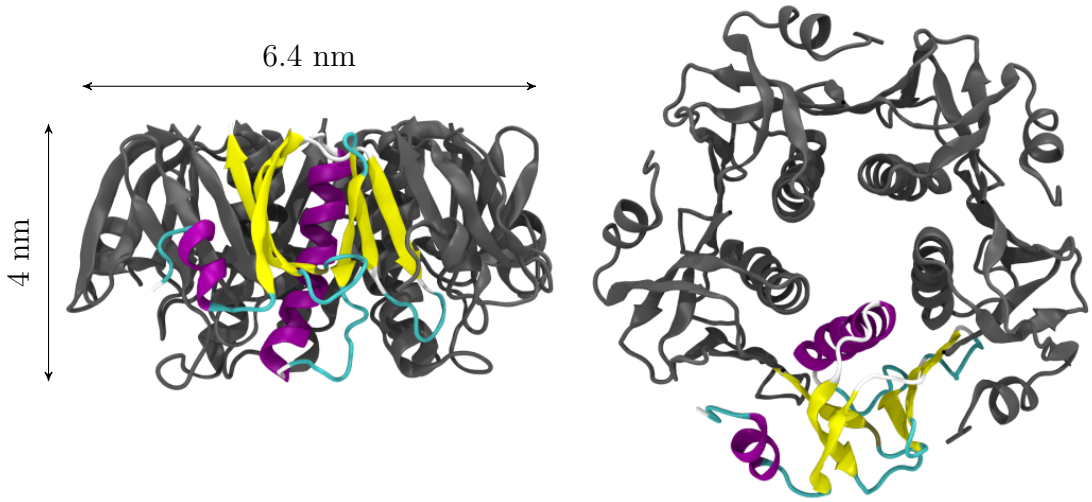

Figure 2.4: B-pentamer with a B-monomer highlighted with colors describing the secondary structure of the protein. On the left, the crystal structure of CT is shown viewed sideways with the surface of the B-subunits containing the binding sites for their membrane receptors facing downwards. On the right CTB is visualized from above.

Holotoxin CT consists of two amino acid sequences, A and B subunits of CT, called CTA and CTB, respectively (see Fig. 2.3). The A subunit contains 240 amino acids while the individual monomer of the B-pentamer contains 103 amino acids. The amino acid sequences and secondary structures for both A and B subunits can be found from Ref. [10]. The A subunit is partially reduced to form A1 and A2 subunits after its arrival in the endoplasmic reticulum (ER). The A1 fragment displays ADP-ribosyl transferase activity, and the A2 fragment mediates interaction with the B-pentamer. The function of the B-pentamer is to bind the holotoxin to the eukaryotic cell receptor. A single Trp residue at the position 88 in CTB being located at the subunit interface in the native B-pentamer is a useful probe for studying CTB assembly [50]. The roles of action of these different fragments are discussed in more detail in section 2.4.3.

The mass of CTA is about 28 kDa. It is proteolytically cleaved by *V. cholerae* between residues 192 (Arg) and 193 (Ser). The resulting residues 1–192 are called the A1 subunit and residues 192–240 are called the A2 subunit. The 23 kDa sized A1 and the 5 kDa sized A2 are linked together by a disulphide bridge. The wedge-shaped enzymatic A1 fragment is organized into three distinct segments. The first, $A1_1$, containing residues 1–132 forms a compact unit comprising a mixture of α-helices and β-strands. The residues 133–161 form an extended bridge between the compact $A1_1$ and $A1_3$ domains, called $A1_2$. $A1_2$ acts as a molecular tether, like the A2 fragment between A1 and B subunits. The third $A1_3$ is formed from 31 residues that

surround the disulphide bridge, linking the A1 and A2 fragments. The A2 domain is an elongated domain, consisting of an α-helix and a part that extends through the pore formed by the B-pentamer (see Fig. 2.3). The interaction between the A and B subunits are almost entirely mediated by the A2 domain and the B-pentamer pore. The A2 fragment shares an extensive interface with the enzymatic A1 chain and the B-pentamer anchoring them together at the same time. The cleft is situated away from the A1/A2 and A/B interfaces and is probably the binding site for both nicotinamide adenine dinucleotide (NAD) and substrate. This enables the A1 chain to act as both an ADP-ribosyltransferase and a NAD-glycohydrolase [51, 52]. The A subunit is loosely held above the plane of the pentameric B subunits. The pore in the B-pentamer is just wide enough to accommodate the A2 chain as a helix. Stabilizing contacts between the A2 chain and the B subunits within the pore are largely hydrophobic, with a few specific hydrogen bonds.

The B-pentamer consists of five individual B-monomers, each with a size of 103 amino acids and a mass of 11.4 kDa, which makes the pentamer to have a size of 57 kDa. The function of the B-pentamer is to bind the holotoxin to the eukaryotic cell receptor. Each monomer has a short α-helix at the N-terminus, a long α-helix, two three-stranded antiparallel β-sheets, and another two β-strands, illustrated in Fig. 2.4. The overall pentamer fold consists of a closed β-barrel formed by six antiparallel β-strands, capped by an α-helix (see Fig. 2.5). The B-pentamer has an overall diameter of approximately 6.4 nm and a height of 4.0 nm. It is a very stable structure stabilized by a variety of interactions. The total number of hydrogen bonds between the B subunits and its neighboring molecules is 30 and each subunit forms seven salt bridges. Further, the B-pentamer is stabilized by the tight interdigitation of hydrophobic groups at the subunit interface. The inner surface, the pore of the ring, is hydrophobic. Looking down the five-fold axis into the central pore (see Fig. 2.4), the monomeric backbones are tightly packed to form a pentamer of interlocking subunits. The parallel α-helices gently bow inward during their course, reducing the diameter of the pore from 1.6 nm (amino terminus) to 1.1 nm (carboxyl terminus, the binding site). When the B-pentamer is formed by the B-monomers, the surface area of each monomer accounts for 39 % of the total accessible surface. The most specific contacts occur at the entrance to the central pore of the B-pentamer, while the contacts within the pore are mainly hydrophobic and water-mediated. Only a few contacts exist between the A1 fragment and the B-pentamer, showing that the A2 domain functions as a linker for the A and B parts of the protein.

In many books and reviews CT is compared with heat-labile enterotoxin (LT) from the bacterium *Escherichia coli*. This is due to the similar structures of CT and LT. 75 % of the amino acid sequence in the A subunits of the toxins are the same. In the case of the B subunit, the similarity is even larger, 77 %. The most striking

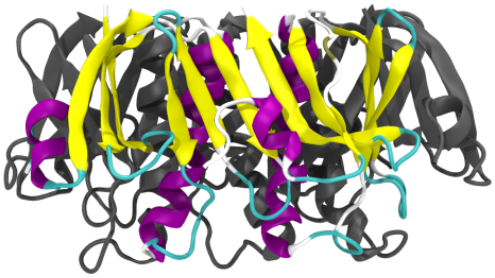

Figure 2.5: The B-pentamer with two B-monomers highlighted with the colors based on the secondary structure of the protein. Six adjacent β-sheets formed by two different B-monomers can be seen.

difference between the structures of CT and LT lies at the carboxyl terminus of the A2 chain. Whereas the last 14 residues of the A2 chain of LT form an extended chain with a terminal loop, the A2 chain of CT remains a continuous α-helix throughout its length [41].

2.4.2 Secretion by the Vibrios

Ever since the discovery in 1959 that cholera toxin is known to be an exotoxin [33, 34] with a total size of about 86 kDa, it has been argued that a biomolecule of this size cannot simply leak through the membranes of the *V. cholerae*. The secretion machinery of the organism *V. cholerae* and the mechanism of secretion of the CT molecule have been studied widely by biochemical, genetic, and structural studies and is now understood as a multistage process. It involves different sets of proteins spanning the inner and outer membranes of the bacterial cell. Two secretory machineries take care of the CT secretion from the *V. cholerae*: the Sec translocase pathway and the type II secretion system (T2SS). Both of them are composed of multiprotein complexes, and especially the type II pathway is selective and allows only specific proteins to be secreted.

In the first phase, the A and B subunits of CT are synthesized with attached N-terminal signal properties [53] in the bacterial cytoplasm and translocated across the inner membrane of the Vibrios as unfolded chains. The translocation process is mediated by secretion machinery that constitutes a protein-conducting channel. Among the gram-negative bacteria, the Sec translocase is the general translocase that transports synthesized proteins across the cytoplasmic membrane in an unfolded state [54, 55]. The Sec machinery is illustrated in Fig. 2.7 and will not be further discussed in this thesis.

After the unfolded subunits are translocated across the inner membrane to the periplasmic space via the Sec-dependent pathway, they are folded to form the three-

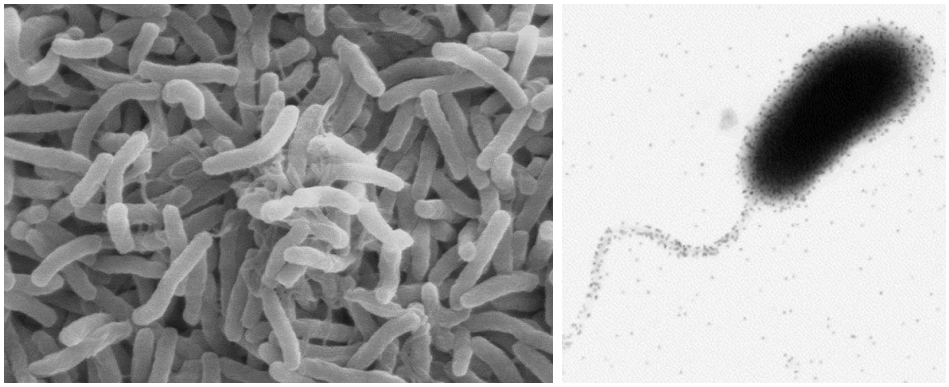

Figure 2.6: On the left, a scanning electron microscope image of *V. cholerae* [56]. On the right, another picture of bacterium *V. cholerae* [29].

dimensional structure of the CT subunits after the polypeptide chains are released from the signal peptides [57]. Further, the folded subunits A and B interact with each other assembling into the complete AB_5 holotoxin [58–60]. Hirst *et al.* noticed that the B-monomers assembled into oligomers with a half-time of around 1 minute, while the half-time for toxin efflux from periplasm was around 13 minutes [59, 60]. The assembly of cholera toxin into AB_5 complexes in the periplasm was investigated both *in vitro* and *in vivo* [50, 61]. First the disassembly and reassembly of CT was done *in vitro* by Finkelstein in 1974 [62], but *in vivo* investigations had difficulties due to the complex periplasmic environment [61]. When purified B-pentamers were denatured in acid and subsequently neutralized, the B-monomers reassembled into stable pentameric complexes [61]. It was noticed that the B-pentamers were secreted to the extracellular environment as efficiently as assembled holotoxins [58–60]. Based on these observations, one could suggest that the AB_5 holotoxin assembly involved the formation of a B-pentamer, followed by association with an A subunit. Instead, evidence of direct association of the A subunit with B subunits in intermediates has been presented. Furthermore, the A subunit was able to accelerate the B subunit assembly *in vivo* [61]. Folding of cholera toxin subunits involves the formation of intrachain disulphide bonds in the A subunit (between Cys187 and Cys199) and in each B subunit (between Cys9 and Cys86). Disulphide bridge (Dsb) proteins are located in bacterial periplasm and they mediate disulphide bond formation, thus helping accelerate the slow steps of folding of cholera toxin subunits. The function of Dsp in a prokaryotic cell corresponds to the functions of protein disulphide isomerase (PDI) protein in an eukaryotic cell.

The fully formed CT holotoxin is translocated through the outer membrane to the extracellular space across the type II secretion system (T2SS) involving both the inner and the outer membrane [63, 64]. The T2SS system is generally termed as the Eps (Extracellular protein system). A large set of accessory proteins, the

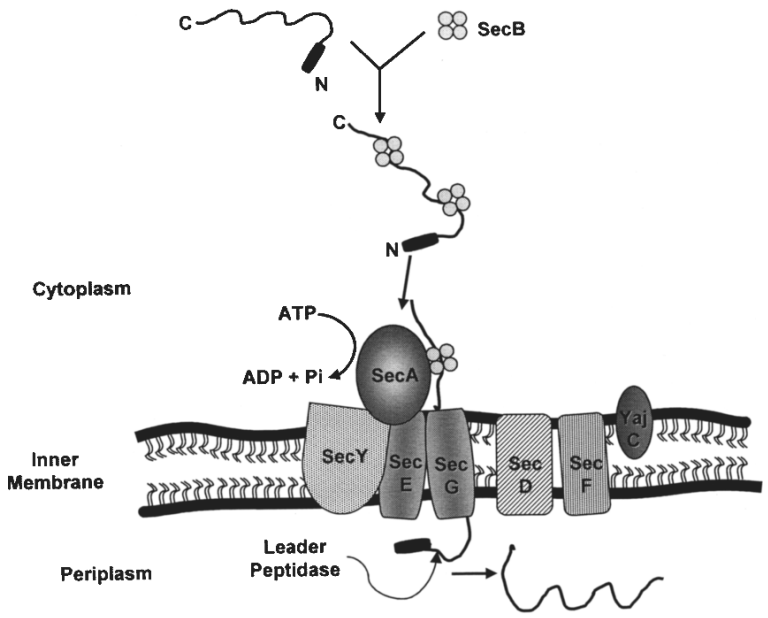

Figure 2.7: A schematic diagram illustrating the translocation of CTA and CTB through the Sec translocase pathway from cytoplasm into the periplasmic space of the *V. cholerae* [10].

components of T2SS, designated EpsA to EpsN, are required [63–67]. The T2SS system can be considered to consist of three subcomplexes: inner membrane platform, pseudopilus, and outer membrane complex. Components of each subcomplex are listed in Table 2.4. The T2SS system is illustrated in Fig. 2.8 and summarized briefly in the following. The cytoplasmic protein EpsE becomes associated with the inner membrane through its interactions with the innermembrane protein EpsL. EpsM interacts with EpsL. EpsG is proposed to generate a structure similar to type IV pilins [68, 69], and the monomers are presumed to form a pilus-like structure which might act as a piston to push CT through the secretin EpsD, which is the only T2SS protein integrated into the outer membrane of *V. Cholerae*. EpsD forms a large pore-like structure involving 12 subunits at the outer membrane. These are the core proteins. Other proteins act to stabilize the Eps structure to facilitate secretion. The minor pseudopilins EpsH, EpsI, EpsJ, and EpsK interact with the major pseudopilin EpsG. EpsC interacts with EpsD in the outer membrane and with EpsL and EpsM in the inner membrane.

2.4.3 Intracellular Journey

In order to produce the outpouring of intracellular fluid containing different electrolytes that leads to the diarrhea typical of the disease cholera, CT must enter the intestinal epithelial cell and reach the cytosol. There it can activate the adenylate cyclase over a long period of time in order to produce an intracellular accumulation

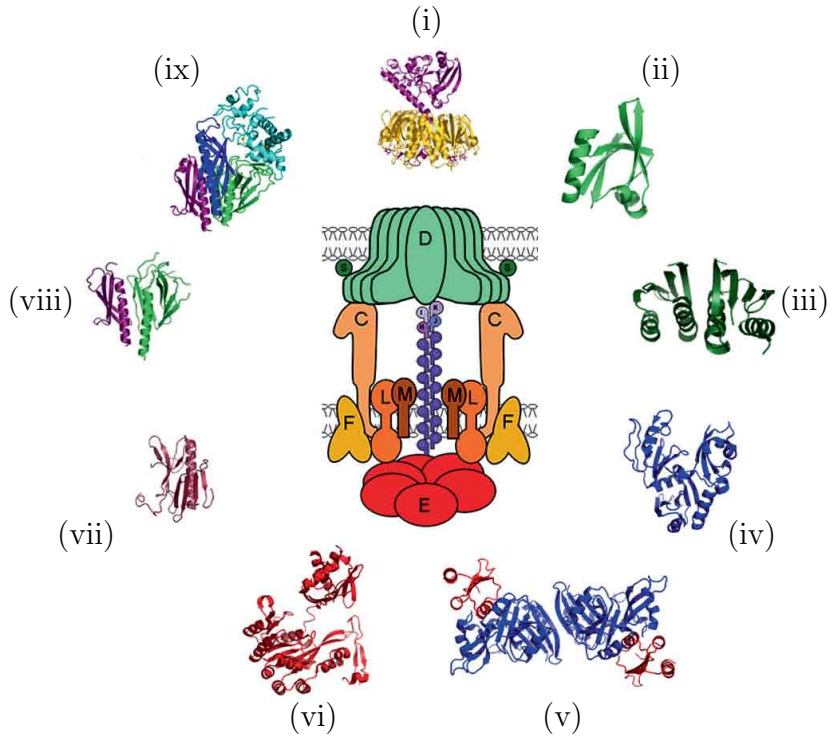

Figure 2.8: The structure of the type II secretion system (T2SS). In the center is an assembled T2SS system and in the periphery are the structures of each component of the T2SS system. The components of T2SS system are presented in clockwise order: (i) cholera toxin molecule, (ii) PDZ-domain of GspC from EpsC, (iii) the periplasmic domain of GspM from EpsM, (iv) the cyto- plasmic domain of GspL from EpsL, (v) the cytoplasmic domain of GspL (blue) in complex with the N1 domain of the secretion ATPase GspE EpsE (red), (vi) the secretion ATPase GspE from EpsE, with the N1 domain removed, (vii) the globular domain of the pseudopilin GspH from EpsH, (viii) the globular domains of pseudopilins GspI or EpsI (purple) from EpsJ (green), (ix) the ternary complex of GspK (light and dark blue), GspI (purple), and GspJ (green). Their PDB identifiers are: 1LTT [70], 2I6V [71], 1UV7 [72], 1YF5 [73], 2BH1 [73], 1P9R [74], 2QV8 [75], 2RET [76], and 3CIO [77], respectively. Figure modified from [10].

Table 2.4: Three different subcomplexes of the type II secretion system (T2SS) [10].

Subcomplex	Components involved
Inner membrane platform	Membrane proteins EpsC, EpsF, EpsL, and EpsM Secretion ATPase EpsE
Pseudopilus	Major pseudopilin EpsG Minor pseudopilins EpsH, EpsI, EpsJ, and EpsK
Outer membrane complex	Large secretin EpsD Pilotin EpsS

of cyclic adenosine monophosphate (cAMP), leading to the heavy outpouring of chloride and other electrolytes. This process takes place in several stages: 1) the attachment of CT to the plasma membrane of epithelial cell, 2) the internalization of CT by endocytosis, 3) retrograde trafficking of CT inside the cell to reach the lumen of the endoplasmic reticulum (ER), 4) unfolding of the A1 fragment and its disassembly from the holotoxin, 5) translocation of the A1 fragment to the cytosol, and 6) reactions of the A1 fragment in cytosol, leading to the activation of the adenylate cyclase, the opening of the chloride channel and the outpouring of the fluid. A current model for the CT cell entry and intoxication is illustrated in Fig. 2.9. The whole journey starts by the binding of CT to the GM1 ganglioside on the cell membrane of intestinal epithelial cells. All the stages are briefly described in the following paragraphs except for the attachment of the CT to the plasma membrane, which will be discussed in more detail in section 2.4.4.

Endocytosis is a mechanism by which an object gains entry into the cell. The endocytosis mechanism may vary depending on the object. CT utilizes lipid rafts in the endocytic mechanism when it is internalized into the cell [78, 79]. The attachment of CT to GM1 partitions in detergent-insoluble glycosphingolipid (DIG)-rich membranes has been demonstrated by different teams [80–83]. GM1 has been noticed to have an ability to transport CT backwards into the Golgi and ER in an intestinal cell. After CT has bound to the GM1 ganglioside in lipid rafts on the plasma membrane of the host cells, the toxin enters the cell by various endocytic mechanisms, including clathrin and caveolin-dependent, as well as caveolin and dynamin-independent mechanisms [84–90]. This involves many different proteins, including V- and T-SNAREs [91, 92]. Endocytosis of CT can take place by different pathways, and these pathways can function simultaneously [93]. It has been proposed that the CT-GM1 complex is associated with the actin cytoskeleton [94] via lipid drafts, and that the actin cytoskeleton plays a role in the trafficking of CT from the plasma membrane to the Golgi or the ER and in the subsequent activation of adenylate cyclase.

Protein translocation channels exist on the endoplasmic reticulum. To get there, CT must first undergo retrograde transport. CT is transported via a glycolipid-dependent pathway [79] where glycolipids act as transport vehicles from the plasma membrane to the ER. The toxin can be found in the early endosome (EE) and the recycling endosome (RE) [95, 96]. In general, the toxins are thought to move from the EE to the trans-Golgi network (TGN), independent of the late endosome pathway [91, 92, 97]. CT is transported directly from the early endosome via different vesicle dockings to the TGN [92, 98, 99], utilising actin and microtubules of the host cell [100]. From the TGN, CT is transported to the ER via a coat protein complex I (COPI)-independent pathway in the human intestinal [101]. It has been shown that

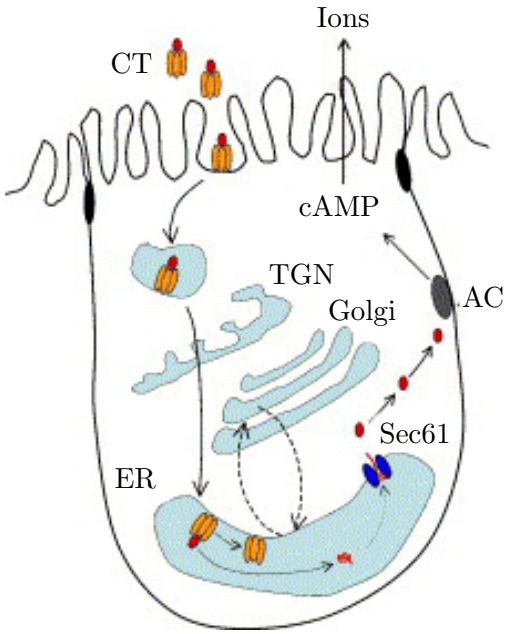

Figure 2.9: An illustration of the intracellular journey of CT from the intestinal lumen to the arising of symptoms [42].

the CT-GM1 complex might bypass the Golgi cisternae, trafficking directly to the ER [101]. CT can also be recycled between the Golgi and the ER [101]. The A subunit of CT harbors a specific amino acid sequence Lys-Asp-Glu-Leu (KDEL)-motif [102] that is not essential for transport to the ER [103], but appears to allow retention in the ER by recycling CT between ER and Golgi cisternae, and enhance interaction with endoplasmic-reticulum-associated proteins (ERAD) for retro-translocation.

CT remains bound to GM1 after entering the ER. The A1-chain must actively be released from the toxin complex, because even after reducing the disulphide bond between the A and B subunits, the subunits remain folded together [104]. This is achieved by the protein disulphide isomerase (PDI) which is a redox-dependent chaperone within the ER lumen [105]. Chaperones are special proteins that can assist in protein folding [106]. PDI unfolds CT [105], while Erp72 works in the opposite direction: it maintains CT in a folded conformation [107]. The recognition between PDI and cholera toxin is not known, but it might be initiated by a relative instability of the fold of the A subunit [108], or by exposure of the hydrophobic C-terminal domain of the A1-chain [109]. The PDI-A1-chain is targeted to a protein on the ER, after which the A1-chain is released from the PDI by Ero1 oxidase [110]. The mechanism is not fully understood, and the PDI may not be the only chaperone responsible for unfolding of the A1-chain. Additional *in vitro* evidence suggests that the Hsp70 chaperone BiP plays a major role in maintaining the A1-chain in a soluble state [111].

The retro-translocation of CT from within the ER to the cytosol has caused many groups to speculate that the CT, like other ERAD substrates [112], crossed the ER membrane through a protein-conducting channel initially thought to be the translocon Sec61 [113, 114]. This was observed by Shmitz *et al.* [115] in 2000. However, there are problems with the idea that Sec61 operates in the observed way [109]. Other possibilities for the identity of the channel have emerged [116, 117], like Hrd1 and gp78 forming the protein-conducting channel from ER into the cytosol [118]. Also the idea that a channel is not required at all has been presented [119].

ERAD substrates exit the ER and enter the cytosol for ubiquitination and degradation by the proteasome [106]. After getting out from the ER into the cytosol, the A1-chain has to rapidly refold into its native, enzymatically active conformation to be able to act and avoid rapid degradation by the 20S proteasome [108, 120]. Rapid refolding of the chain might act as a molecular ratchet to provide the driving force for retro-translocation [121]. However, it has been shown that the A1-chain is thermally unstable [108, 120] and not likely to refold spontaneously. Such instability challenges the idea of self-folding as a molecular ratchet. Another idea is that the A1-chain might require binding to a cytosolic chaperone or other CT binding proteins to stabilize its native conformation. Also, the lack of lysines in the A1 chain [122] may affect on the really slow degradation after retro-translocation because lysines are the sites for polyubiquitination [122]. Polyubiquitination is the primary motif for targeting proteins to the proteasomes which degrade proteins. However, the proteasome can also recognize and degrade unfolded proteins in the absence of polyubiquitination. Thus, it is probable because of the paucity of lysines in the A1 chain together with its ability to refold rapidly protects the A1 chain from degradation in the cytosol [79, 121]. Other factors must also be involved, since a mutant form of the A1 chain with the same lysine residues undergoes retro-translocation but is rapidly degraded by the proteasome after being ubiquitinated at the two lysine residues [123]. It is possible that CT avoids the ubiquitination machinery due to cytosolic chaperones or rapid refolding of the A1 chain upon entry into the cytosol [123]. A cofactor for the enzymatic activity, ADP ribosylation factor 6 (ARF6), was found to stabilize the A1 chain and protect it from degradation by the proteasome [108, 120]. Thus, binding of ARF6-GTP to the A1 chain restores order to the toxin, and this might explain how the toxin avoids rapid degradation and induces toxicity.

The last step in toxin activity in cytosol is diffusion-limited, where the A1 chain catalyzes the ADP-ribosylation of the heterotrimeric guanine nucleotide-binding protein (G protein) to activate the adenylate cyclase (AC). Adenylate cyclase is not directly activated by the binding of any hormone. Instead, it is stimulated by the G protein which binds guanyl nucleotides guanosine triphosphate (GTP) or guanosine diphosphate (GDP). Only the GTP complex of the G protein activates the adenylate

cyclase. The AC is a transmembrane protein which passes through the membrane 12 times and the functionally important parts are located in the cytoplasm. The cytoplasmic part consists of two regions which form a catalytic dimer which binds ATP and is converted to cyclic AMP (cAMP). Thus, the net effect of the cholera toxin is to cause cAMP to be produced, which stimulates mucosal cells to pump large amounts of chloride ions into the intestinal contents by stucking the chloride channels in the "open position" [4].

2.4.4 Binding to Plasma Membrane

The heterogeneous lipid composition of the plasma membrane (PM) has been shown to be important for the function of CT. It is generally known that lipids are organized into "lipid rafts", specialized membrane microdomains rich in cholesterol and glycosphingolipids (GSL) [124, 125]. They are recognized to play roles in signaling and membrane trafficking [126, 127]. The structure of these microdomains has proven to be difficult to obtain with conventional imaging methods due to resolution limits. It has been revealed that a raft may be very small in size and highly dynamic, existing for 10 to 20 ms and having a diameter of less than 20 to 50 nm [128]. By using the Saffman-Delbrück model [129], the estimated radius of the raft varies between 13 and 39 nm [130]. It is confirmed that association with raft is required for efficient uptake at the plasma membrane [131]. The CTB subunit tethers the holotoxin to the membrane, leading to the association of CT with lipid rafts, which are required for toxin function [79, 80]. CT interference with cholesterol has been shown to inhibit endocytosis and intracellular transport [81, 132].

The association of CT with lipid rafts appears to be crucial for toxicity [134]. CTB has a high affinity for GM1 ganglioside, which is found in the outer leaflet of the plasma membranes of virtually all cell types, including enterocytes and lymphocytes [3, 135, 136]. Clustering of CT to GM1 ganglioside increases the efficiency of retrograde trafficking to the ER, perhaps by stabilizing lipid raft microdomains, by inducing membrane curvature [137], or by enhancing the affinity for GM1 binding [138]. Interestingly it has been noticed that CT does not bind with a high affinity to other gangliosides like it does to GM1 [3, 139, 140]. Thus, the endogenous addition of GM1 allows immune cells to be attacked and intoxicated by CT [141].

Fishman *et al.* [142] showed in 1978 that five GM1 molecules on the membrane surface are bound by the B-pentamer consisting of five identical binding sites. The binding of GM1 to the five sites is suggested to be cooperative [143]. Merrit *et al.* revealed in 1994 by utilising X-ray crystallography that each B subunit has a GM1 binding pocket. B subunits interact mainly with the terminal galactose, and to a lesser tend with the sialic acid and N-acetylgalactosamine of GM1 [144]. Structure determination showed that the specific portion of the cell surface receptor interacts

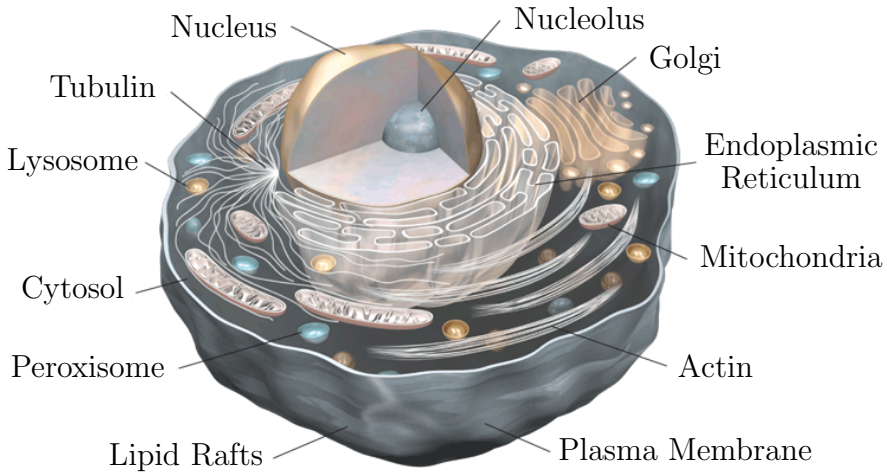

Figure 2.10: A schematic picture of the interior of the cell. Figure modified from [133].

with toxin side chains.

The receptor-toxin binding interaction may be described as a "two-fingered grip" because a large majority of interactions involve the two terminal sugars of GM1, galactose and sialic acid, illustrated in Fig. 2.11. The galactose part plays the role of the forefinger and sialic acid the role of the thumb when pinching an object with a human hand. The longer Gal-GalNac terminal is fairly deeply buried in the toxin-pentasaccharide complex while the shorter branch, the thumb, lies along the toxin surface. The binding site against the forefinger of GM1 is notable for comprising a complex net of hydrogen-bonding interactions tying all of the galactose hydroxyl oxygens to the protein, either directly or via tightly associated water molecules. All of the binding sites of AB_5 holotoxin are located on the opposite side of the catalytic A1 domain [145].

Several key residues in the B-pentamer have been found to be necessary for receptor binding. One of them is the single tryptophan residue Trp88, shown by chemical modification and site-directed mutagenesis studies [146–148]. Upon receptor binding, the toxin-GM1 complex is stabilized due to a flexible loop comprising amino acids 51-58 becoming more ordered. This is caused by hydrogen bond interactions with the GM1 pentasaccharide [144]. Merrit *et al.* suggested also other residues which may be important for the binding, like Glu11, His13, Glu51, Gln56, Gln61, Asn90 and Lys91.

The saccharide moiety of GM1 is bound by the complete AB_5 hexamer and the mere B-pentamer but not by the monomeric B subunit [146]. Thus, the B-pentamer is capable of target cell recognition and binding, even in the absence of the A subunit, but actual intoxication follows only from exposure to the AB_5 holotoxin.

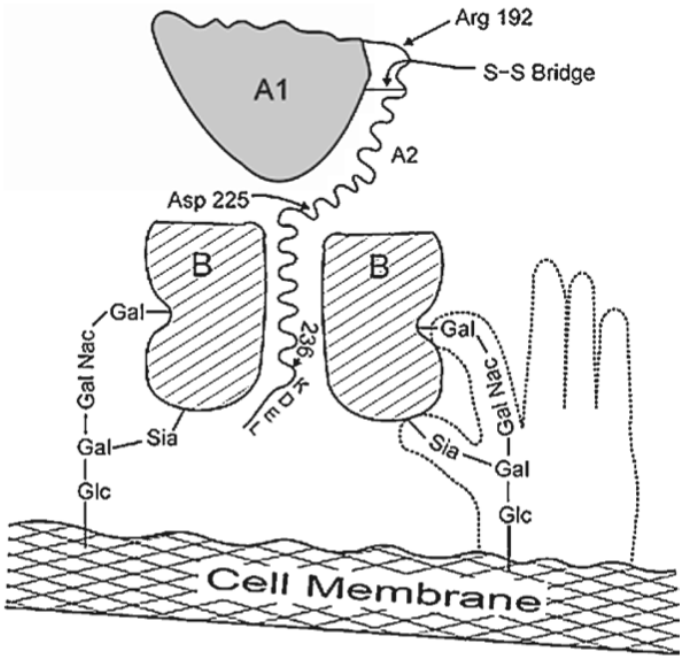

Figure 2.11: A schematic drawing showing the "two-fingered" grip binding of CT to the GM1 pentasaccharides. Figure modified from [10].

2.4.5 Possible Approaches to a Structure-Based Drug Design

Based on the known structure of the CT and its binding to the cell membrane, the sites where the inhibitor may act to inhibit the action of CT have been revealed [149]. One is achieved by blocking the active site of A1 in a manner in which it cannot catalyze the ADP-ribosylation reaction. The second approach to inhibit the action of CT could be by blocking the interaction between the A2 fragment and the B-pentamer, and thus the assembly of the holotoxin. The third approach could be to prevent the binding of the B-pentamer to the cell surface receptor GM1.

In addition to structure-based drug design, there are other aspects which can be used to develop new drugs against cholera. These include the synthesis of the toxin, its assembly into the three-dimensional structure in the periplasmic space, its secretion into the extracellular medium by the complex secretory mechanism evolved by the bacteria, or its entry and retrograde voyage into the epithelial cell of the host. These are just a few ideas to be mentioned. These methods provide many opportunities to disturb the action of the toxin molecule. All these possibilities and other methods of molecular biology enable us to design new effective methods for inhibiting the physiological action of the toxin and thus preventing the onset of the disease cholera.

3. FLUORESCENCE

Luminescence is emission of light by any substance. It includes the emission of photons from atoms excited in the course of chemical reactions, biochemical reactions, or upon oxidation or reduction at an electrode [150]. Luminescence is formally divided into two categories: fluorescence and phosphorescence, depending on the nature of the excited state. However, the distinction between fluorescence and phosphorescence is not always clear. In excited singlet states, the electron in the excited orbital is paired by the opposite spin to the second electron in the ground-state orbital. Phosphorescence is emission of light from triplet excited states, in which the electron in the excited orbital has the same spin orientation as the ground-state electron. Transitions to the ground state are forbidden and the emission rates are slow [151]. Fluorescence is a methodology used in biotechnology, flow cytometry, medical diagnostics, DNA sequencing, and genetic analysis, to name a few.

Fluorescence is based on the fluorescent molecules, also called fluorophores. In a fluorophore an electron absorbs a photon from excitation light. Due to the excitation photon, the energy level of the electron of the fluorescent particle is raised to an excited state (see Fig. 3.1). Some of the energy is dissipated by molecular collisions or transferred to a proximal molecule during a short excitation period. The remaining energy is emitted as a photon to relax the electron back to the ground state. The emitted fluorescence can be distinguished from the excitation light because the emitted photon carries less energy, therefore having a longer wavelength and smaller frequency than the excitation photon. The whole fluorescence process is cyclical as the fluorophore can be repeatedly excited.

Both the excitation and emission wavelengths are specific characteristics for each fluorophore. While these wavelengths are discrete for monatomic fluorophores, polyatomic fluorophores exhibit broad excitation and emission spectra. The spectra indicate the wavelengths that correspond to the minimum and maximum excitation and emission signal intensity. This is illustrated in Fig 3.1.

The distance between the excitation and the emission peaks in a spectrum is called the Stokes shift (see Fig. 3.1). It is a distinct characteristic of each fluorophore and a key aspect in the detection of the emitted fluorescence in biological applications. For fluorophores with very small Stokes shifts, the detection of the emitted fluorescence can be difficult to distinguish from the excitation light because of the overlap of the

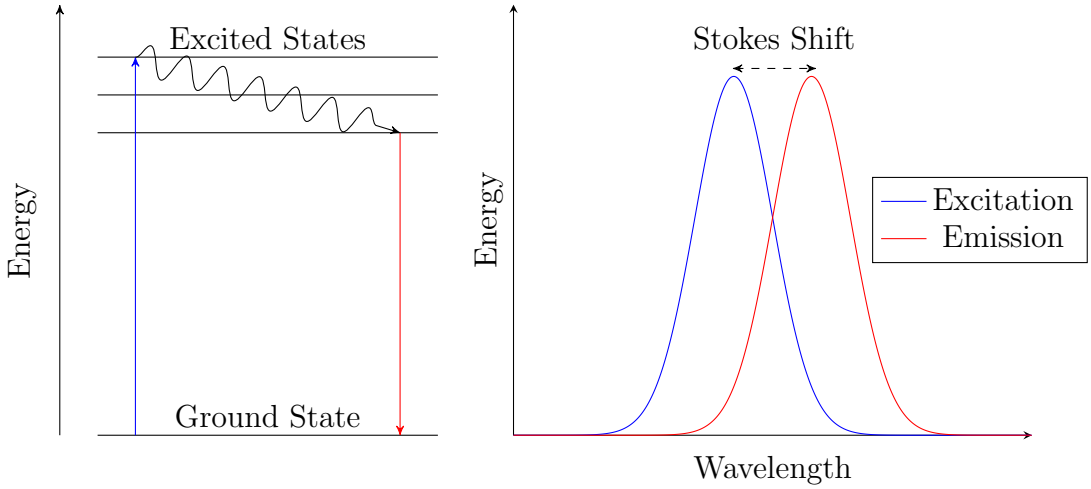

Figure 3.1: On the left, illustrative diagram of the nature of the fluorescence phenomenon. Blue arrow represents the absorbed excited photon and the red arrow the emitted fluorescent light. On the right, shematic figure of the excitation and emission spectra of a fluorophore. Stokes shift is marked in the picture. Picture modiefied from [151].

excitation and the emission wavelenghts. Conversely, fluorophores with large Stokes shifts are easy to distinguish and therefore they are preferred to the ones with small Stokes shift.

Fluorescence techniques offer high spatial resolution reaching the limit of single molecules. The scale of fluorescence lifetime can be as short as 10^{-8} to 10^{-10} s, which makes fluorescence techniques really fast. However, the greatest advantage of the techniques is their versatility [150]. Fluorescence sensing can be provided in solid, liquid and gaseous media. All kinds of interfaces between these phases are also able to be studied. This is due to the fluorescence reporter and the detecting instrument which are connected via light emission. Fluorescence detection can be made non-invasive and for sensing different targets within the living cells.

Many factors can influence fluorescence emission and detection. Fluorophore emission can be directly influenced by interaction with other fluorescent or non-fluorescent molecules, which can "quench" the emitted fluorescence from the excited fluorophore. Fluorophore detection can be disturbed by high background fluorescence, usually caused by insufficient removal of nonbound fluorescent probes. The low fluorescence intensity can also limit the detection of the target fluorophore, especially in the case of high background fluorescence. High-intensity excitation light or prolonged exposure can cause the photochemical destruction of a fluorophore. This is called photobleaching. It can be minimized by exposing the fluorophore to the lowest possible level of excitation light intensity for the shortest length of time that still yields an adequate signal detection.

3.1 Fluorescent Labeling

Fluorophores can be broadly divided into two main classes: intrinsic and extrinsic fluorophores [152]. Intrinsic fluorophores are those that occur naturally including the aromatic amino acids, flavins, derivatives of pyridoxyl, and chlorophyll. Extrinsic fluorophores are added to the sample to provide fluorescence or to change the spectral properties of the sample. Extrinsic fluorophores include fluorescein, rhodamine, dansyl, and numerous other substances.

One can compare different fluorophores by the brightness of a fluorophore which is determined by the molar extinction coefficient and the quantum yield. The molar extinction coefficient ϵ is defined as the quantity of light absorbed by a fluorophore at a given wavelength. The quantum yield Φ is the number of emitted photons divided by the number of absorbed photons. The brightness of a fluorophore is the product of ϵ and Φ. Other important properties of a fluorophore include the amount of times the fluorophore can be excited and the lifetime of the excited state.

Fluorescent labelling is the process of covalently attaching a fluorophore to another molecule. The most commonly labelled molecules are antibodies, but other molecules, such as proteins and nucleic acids are also used as specific probes. If a particle like a protein or a lipid is labelled with an extrinsic fluorophore, the fluorophore is termed as a fluorescent dye.

In order to measure membrane nanostructures, specific visualizations of lipids and proteins are required. This can be done by adding a fluorescent label to the molecule of interest. One of the most well-known proteins, the green fluorescent protein (GFP), enables direct observation of proteins both in their native environment and in the synthetic systems [153–155]. In the case of lipids, such a universal probe does not exist. To probe the lipid environment sensitively and selectively [156], incorporation of synthetic fluorescent analogs of native lipids into cell membranes has become a common protocol for optical investigation of membranes. Fluorescent analogs of cholesterol [157–160], sphingomyelin [159, 161–163], GM1 [161, 164–166], PC, and PE [153] were used. When using extrinsic dyes, the addition of a fluorophore may drastically affect native lipid behavior, especially if the dye contains hydrophilic groups [153]. This has to be taken into account when dealing with lipid rafts because they require specific structural features which allow their condensation into an ordered domain. Correspondingly, most fluorescent raft lipid analogues do not enter the raft-mimetic liquid-ordered phase of model membranes [153, 164, 167–170].

3.2 BODIPY Fluorophores

Compounds in the series of BODIPY fluorophores have an indacene-like structure (see Fig. 3.2). BODIPY is a trademark of Molecular Probes Inc and refers to a family

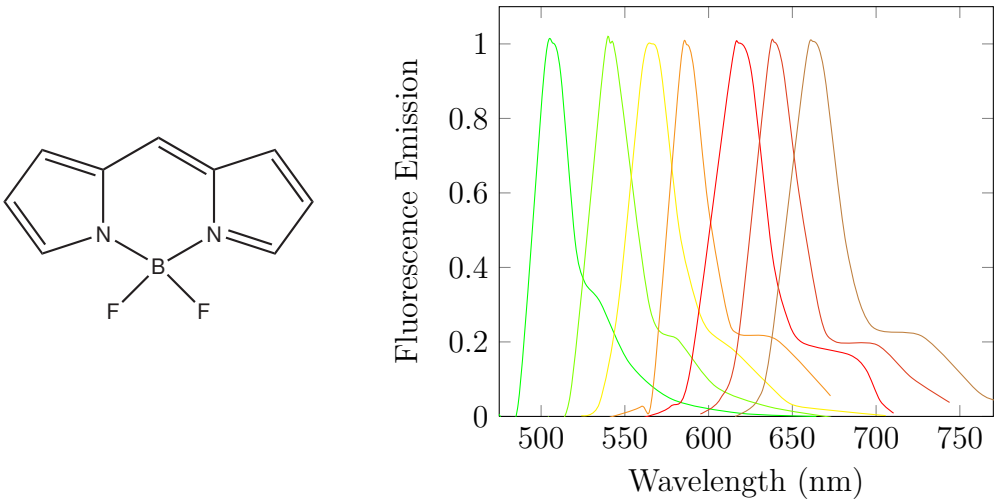

Figure 3.2: On the left, the molecule structure of a parent BODIPY fluorophore. On the right, normalized emission spectra of (——) BODIPY FL, (——) BODIPY R6G, (——) BODIPY TR, (——) BODIPY581/591, (——) BODIPYTR, (——) BODIPY 630/650 and (——) BODIPY 650/665 dyes in methanol. Figure modified from [133].

of dyes based on 4,4-difluoro-4-bora-3a,4a-diaza-s-indacene [151]. The framework can be considered as a rigidized monomethine cyanine dye by introduction of a linking group between the two nitrogen atoms. The resulting dipyrrometheneboron difluoride structure is quite rigid, which leads to high fluoroscence quantum yields [171].

BODIPY fluorophores are extremely versatile with their derivatives spanning the visible spectrum (see Fig. 3.2) [172]. Alkyl-substituted derivatives have a green, fluorescein-like fluorescence. Substitution by conjugated units on one or both pyrrole moieties causes extension of the conjugation of the π-electrons occurring along the organic backbone. The emission wavelength maxima range thus from 510 to 675 nm (see Fig. 3.2) and even emission maximum wavelengths greater than 750 nm are possible [171]. BODIPY molecules are also uncharged. They are insensitive to polarity and solvent pH [150]. They possess a high molar absorbance $\left(\epsilon \approx 80000 \frac{1}{\mathrm{cm} \times \mathrm{M}}\right)$ and a quantum yield Φ that is approaching 100 %, even in water. The application of these dyes is extremely versatile. Due to their relatively long lifetime, 4 ns or longer, they are particularly useful for fluorescence polarization-based assays.

BODIPY fluorophores offer many advantages: high fluorescence quantum yields, good solubility, and an excellent stability in thermal, chemical and photochemical perspective. Since they are rather insensitive to environmental effects, like polarity and pH, they are suitable as tracers in biology. They are in fact commonly used for labelling amino acids, nucleotides, and other low molecular weight ligands [171]. Further, BODIPY has been used as a fluorescent marker attached to the GM1 ganglioside, the interest of this study [164, 165].

4. MOLECULAR DYNAMICS

In this thesis, interactions between cholera toxin and various lipid bilayers are studied with the aid of molecular dynamics (MD) which is often the simulation method of choice when there are thousands of molecules in the system whose analysis requires atomic scale accuracy [173]. In this study the GROMACS simulation package was used [174, 175]. This chapter gives an overview of MD simulation methods based on the user manual of GROMACS [176], as well as Refs. [177], [178], and [179].

Molecular dynamics simulations represent an approach to statistical mechanics with the aid of computers [179]. MD simulation is a classical technique for computing the equilibrium and transport properties of a classical many-body system [180]. For simplicity, the system is assumed classical, meaning that quantum effects are ignored so that the nuclear motion of the constituent particles obeys the laws of classical mechanics. Only when considering translational or rotational motion of light atoms like helium or light molecules like H_2 or vibrational motion with a frequency larger than $k_B T/h$, one should consider quantum effects [177].

Experiments and MD simulations have many similarities to each other. An experiment begins with preparing a sample one wishes to study and continues by attaching it to a measuring instrument. Then the property of interest is measured during a certain time interval. Exactly the same approach is followed in MD simulations. At first, a model consisting of N particles has to be selected. Then it will be simulated by Newton's equations of motion for the system until the properties of the system no longer change with time. In other words, we equilibrate the system. After the equilibration period, the actual measurement is performed.

Experimental measurements are difficult to perform in small scales — in nanoscales this is almost impossible. The aim of molecular dynamics is to provide a better understanding of or to predict macroscopic phenomena observed in experiments. MD simulations allow the study of properties which are beyond the access of experimental techniques. MD simulations are also cheap to implement, which is the second significant advantage of MD simulations compared to experiments. On the other hand, the MD technique has a number of limitations which are going to be discussed in section 4.6 in more detail.

MD simulation begins with creating the initial structure and giving the required parameters for the system to be simulated. After this, the MD algorithm iteratively

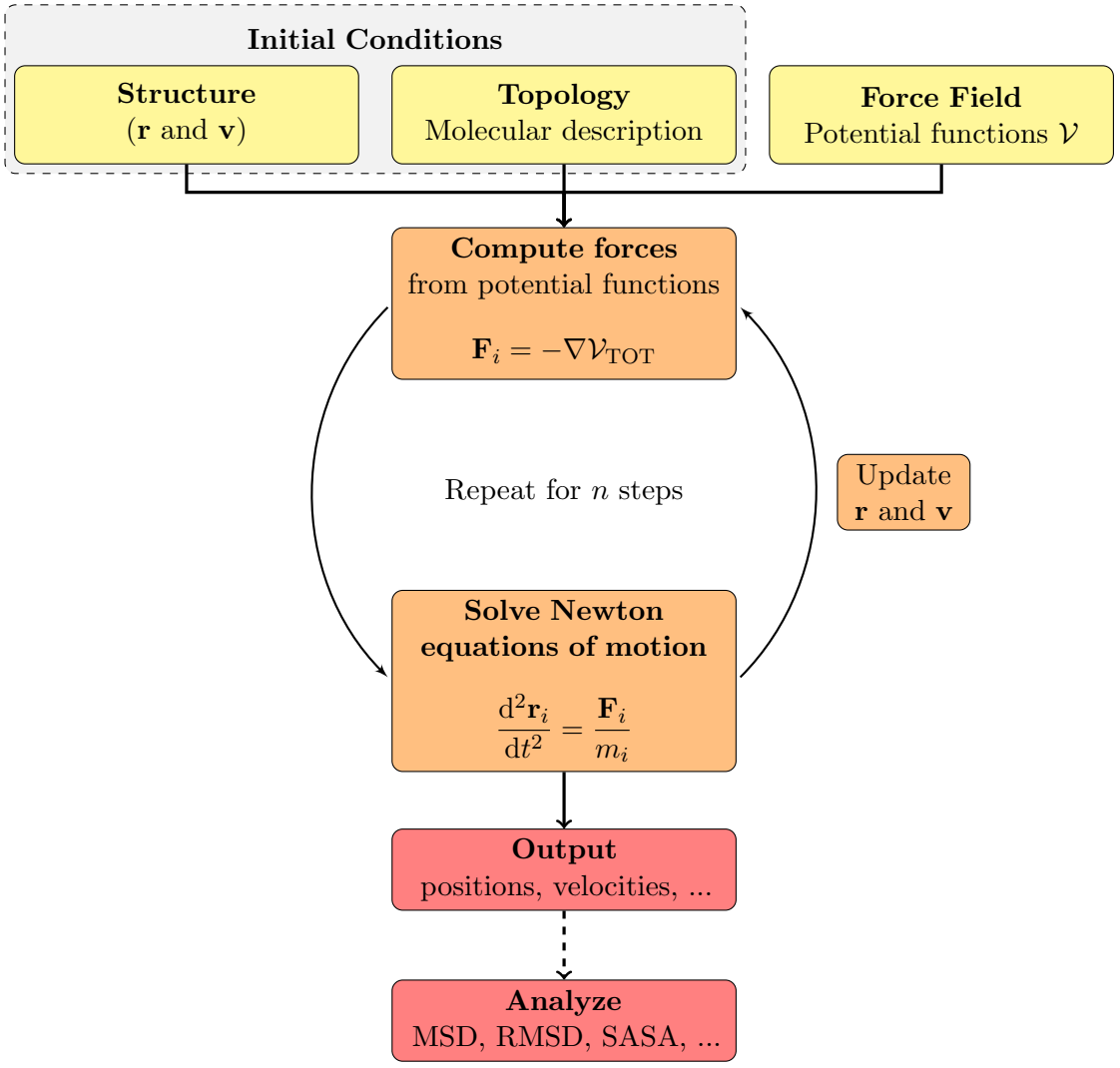

Figure 4.1: General MD algorithm.

computes the actions on all particles, integrates Newton's equation of motion, and updates the new positions and velocities for each particle [174]. These steps are then repeated for the required number of steps. The schematic picture of MD workflow is presented in Figure 4.1.

4.1 Initial Conditions

Before the MD simulation can be initiated, the systems need to be adequately prepared. To prepare a system, one needs not only to construct the topology with the description of force field, but also to set the positions and velocities of all the particles. Because the results of the study are usually dependent on the initial conditions, this should be done very carefully. Usually the assignment of the positions is based on experimental findings and an established theoretical model.

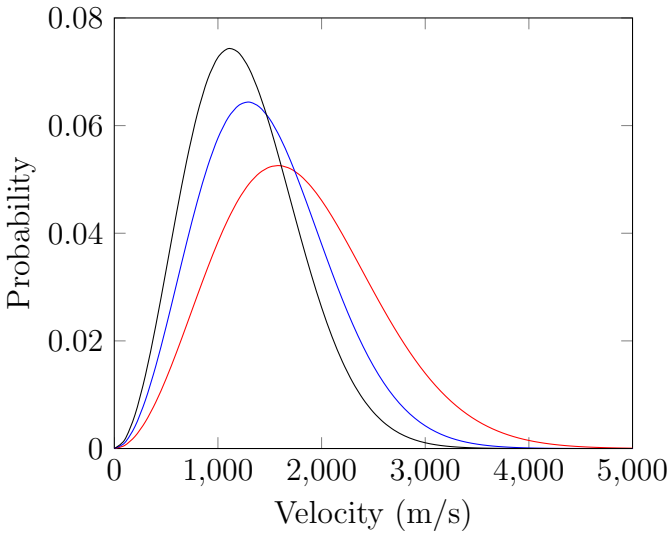

Figure 4.2: Maxwell–Boltzmann velocity distributions calculated with the temperature of 300 K. Different colors represents different masses as: ——: 2u, ——: 3u, and ——: 4u.

Starting velocities for each particle can be set by the user or they can be generated accordingly to a Maxwell–Boltzmann distribution at a given absolute temperature T. The distribution function has the following form:

$$p\left(v_i\right) = \sqrt{\frac{m_i}{2\pi k_\mathrm{B} T}} \exp\left(-\frac{m_i v_i^2}{2 k_\mathrm{B} T}\right), \tag{4.1}$$

where m_i is a mass of the particle i, k_B is the Boltzmann's constant, T is the temperature and p is a probability as a function of velocity v_i for each particle i. A schematic picture of distributions for particles with different masses are illustrated in Fig. 4.2.

All the MD simulations require a molecular description of the particles that are simulated. The description is the so called topology which contains parameters attributed to atoms and their interactions. These parameters describe physical properties of atoms like atom type, mass and charge, as well as relations between them like bonds, angles and dihedrals. It is important to emphasise and remember that all the information in topology is static: it is never modified during the simulation which means that, for example, new bonds cannot be created during the MD simulation.

After the system has been constructed, it has to be energy minimized before starting the real simulations. Energy minimization is performed in order to eliminate all the high-energy interactions which might cause instability in the system.

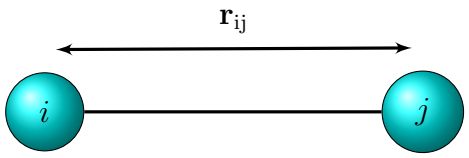

Figure 4.3: Bond stretching

4.2 Force Field

The force field is a set of potential functions which describe the interactions between simulated particles by certain potential functions. Further on, the parameters in the topology, as mentioned before, are included as constant coefficients in the potential functions. Force fields are used to calculate forces acting on the atoms during the run of a simulation. Two main kinds of interactions are discussed in the following sections: bonded and non-bonded interactions. The total potential function is sum of all the potential functions:

$$\mathcal{V}_{\mathrm{TOT}} = \mathcal{V}_{\mathrm{bonded}} + \mathcal{V}_{\mathrm{non-bonded}}. \tag{4.2}$$

In this study, the OPLS all-atom force field was implemented [181].

4.2.1 Bonded Interactions

Bonded interactions involve atoms which are chemically attached to each other. However, the bonded interactions include not only the interactions between two atoms but also 3- and 4-body interactions. Generally 2-body interactions are denoted as bond stretching, 3-body interactions as valence angle bending, and 4-body interactions as dihedral angle rotation.

The bond stretching between two covalently bonded atoms i and j (see Fig. 4.3) is often modelled by a harmonic term following Hooke's law and can be described by a harmonic potential

$$\mathcal{V}_{\mathrm{bonds}} = \sum_{\mathrm{bonds}} k_{r,ij}(r_{ij} - r_{ij,r})^2, \tag{4.3}$$

where $k_{r,ij}$ is the force constant which describes the rigidity of the bond, r_{ij} is the distance between particles and $r_{ij,r}$ the reference bond length value.

The valence angle is determined by the hybridization of the atomic orbitals of three consecutively covalently bonded i, j and k atoms shown in Fig. 4.4. It provides general information about the geometry of the molecular fragment. They can be described by valence angle potentials which have the form of harmonic functions as

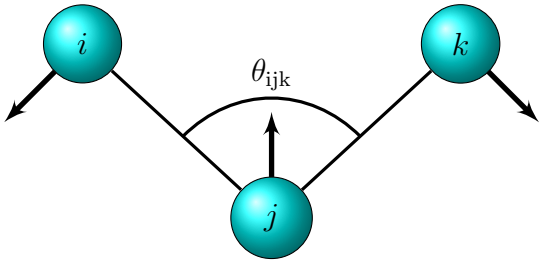

Figure 4.4: Angle bending

well:

$$\mathcal{V}_{\text{angles}} = \sum_{\text{angles}} k_{\theta,ijk}(\theta_{ijk} - \theta_{ijk,r})^2, \tag{4.4}$$

where $k_{\theta,ijk}$ is the force constant, θ_{ijk} is the angle between the three atoms and $\theta_{ijk,r}$ is the reference angle when j is the middle atom.

The dihedral angle is a torsional angle between four sequential bonded atoms. There are different types of dihedrals, each described by a different potential function. Improper dihedrals are meant to keep planar groups like aromatic rings planar. The simplest improper dihedral potential is a harmonic potential:

$$\mathcal{V}_{\text{improper dihedrals}} = \sum_{\text{improper dihedrals}} \frac{1}{2} k_\omega \left(\omega_{ijkl} - \omega_{ijkl,r}\right)^2, \tag{4.5}$$

where k_ω is a force constant, ω_{ijkl} stands for the torsional angle and $\omega_{ijkl,r}$ for reference angle.

Proper dihedral angles are defined according to the IUPAC/IUB convention, where ω is the angle between the ijk and the jkl planes (see Figure 4.5). For proper dihedrals there are two different most commonly used potential functions: periodic or Ryckaert-Belleman potential. The form of the periodic potential function is

$$\mathcal{V}_{\text{dihedrals}} = \sum_{\text{torsion}} k_\omega \left(1 + \cos\left(n\omega - \omega_r\right)\right), \tag{4.6}$$

where n is a constant and ω_r the reference torsional angle. The Ryckaert-Belleman potential function for proper dihedrals has the following form:

$$\mathcal{V}_{\text{dihedrals}} = \sum_{\text{torsion}} \sum_{i=0}^{5} C_n \left(\cos\left(\omega - 180^\circ\right)\right)^n, \tag{4.7}$$

where C_n is a constant defined in the topology. The first three of cosine terms of Fourier dihedrals (derived from 4.7) are used in the OPLS potential function

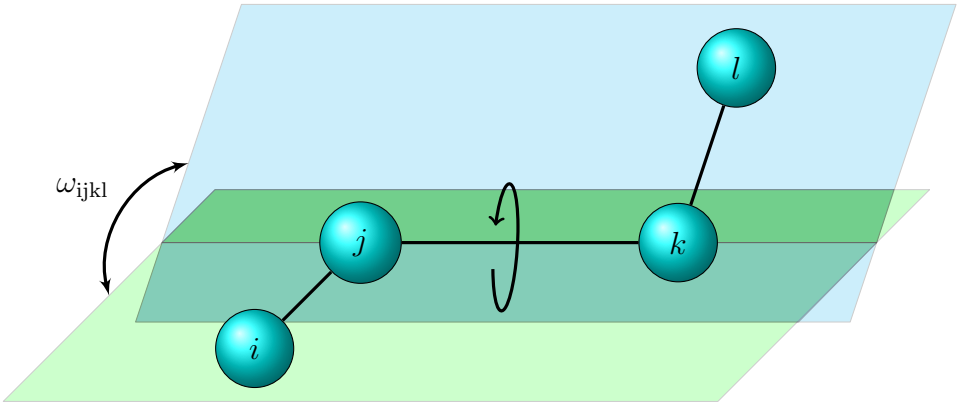

Figure 4.5: Dihedral Bending

[181, 182], which yields the following potential function:

$$\mathcal{V}_{\text{dihedrals}} = \sum_{\text{torsion}} \left(\frac{V_1}{2}(1 + \cos \omega_{ijkl}) + \frac{V_2}{2}(1 - \cos 2\omega_{ijkl}) + \frac{V_3}{2}(1 + \cos 3\omega_{ijkl}) \right), \tag{4.8}$$

where V_1, V_2, and V_3 are constants and ω_{ijkl} is the torsion angle.

4.2.2 Non-Bonded Interactions

The non-bonded interactions are pair-additive and centro-symmetric. They are computed on the basis of a list of non-bonded atoms within a certain radius. The list is called as a neighbour list. Two atoms which are connected via bonded interactions are excluded from the list. Non-bonded interactions consist of Lennard-Jones (LJ) or Buckingham potential and Coulomb interactions.

Repulsion and dispersion terms are combined in, for example, the LJ or the Buckingham potential. In this study the LJ potential function was used:

$$\mathcal{V}_{\text{LJ}} = \sum_{i<j} 4\epsilon_{ij} \left(\frac{\sigma_{ij}^{12}}{r_{ij}^{12}} - \frac{\sigma_{ij}^{6}}{r_{ij}^{6}} \right) f_{ij}, \tag{4.9}$$

where ϵ_{ij} and σ_{ij} defines the reference length and the strength of non-bonded LJ interactions which are individual for each atom pair ij, respectively. r_{ij} is the distance between particles i and j. f_{ij} is equal to zero when there is up to two covalent bindings between particles i and j. When there are three bonds, f_{ij} is equal to 0.5; these are so-called 1-4 interactions. In all other cases, f_{ij} gets a value of 1. r_{ij}^{12} represents the steep repulsive interaction and r_{ij}^{6} the attractive van der Waals interaction between two particles. Since van der Waals forces act within a short range, the interaction potential is rapidly decaying. Therefore, these interactions are

computed only for neighbour atoms within a certain cut-off radius.

The electrostatic interaction between two charged particles is described by the classical Coulombic potential

$$\mathcal{V}_{\text{coulomb}} = \sum_{i<j} \frac{1}{4\pi\epsilon_0} \frac{q_i q_j}{\epsilon_r r_{ij}} f_{ij}, \tag{4.10}$$

where q_i and q_j are the charges of particles i and j, ϵ_0 is the permittivity of the vacuum, ϵ_r the relative permittivity of the medium, r_{ij} the distance between two particles and f_{ij} is the same as in the LJ potential function (4.9). Comparing to van der Waals interactions, the Coulomb potential is a slowly decaying function. Evaluation of these interactions for each pair increases the computational complexity of the simulation significantly. Fast-electrostatic algorithms, such as Ewald methods [183, 184], can be implemented in order to address this problem.

4.3 Equations of Motion

To compute the time evolution of positions and velocities for a system consisting of N particles, the forces acting on the particles have to be calculated first. The force $\mathbf{F}_i$ acting on a particle is a negative gradient of the sum of the potential functions V defined in the force field:

$$\mathbf{F}_i = -\nabla \mathcal{V}_{\text{TOT}}. \tag{4.11}$$

The solving of the forces in the system is the most time consuming part of a MD simulation, despite using efficient techniques which allow for much faster evaluation. In order to minimize the needed computer resources, a common approach is to calculate the forces only for a certain group of atoms that lie within the cut-off radius for the interaction.

After the forces acting on each particle have been calculated, the motion of the particles can be found by solving the Newton's equations of motion:

$$\mathbf{F}_i = m_i \frac{\mathrm{d}^2 \mathbf{r}_i}{\mathrm{d}t^2}, \tag{4.12}$$

where m_i is the mass and $\mathbf{r}_i$ is the position of a particle i.

In order to calculate new positions and velocities, equations (4.11) and (4.12) are computed simultaneously in short time steps. There are several different time integrating algorithms for that purpose [185]. The default MD integrator in GROMACS is a commonly used leap-frog algorithm [186, 187], which produces identical trajectories to the Verlet algorithm [188].

The leap-frog algorithm uses coordinates $\mathbf{r}_i$ at time t and velocities $\mathbf{v}_i$ at time

$t - \frac{\Delta t}{2}$ to update new positions and velocities by calculating forces $\mathbf{F}(t)$ at time t. In practice, this means that GROMACS calculates the coordinates and the velocities to each particle alternately. The mathematical format for the new position is

$$\mathbf{r}_i\left(t + \Delta t\right) = \mathbf{r}_i\left(t\right) + \mathbf{v}_i\left(t + \frac{\Delta t}{2}\right)\Delta t, \tag{4.13}$$

where $\mathbf{r}_i$ and $\mathbf{v}_i$ are place and velocity of a certain particle, t is a point in time which is studied and Δt is the size of time step. The mathematical formula for velocity in the leap-frog algorithm is:

$$\mathbf{v}_i\left(t + \frac{\Delta t}{2}\right) = \mathbf{v}_i\left(t - \frac{\Delta t}{2}\right) + \frac{\mathbf{F}_i\left(t\right)}{2m_i}\Delta t, \tag{4.14}$$

where m_i is the mass of particle i and $\mathbf{F}_i$ is the force directed to it. Other variables are the same is in equation (4.13).

4.4 Temperature and Pressure Coupling

In a basic MD simulation, one can study a system consisting of N particles in volume V, while the energy of the system E is constant. This corresponds to a microcanonical (constant-NVE) ensemble. However, this is not often the case in real experiments where conditions like constant temperature and pressure (NpT) or constant temperature and volume (NVT) are more often used. In order to simulate systems in such ensembles, temperature and pressure coupling are often implemented.

One commonly used method to control the temperature in MD simulation is to use the Berendsen weak coupling algorithm [189]. Nosé–Hoover thermostat [190, 191] and velocity rescaling [192] schemes are also used to sustain constant temperature.

The Berendsen weak coupling algorithm can be understood as coupling the system to an external heat bath with a given temperature T_0. Comparison with the Nosé–Hoover scheme has been discussed in detail in Ref. [193]. As a result, the temperature difference in the Berendsen weak coupling method decays exponentially with a time constant τ:

$$\frac{\mathrm{d}T}{\mathrm{d}t} = \frac{T_0 - T}{\tau}. \tag{4.15}$$

The strength of the coupling can be varied to adapt to user requirements, which is a great benefit of the Berendsen method. In order to correct the kinetic energy distribution, an additional stochastic term is added to the velocity rescaling thermostat

applied in this study:

$$\mathrm{K} = (K_0 - K)\,\frac{\mathrm{d}t}{\tau_T} + 2\sqrt{\frac{KK_0}{N_f}}\,\frac{\mathrm{d}W}{\sqrt{\tau_T}}, \tag{4.16}$$

where K is the kinetic energy, N_f the number of degrees of freedom, and $\mathrm{d}W$ a Wiener process. In this approach the velocities of all the particles are rescaled by a properly chosen random factor. The velocity rescaling method has advantages over the Berendsen thermostat and still produces a correct canonical ensemble.

In order to simulate the system at a constant pressure, pressure coupling, similar to the temperature coupling, can be used. The Berendsen algorithm [189] is a commonly used algorithm for this purpose. It rescales the coordinates and the box size to sustain a given reference pressure $\mathbf{P}_0$ in a following way:

$$\frac{\mathrm{d}\mathbf{P}}{\mathrm{d}t} = \frac{\mathbf{P}_0 - \mathbf{P}}{\tau_p}. \tag{4.17}$$

A scaling matrix μ_{ij} given by

$$\mu_{ij} = \delta_{ij} - \frac{n_{\mathrm{PC}}\Delta t}{3\tau_p}\beta_{ij}\left(\mathbf{P}_{0ij} - \mathbf{P}_{ij}(t)\right), \tag{4.18}$$

is used, where δ_{ij} is Kronecker delta (one when i and j are equal and zero otherwise), n_{PC} the number of steps between pressure rescaling, τ_p the pressure constant, β the isothermal compressibility of the system, and $\mathbf{P}_{0ij}$ the target pressure.

The Parrinello–Rahman coupling [194, 195] is used in cases where it is important to calculate the thermodynamical properties of the system accurately. It is similar to the Nosé–Hoover temperature coupling and in theory it gives the true NpT ensemble. The box vectors represented by the matrix $\mathbf{b}$ obey the matrix equation motion

$$\frac{\mathrm{d}\mathbf{b}^2}{\mathrm{d}t^2} = V\mathbf{W}^{-1}\mathbf{b}'^{-1}\left(\mathbf{P} - \mathbf{P}_{\mathrm{ref}}\right), \tag{4.19}$$

where V is the volume of the box, $\mathbf{W}$ a matrix parameter which determines the strength of the coupling, $\mathbf{P}$ and $\mathbf{P}_{\mathrm{ref}}$ the current and reference pressure, respectively.

Parrinello–Rahman and Berendsen barostats can be combined with any of the temperature coupling methods in GROMACS and they both allow either isotropic scaling of all dimensions or anisotropic deformations, scaling the three dimensions separately. It must be remembered that if the simulation aims to study the thermodynamical properties of the system very accurately, it is reasonable to use more sophisticated coupling algorithms than those described in this section.

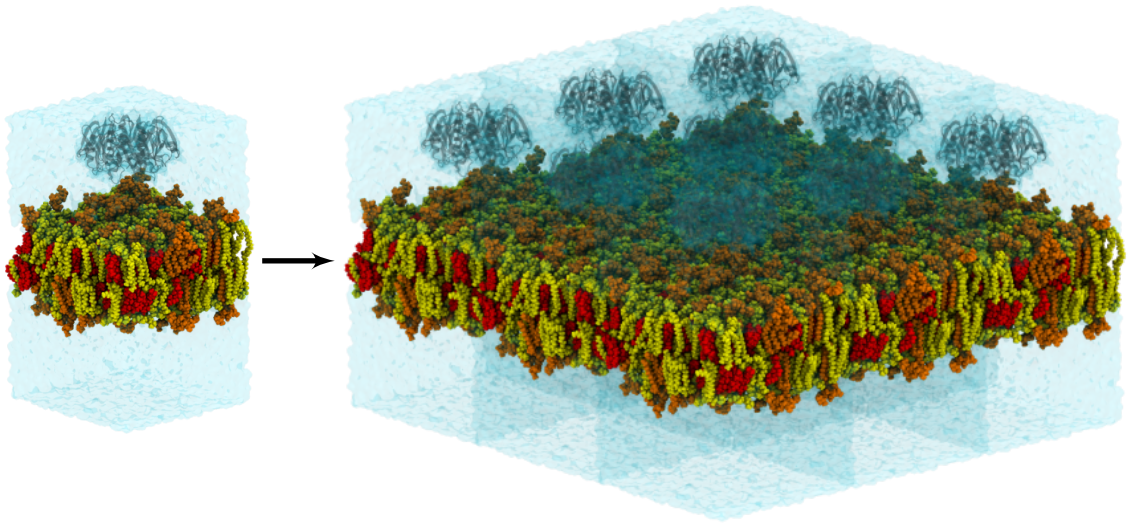

Figure 4.6: A schematic picture of PBCs in xy-plane in a three dimensional space.

4.5 Periodic Boundary Conditions

The size of the system in MD simulations is limited. In order to minimize the edge effects, there are several ways to treat the boundaries of the simulation box. The traditional way is to use periodic boundary conditions (PBC) where the space is filled with identical cells containing translated copies of the system, thus forming an infinite lattice. This is illustrated in Fig. 4.6. Therefore, if the particle crosses one side of the simulation box, it re-enters the box from the opposite site immediately. In this manner there are no undesired boundaries in this arrangement, though new artifacts related to periodic conditions may occur. If the size of the box is too small so that a particle residing near the box boundaries will experience the interactions caused by other particles more than once, unwanted edge effects ruining the whole data from the MD simulation might occur. Therefore, attention to the size of the box should be paid.

4.6 Limitations of MD simulations

To be able to understand and analyze the results of MD simulations, the user should be aware of the limitations of MD simulations. Since the MD method is based on a number of assumptions and approximations, there are several limitations.

Firstly, MD simulations are classical which means that the motion of particles is described by classical mechanics. Although there are corrections to the parameters of the force field used in MD, taking into account quantum phenomena, the study of real quantum behaviour with MD is impossible. For most atoms at normal temperatures this is a correct approach, but there are cases when quantum phenomena play an

important role and such systems cannot be studied by simulations based on classical mechanics.

Secondly, there are many force fields which can be chosen. In addition, all of them are approximate because the potential energy, determined on the basis of rather simply assumed pair-additive potential functions, is highly approximate, yet the simulation results depend on them. Furthermore, cut-off radii are used in the calculation of interactions.

Moreover, the boundaries of a small system can result in edge effects. On the other hand, by introducing PBCs one can avoid this kind of real face problems, but especially for small systems this may bring unwanted artifacts related to periodicity. Thus, it is important to be aware of the influence of the system size on these effects.

Finally, the computational cost of MD simulations is a challenge. If one aims to study protein folding, hundreds of microseconds of simulation time, or even milliseconds will be needed. Taking into account that membrane-protein systems contain hundreds of thousands of atoms and the fact that one simulation does not offer much of statistics, simulating these kinds of systems will cost a lot. Usually, the simulation time has to be decided from the relation between the computational cost and the amount of obtained data.

In conclusion, performing MD simulation is very challenging, although the basic principles of MD are relatively simple. One has to be really careful with initial conditions, algorithms and integrators, as well as analysis of the huge amounts of obtained data when dealing with MD simulations.

5. SIMULATION MODELS AND ANALYSIS METHODS

This thesis does not include any kind of experimental measurements. Instead, MD simulations described in the previous chapter were employed to study the binding of cholera toxin to various kinds of lipid bilayers. The simulated systems consisting of about 500,000 atoms are computer-intensive. It would have taken approximately 17 years to calculate each simulated system with a single core computer. Thus, all the systems were simulated by using the computing facilities offered by the Finnish IT Centre for Scientific Computing (CSC) and Tampere Center for Scientific Computing (TCSC).

5.1 Systems Studied

The purpose of this study was to investigate the binding of cholera toxin to lipid bilayers of various compositions. Cholera toxin itself consists of about 12,000 atoms. Instead of simulating the whole holotoxin, only the binding part, B-pentamer, involving about 8100 atoms was simulated with the lipid bilayers. This is relevant because the CTB is responsible for the toxin binding. In addition to a smaller number of atoms in the toxin, the system size was greatly reduced due to the smaller number of water molecules needed in the simulation box compared to the case of simulating the whole holotoxin.

To mimic different kinds of lipid bilayers, numerous types of lipids are needed. To be able to choose appropriate lipids for this study, the basic knowledge of the structure of the lipid bilayer is essential. Both the plasma membrane (PM) and the endoplastic reticulum (ER) are formed of two layers of lipids comprised of fatty acid chains and a head group linked together by a glycerol backbone, and proteins embedded in the membrane. The lipids are naturally arranged in such a way that their hydrophobic tails face each other while their hydrophilic heads are exposed to water on the outer sides of the leaflets. An illustrative picture of a cell membrane can be seen in Fig. 5.1.

Lipid bilayers can adopt an ordered gel-like phase, a liquid-ordered (l_o) phase, or a disordered liquid (l_d) phase depending on the lipid composition and the temperature of the system. The types of the membrane lipids strongly affect on the membrane properties [197]. Long saturated fatty acid chains can pack together tightly, forming

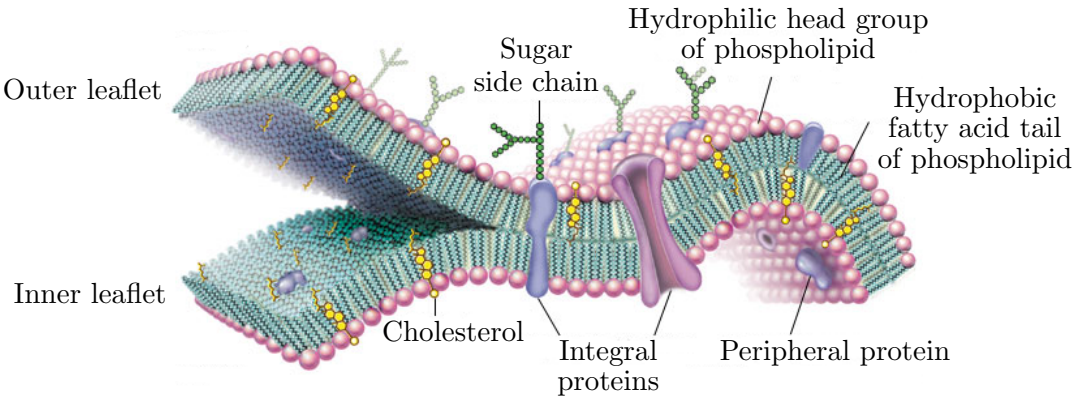

Figure 5.1: A schematic drawing of a cell membrane. Figure modified from Ref. [196]

a rigid structure, whereas kinks in the hydrocarbon chains due to unsaturated bonds cause the bilayer structure to be much more loose and disordered [198]. Thus, the fluidity of the lipid bilayer is greater in the l_d phase. Cholesterol is known to interact with the hydrophobic tails of other lipids, immobilizing them by restricting the random diffusion and hardening the structure of the bilayer by increasing the order of the lipid tails [102, 199]. Sphingomyelin has been noticed to make the bilayer thicker and more gel-like due to its ordered structure [102]. Many membrane events such as membrane fusion, protein sorting, and signaling are related to the phase behavior of the membrane [106].

The chemical structures of different lipids may vary a lot although they have many common features, such as insolubility in water. Lipids consist of either unsaturated or saturated fatty acid chains depending on whether they contain double bonds or not. Five types of lipids were used in our model membranes: cholesterol, GM1, GM1-b, DOPC, and SSM. The chemical structures of all these lipids are presented in Fig. 5.2.

Cholesterol is an amphiphilic molecule consisting of a polar hydroxyl group and a rigid nonpolar steroid fragment consisting of four carbon rings. A stable bilayer structure cannot be formed spontaneously with only cholesterol since the molecules are too hydrophobic due to the sterol group. However, cholesterol plays a major role in stiffening the membrane structure in mixed bilayers.

GM1 (Gal5-β1,3-GalNAc4-β1,4-(NeuAc3-α2,3)-Gal2-β1,4-Glc1-β1,1-Cer) is a ganglioside composed of a glycosphingolipid with one sialic acid residue linked on the sugar chain. Glycosphingolipid consists of a ceramide portion joined to a oligosacharide head group. There are five sugar units in the oligosaccharide of GM1: glucose, two galactose, N-acetylgalactosamine and N-acetylsneuraminic acid (NANA) groups (see Fig. 5.2). Due to the sialic acid, the head group of GM1 is anionic. In order to simulate the GM1 used in fluorescence spectroscopy, we replaced one of the

Table 5.1: Simulated systems.

System	CTB	DOPC	SSM	Chol	GM1	GM1-b	Time (ns)
l_d/GM1	1	440	0	0	40	0	500
l_d/GM1-b	1	440	0	0	0	40	500
l_o/GM1	1	0	220	220	40	0	500
l_o/GM1-b	1	0	220	220	0	40	500
l_d/GM1 ref.	0	440	0	0	40	0	200
l_d/GM1-b ref.	0	440	0	0	0	40	200
l_o/GM1 ref.	0	0	220	220	40	0	200
l_o/GM1-b ref.	0	0	220	220	0	40	200

tails of native GM1 with a BODIPY molecule. This is illustrated in Fig. 5.2.

DOPC, or 1,2-dioleoyl-*sn*-glycero-3-phosphocholine, is a phospholipid which is representative for phosphatidylcholines — a major component of biological membranes found in every cell of the human body. DOPC consists of two oleic acid chains joined together by a glycerol backbone which is connected to a positively charged phosphatidylcholine (PC) head group. The oleic tail is unsaturated due to a *cis*-double bond in it, creating a kink in the structure of the tail. It is also one of the most common fatty acids found in cells.

Stearoylsphingomyelin (SSM or N-stearoyl-d-erythro-sphingosylphosphorylcholine) belongs to a family of sphingolipids which are derivatives of sphingosine, an amino alcohol with a long hydrocarbon tail, containing an additional fatty acid chain attached to the sphingosine amino group. SSM consists of a ceramide backbone joined to a phosphatidylcholine head group. Due to the hydrogen bonding caused by the hydroxyl group in SSM and other sphingolipids, SSM is thought to have a stabilizing effect on the membrane structure.

In this study, four different lipid bilayers of various compositions were constructed. In order to mimic the liquid-disordered phase, a bilayer composed of DOPC lipids was built. For the liquid-ordered phase, a 1:1 cholesterol/SSM bilayer was constructed. In addition, both of these membranes were enriched with 9 mol-% of either native GM1 or BODIPY-labeled GM1 (GM1-b) resulting in four different lipid environments. Additionally, all the systems were simulated without CTB on the bilayer as a reference. Detailed compositions of all the simulated systems are shown in Table 5.1.

All the systems were prepared in a following manner. First, all the bilayers were hydrated and salt was added in a physiological concentration of 150 mM NaCl. In order to get the zero net charge for all the systems, 40 Na^+ counterions were added into all the systems due to the net charge of $-e$ of each GM1 ganglioside. These systems were simulated for 20 ns in order to equilibrate the bilayers. After equilibration, the B-pentamer was added to the systems. The distance between the

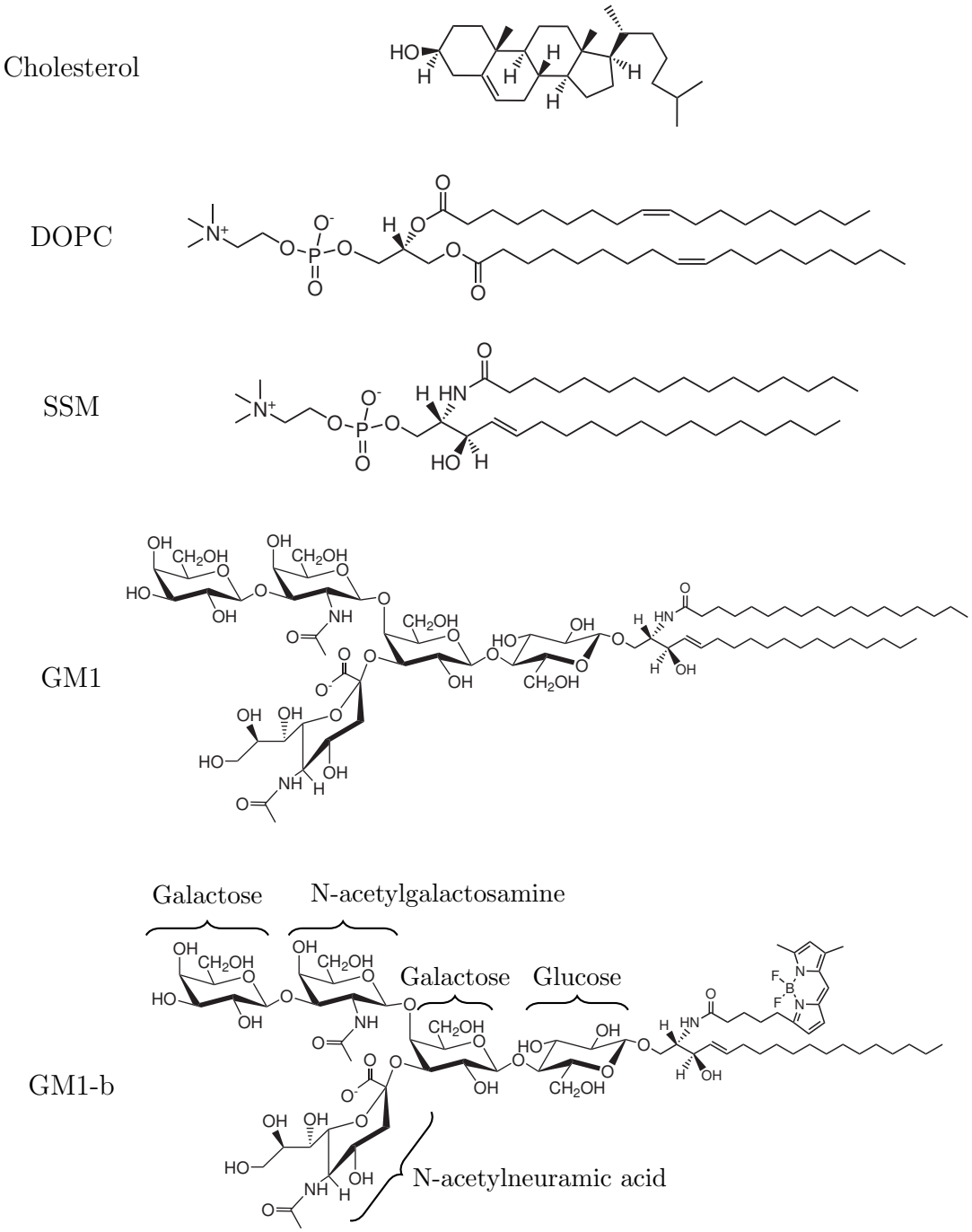

Figure 5.2: Molecular structures of the lipids used in this study. Carbohydrates in the head group of GM1 and GM1-b are shown in the molecular structure of GM1-b [159]. Molecular structures modified from Ref. [200].

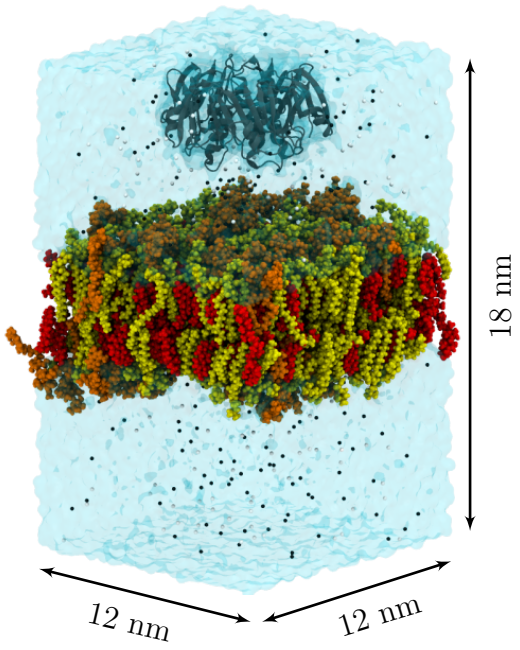

Figure 5.3: Illustrative picture of the simulated system consisting of libid bilayer in l_o phase with native GM1 and cholera toxin in 150 mM NaCl solution.

surface of the membrane and CTB was about 2 nm in each system. The coordinate file for CTB was acquired from the Protein Data Bank under the identifier 1RF2 [201]. Initial configuration of the l_o/GM1 system is illustrated in Fig 5.3.

5.2 Simulation Parameters

Before running the real simulations, energy of each system was minimized using the steepest descent algorithm. All the actual simulations were performed under NpT conditions. The temperatures were controlled with the v-rescale method [202] with separate heat baths for the solute and the solvent. Reference temperatures for all the simulated systems were set at 300 K with time constants of 0.1 ps. For pressure coupling, the Parrinello–Rahman [194] semi-isotropic barostat was used with a time constant of 0.2 ps. The reference pressure was set at 1 bar.

The OPLS all-atom force field [203] was used to parameterize all the molecules and ions. For water, the TIP3P model that is compatible with the OPLS parameterization was employed [204]. A time step of 2 fs was used for integration and all bonds were constrained using the LINCS algorithm [205]. The simulation times for the systems with and without the protein were 500 and 200 ns, respectively. The van der Waals interactions were cut off at 1 nm. For the long range electrostatic interactions, the particle-mesh Ewald (PME) [206] method was used.

6. RESULTS AND DISCUSSION

In this study, the effect of various kinds of lipid bilayers on the binding of cholera toxin was investigated. A total of four MD simulations were performed with similar initial structures and equal simulation times. Additionally, the same systems were simulated without the toxin as a reference. The systems with the toxin were simulated for 500 ns, whereas the systems without the toxin were simulated for 200 ns. This chapter presents the most important findings obtained from the simulations. All the snapshots were prepared using VMD, which is a program used for visualization of biomolecular systems [38]. All the graphs were made using MATLAB® and LaTeX.

6.1 Stability of the Protein

Simulated system requires a certain time to reach the equilibrium. In this study, the equilibration of the protein is studied through the root mean square deviation (RMSD) calculation, which is usually utilised to evaluate the deviation of the simulated structure from the initial configuration over the course of a simulation. In general, the smaller the obtained RMSD value, the smaller the deviation between the final and the initial structure.

In order to calculate the RMSD for the protein, the GROMACS tool `g_rmsd` was employed. The RMSD was calculated for the backbone of the CTB. The RMSDs of the protein backbone for each system are plotted as a function of time in Fig. 6.1. The RMSDs stabilize at about 0.2 Å in all the systems, which confirms the stable structure of the protein. The changes on the order of 0.1 to 0.3 nm in RMSD are acceptable and expected [207]. The result indicates that the secondary structure of the protein is stable and unfolding events are not observed.

In addition to the root mean square deviation, also the root mean square fluctuations (RMSFs) were calculated for the CTB in each system. For that purpose, the GROMACS tool `g_rmsf` was utilised. The results are shown in Fig. 6.1. Some successive residue regions which are moving more than the others can be noticed from the graphs. In general, these groups are the loops in the protein. From the loops in the protein, the residue numbers 1–4, 11–14, 32–36, 50–58, and 89–93 are in the binding site of the protein, and the residue numbers 23–24, 43–46, 79–80, and 103 are in the opposite site of the protein, thus not affecting the binding. Due to the flexibility of the loops, CTB can attach to the plasma membrane (PM) easily, by

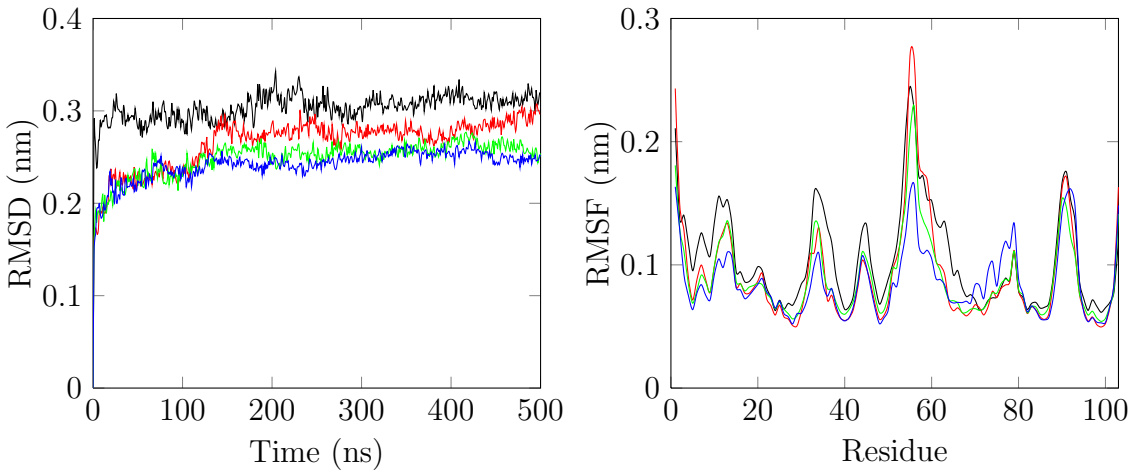

Figure 6.1: On the left, the root mean square displacement (RMSD) profiles of CTB and on the right root the mean square fluctuation (RMSF) profiles of CTB in each system during the 500 ns simulation. The different colours represents CTB in different systems with: ——: l_d/GM1, ——: l_d/GM1-b, ——: l_o/GM1, ——: l_o/GM1-b.

adjusting the positions of the residues to the surface of the membrane.

6.2 Binding of Cholera Toxin

During the 500 ns simulation, cholera toxin bound to all the simulated membranes. Snapshots of the final structures are presented in Fig. 6.2. To present the binding of CTB to the membrane in a more quantitative manner, the distances between the center of mass (COM) of CTB and the COM of the membrane are shown in Fig. 6.3. From all the curves one finds that the binding of CTB takes less than 100 ns. In order to describe the binding process more specifically, further analysis will be shown below.

6.2.1 Hydrogen Bonding

A hydrogen bond is an attractive electrostatic interaction between a polar hydrogen atom (donor) and an electronegative atom (acceptor), such as oxygen or nitrogen. A hydrogen bond may be formed either directly between the donor and the acceptor, or via a water molecule. It is stronger than the van der Waals interaction, but weaker than a covalent bond. In this study, the GROMACS tool `g_hbond` was utilised to calculate the number of hydrogen bonds over the course of the simulations. The GROMACS tool analyzes the hydrogen bonds between all possible donors and acceptors of given groups. A distance criterion of 0.35 nm, and an angle of 30° as a geometric criterion were used as operational definitions for hydrogen bonding.

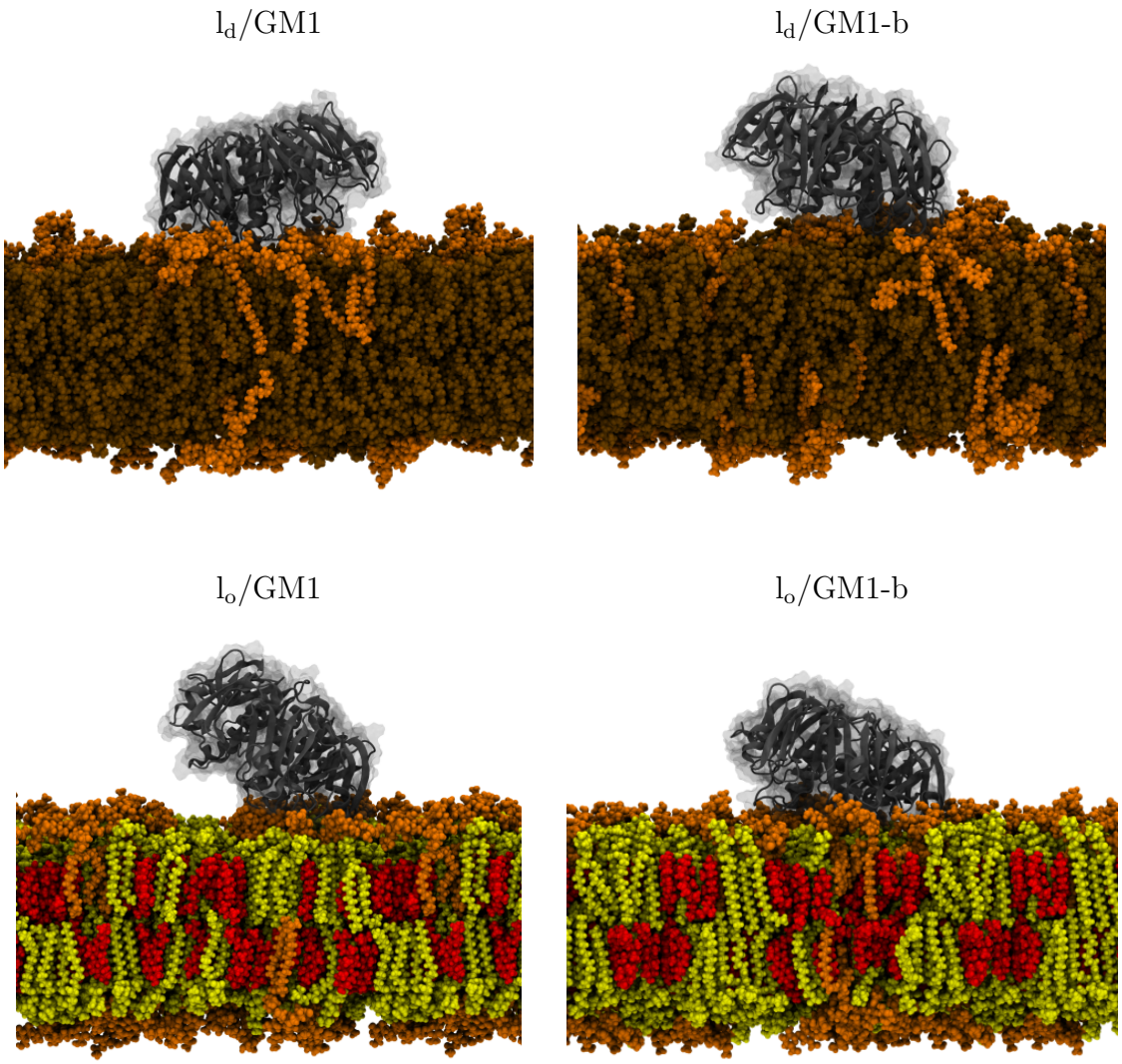

Figure 6.2: Final structures of each system after the 500 ns simulations. On the upper row are the systems with a membrane in the liquid-disordered phase, and on the lower row are the systems with a membrane in the liquid-ordered phase. On the left column are the systems with native GM1, while on the right are the systems with BODIPY-labelled GM1 lipids. In the pictures different molecules are represented as follows: gray; CTB; red; cholesterol; yellow; SSM; orange; GM1 or GM1-b; and brown; DOPC. The pictures are visualized with VMD (Visual Molecular Dynamics) [38] and rendered using the Tachyon ray tracing library [39].

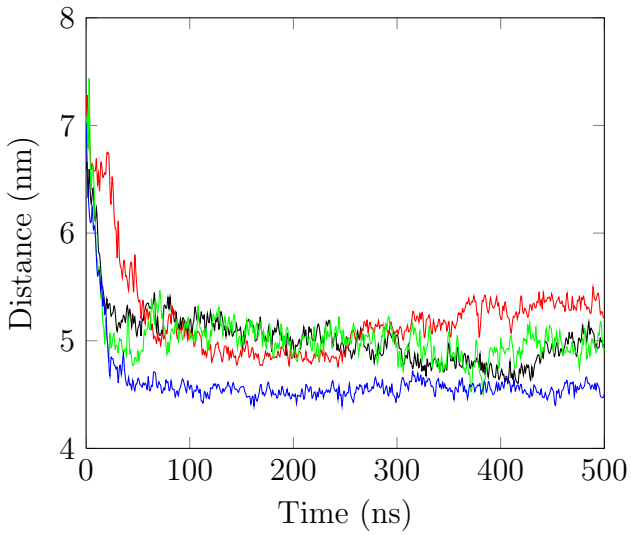

Figure 6.3: The distance in z direction between the COM of CTB and the COM of membrane as a function of time for each system. The different colours represent different systems as: ——: l_d/GM1, ——: l_d/GM1-b, ——: l_o/GM1, ——: l_o/GM1-b.

The number of hydrogen bonds between CTB and GM1/GM1-b as a function of time are depicted in Fig. 6.4. From the data shown, a few issues are worth emphasizing. First, there are hydrogen bonds between the cholera toxin and GM1/GM1-b in all the simulated systems. This supports the idea presented in previous studies (discussed in chapter 2) that the cholera toxin binds to the GM1 ganglioside, while GM1 plays a role of a receptor in the PM and cholera toxin is its ligand. Second, a difference in the number of hydrogen bonds in the different systems can be noticed. However, in addition to fluctuations, also the initial configuration and stochasticity of each system play a major role in this data, as if all the simulations were repeated, the results might be different. For instance, if cholera toxin binds with three different GM1 molecules in the first run, but only with one in the beginning of the second run, the fluctuations in the number of hydrogen bonds are expected to be significant. Furthermore, if the CTB binds only to one GM1 molecule, no matter if it attracts more than one GM1 molecule or not, the simulation time of 500 ns does not allow five GM1 lipids to move to the right places within the membrane as the probability for this process is too low. Also, the binding of the protein may disturb the movement of the lipids by binding on them, which increases the role of the used time scale. In general, although the size of the simulated systems does not allow to simulate them for a longer time, the phenomena described here might require longer time scales. Nevertheless, computational resources used in this study were already state-of-the-art at the current computational facilities.

The average number of hydrogen bonds during the interval of 300–500 ns in each

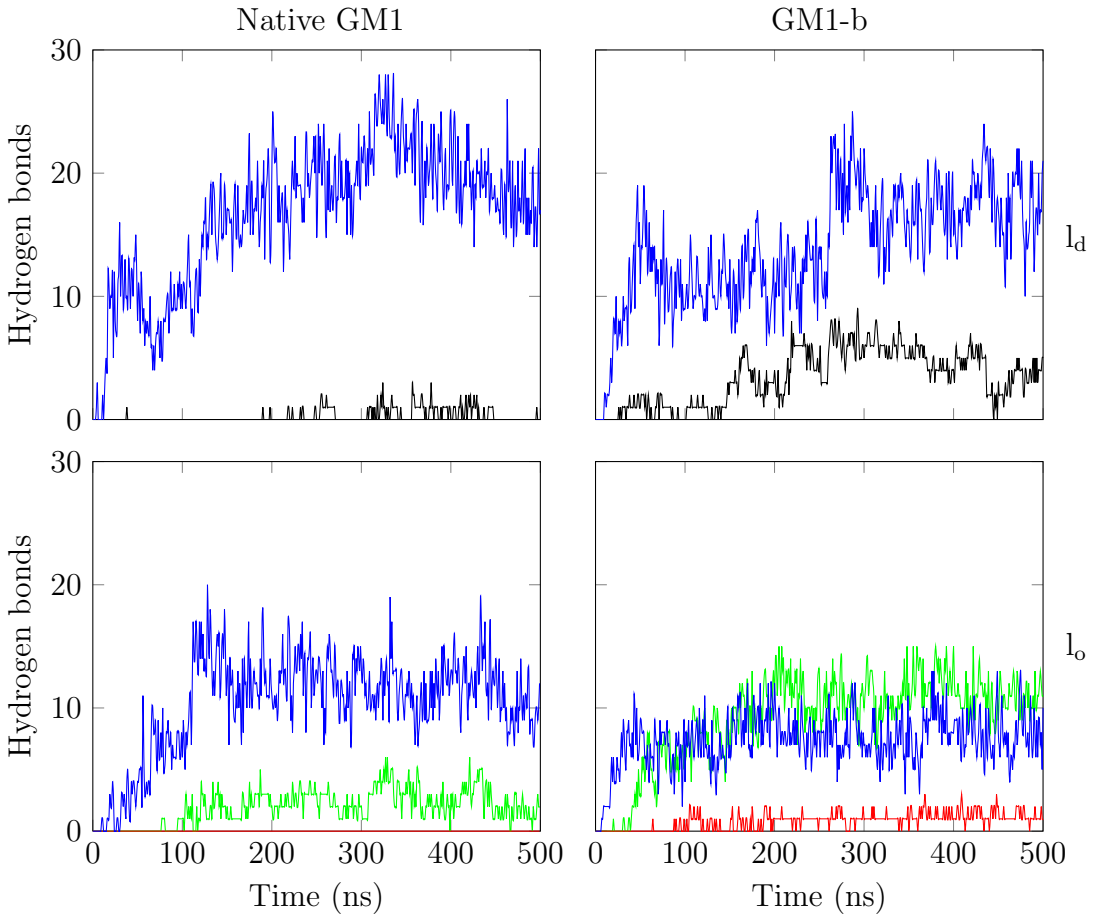

Figure 6.4: Number of hydrogen bonds in each system: Upper left corner (l_d/GM1), upper right (l_d/GM1-b), lower left (l_o/GM1), and lower right (l_o/GM1-b). The different colours represents different lipids with: ——: cholesterol, ——: DOPC, ——: GM1 or GM1-b, depending on the system, and ——: SSM.

Table 6.1: Average number of hydrogen bonds between CTB and different lipids in each system during the interval 300-500 ns.

	l_d	l_o
GM1	20.46 (± 3.35)	11.25 (± 2.09)
GM1-b	17.09 (± 2.64)	7.85 (± 1.97)
DOPC (with GM1)	0.53 (± 0.67)	-
DOPC (with GM1-b)	4.59 (± 1.51)	-
SSM (with GM1)	-	2.59 (± 1.29)
SSM (with GM1-b)	-	11.10 (± 1.78)

system are presented in Table 6.1. The number of hydrogen bonds between CTB and different lipids is the highest in the case of GM1. Because the binding process betweenCTB and GM1 was suggested before in other studies, the hydrogen bonds between GM1 and each residue of the CTB were calculated. As can be seen from Table 6.2, some residues of CTB play a significant role in binding, i.e. Thr1, Glu11, His13, Lys34, Arg35, Ser55, Gln56, Asp59, Lys62, and Lys91. Out of these ten residues, three are Lysine (Lys), one is Histidine (His), and one is Arginine (Arg), which all have positively charged side chains. Otherwise, Glutamic acid (Glu) and Aspartic acid (Asp) residues have negatively charged side chains. The rest of the residues, Thr, Ser, and Gln, have a polar uncharged side chain. By looking at the results, there are no amino acid residues which contain a hydrophobic side chain. Furthermore, the electrostatic potential of the membrane may play a major role in the binding process. Comparing to the residues suggested by Merrit *et al.* [144], any hydrogen bonds between Glu51, Gln56, Gln61, and Asn90 residues and CTB were not observed. Moreover, in addition to the residues mentioned by Merrit *et al.*, hydrogen bonds between GM1 and many other CTB residues presented in Table 6.2 were found.

6.3 Geometry of GM1

In order to describe the geometry of GM1 and GM1-b molecules, three vectors within the head group of GM1 were chosen and the angles between the vectors and the membrane normal were calculated. The chosen vectors are referred to as forefinger, thumb, and neck, and they are illustrated in Fig. 6.5 together with the reference vector — the normal of the membrane. A more specific picture of the vectors within the head group of GM1 is shown in Fig. 6.6.

There are only a few GM1 molecules which are bound to the toxin in all the systems in total, and the time scale is rather short. Due to poor statistics, it is not possible to give well-defined orientations for the different components in the head group of GM1 while the toxin is bound to the membrane. Instead of studying only a

Table 6.2: Average number of hydrogen bonds between the GM1 or GM1-b and each residue of the CTB in different systems during the 300–500 ns interval.

	l_d/GM1	l_o/GM1	l_d/GM1-b	l_o/GM1-b
Thr1	1.342 ± 0.496	3.743 ± 1.173	0.653 ± 0.487	0.010 ± 0.099
Asp7	-	-	0.020 ± 0.140	-
Ala10	-	-	0.005 ± 0.070	-
Glu11	0.114 ± 0.318	0.955 ± 0.576	0.500 ± 0.888	0.089 ± 0.286
Tyr12	-	0.059 ± 0.237	0.064 ± 0.246	-
His13	0.074 ± 0.298	0.020 ± 0.140	0.772 ± 0.738	0.213 ± 0.434
Asn14	0.010 ± 0.099	0.015 ± 0.157	0.193 ± 0.432	0.634 ± 0.680
Gln16	-	0.158 ± 0.417	0.050 ± 0.218	-
Ile17	-	0.035 ± 0.183	-	-
His18	-	0.010 ± 0.099	-	-
Thr19	-	0.005 ± 0.070	-	-
Gly33	0.015 ± 0.121	-	0.208 ± 0.407	-
Lys34	5.480 ± 1.309	2.654 ± 0.992	1.183 ± 0.583	0.965 ± 0.687
Arg35	6.817 ± 0.893	2.055 ± 0.286	2.168 ± 0.388	0.005 ± 0.070
Glu51	-	-	1.698 ± 0.979	-
Pro53	0.025 ± 0.156	-	-	0.005 ± 0.070
Gly54	0.059 ± 0.237	-	-	-
Ser55	0.985 ± 1.005	0.416 ± 0.523	0.371 ± 0.578	0.728 ± 0.952
Gln56	0.347 ± 0.606	0.718 ± 0.627	0.708 ± 0.719	0.163 ± 0.444
His57	1.084 ± 0.784	0.010 ± 0.099	0.337 ± 0.504	-
Ile58	-	0.015 ± 0.121	0.173 ± 0.379	-
Asp59	0.837 ± 0.891	0.134 ± 0.355	1.183 ± 0.632	1.619 ± 0.919
Ser60	0.020 ± 0.140	0.015 ± 0.157	-	-
Gln61	-	0.015 ± 0.121	0.035 ± 0.183	-
Lys62	2.936 ± 0.847	0.015 ± 0.121	0.535 ± 0.799	1.579 ± 0.730
Lys63	-	-	0.619 ± 0.778	1.787 ± 0.810
Trp88	-	-	0.005 ± 0.070	-
Asn89	-	0.070 ± 0.273	0.015 ± 0.121	-
Asn90	-	0.139 ± 0.361	1.708 ± 0.697	-
Lys91	0.252 ± 0.447	0.035 ± 0.183	1.980 ± 0.919	0.030 ± 0.170
Thr92	-	0.074 ± 0.281	0.138 ± 0.387	-
His94	-	0.005 ± 0.070	-	-

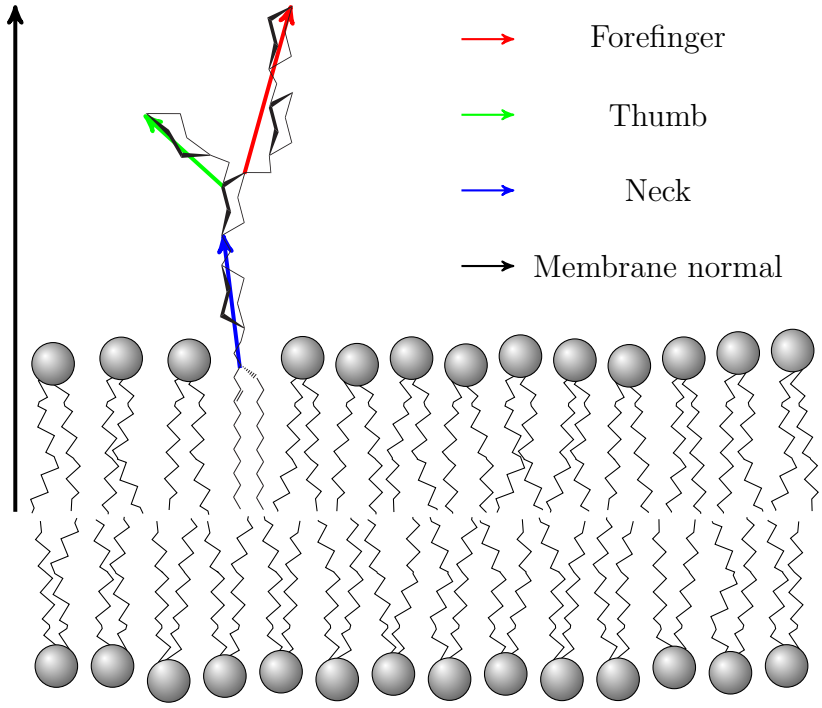

Figure 6.5: An illustrative figure of the chosen vectors from the head group of GM1 and the reference vector — normal of the membrane. The different colours represents different vectors and names as: ——: forefinger, ——: thumb, ——: neck, and ——: membrane normal.

Table 6.3: Average angle during the 500 ns simulation.

Vector	System	Average angle (°)
Forefinger	l_d/GM1	82.1
Forefinger	l_d/GM1-b	85.4
Forefinger	l_o/GM1	83.3
Forefinger	l_o/GM1-b	84.7
Thumb	l_d/GM1	70.6
Thumb	l_d/GM1-b	65.0
Thumb	l_o/GM1	69.5
Thumb	l_o/GM1-b	63.6

few lipids, the data of all the GM1 gangliosides in both leaflets and in both systems (normal and reference) were used to calculate the orientation of the head groups of GM1 and GM1-b. The angles between the normal of the membrane and the different vectors were calculated separately for both leaflets so that the reference vector was the membrane normal facing towards the water phase.

The results calculated for the systems with BODIPY-labelled GM1 are shown in Fig. 6.6. In the histograms, more peaks can be seen in the system with the l_o bilayer compared to the bilayer in the l_d phase. This makes sense due to the freedom of movement of lipids in the l_d phase which allows more flexibility to the orientation of lipids and their head groups. On the contrary, in the l_o phase the structure of the lipids is more rigid which constraints the movement of molecules, and this may also disturb the binding of CTB to GM1. This may decrease the probability of interaction between the receptor and its ligand due to a favorable conformation of GM1 for the toxin binding.

The angle distribution as a function of time for the forefinger and the thumb vectors in the systems with the protein are shown in Fig. 6.7. The averages of the angles after 300 ns of simulation in each system are shown in Table 6.3. A slight increase in the angle between the normal of the membrane and the forefinger vector is observed when native GM1 is replaced with GM1-b. However, this change is not significant enough to make strict conclusions. Instead, the change in the angle between the normal of the membrane and the thumb vector is more significant when the native GM1 is replaced with the BODIPY-labelled GM1. The decrease of this angle means that the thumb bends towards the water phase when the BODIPY probe is attached to GM1. Due to this bending of the thumb, the binding of cholera toxin may be distracted due to the change in geometry of the head group of GM1.

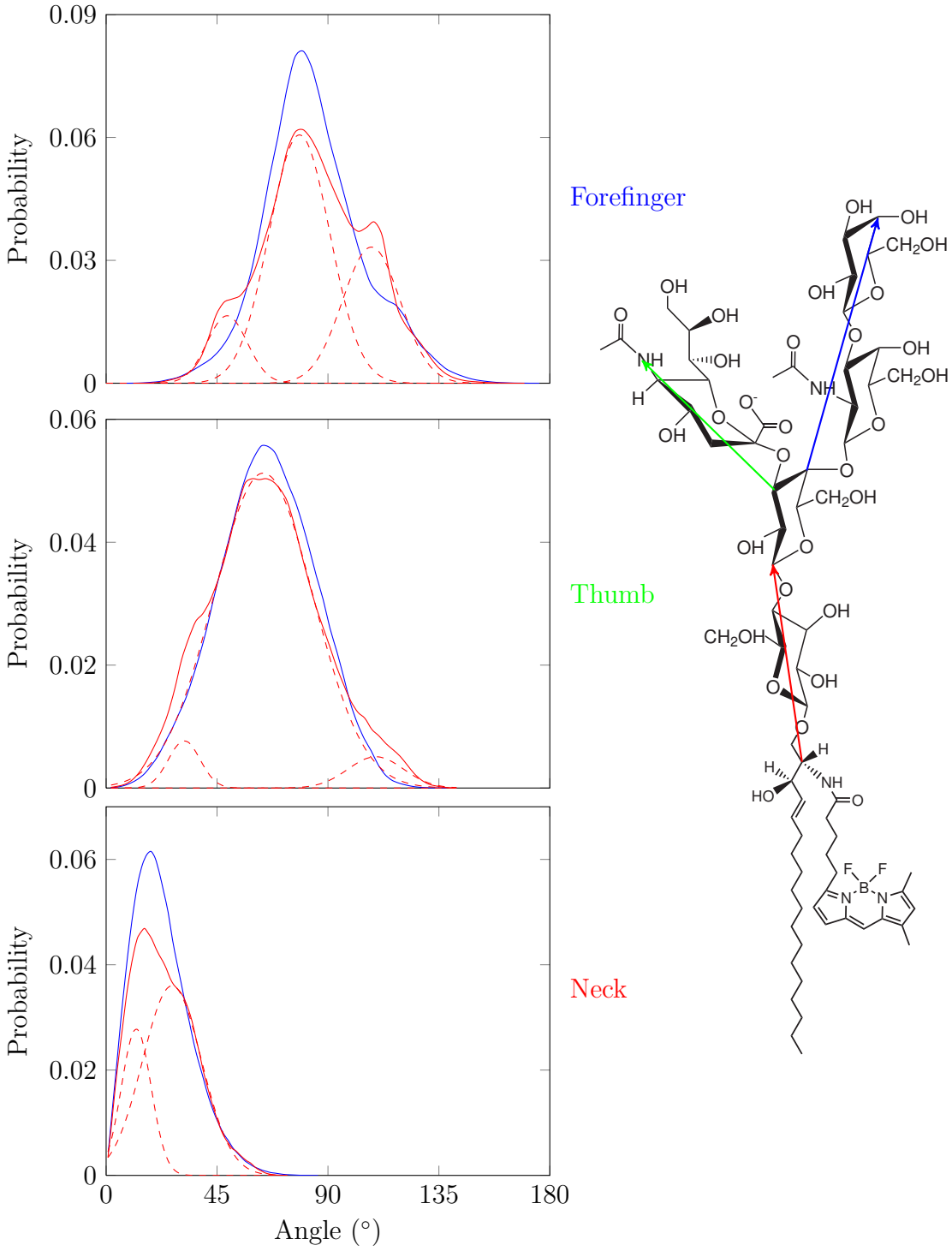

Figure 6.6: On the left, angle distributions for the angle between the membrane normal and the different vectors chosen from the GM1-b head group. The chosen vectors can be seen on the right. The different colours in the graphs represent different systems as: ——: the system with the membrane in the l_o phase, ——: the system with the membrane in the l_d phase. For all the angle distributions in the l_o phase, three Gaussian fits are shown for the forefinger and the thumb, and two fits for the neck.

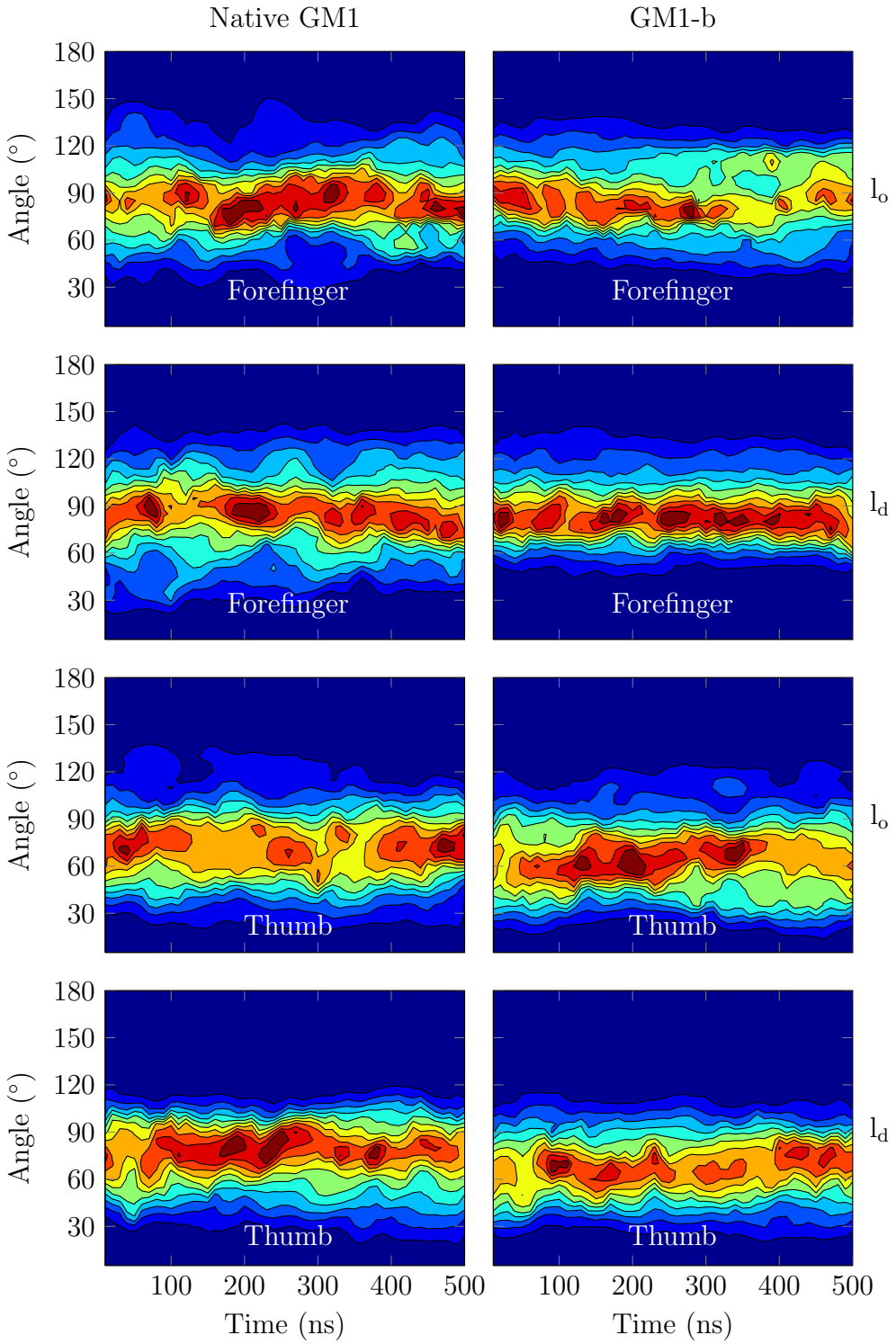

Figure 6.7: Angle distributions plotted as a function of time. On the left column, shown are the systems with native GM1, and on the right, are the data for BODIPY-labelled GM1 systems. The first and the third row show results for the l_o systems, while the rest describe the results for the l_d systems. Angles are described in more detail in the text.

6.4 Membrane Properties

In order to investigate the binding of cholera toxin to different lipid bilayer compositions, it is important to understand the properties of these bilayers. Lots of different quantities were calculated during this study. However, only the most relevant results are presented in this thesis.

6.4.1 Order Parameter

The order parameter is a commonly used quantity to describe the order-disorder transition of alloys or other materials [208]. Furthermore, it can be used to describe the long-range order in structural or thermodynamic properties. Thus, the order parameter is more used to get information about long carbon chains in a biological environment, such as lipid tails.

In this study, the order parameter was calculated for one chain of SSM, DOPC, GM1, and GM1-b lipids by using the GROMACS tool `g_order`. In general, the order parameter can vary between 1 and $-1/2$. One means full order along the interface normal, $-1/2$ the full order perpendicular to the normal, and zero corresbonds to an isotropic (random) orientation.

The deuterium order parameter (S_{cd}) [209] was calculated for both the native GM1 and GM1-b. The results are shown in Fig. 6.8. As can be seen, S_{cd} of GM1 and GM1-b is higher in the membrane consisting of cholesterol and SSM compared to the membrane consisting of DOPC, which means that the tails are more ordered in the lipid bilayer comprised of cholesterol and SSM. By comparing native GM1 and GM1-b with each other, the BODIPY probe decreases the order of the tail. As can be seen from Fig. 6.9, the BODIPY fluorophore does not only make the GM1 tail more disordered but also induces order in the tails of the surrounding lipids.

6.4.2 Area per Lipid

In order to get more understanding of the geometry of lipids discussed in section 6.3, the area per lipid is a relevant quantity to be investigated. In this study, the area per lipid was calculated for each system in a very simple manner. First, the area of the system in the xy-plane (membrane plane) was calculated at every time step by using the GROMACS tool `g_traj`. Secondly, the area was divided by half the number of lipids, which is 240 in our systems. Results of the calculation are given in Table 6.4.

In section 6.3 it was noticed that in the l_o phase the head group of GM1 is more constrained when compared to the l_d phase. Area per lipid calculations can explain this because the area per lipid is much smaller in the l_o phase than in the l_d phase, as there is less space for the head group of GM1 to move in the liquid-ordered phase. Although the lipid packing is more dense within the membrane in the l_o phase,

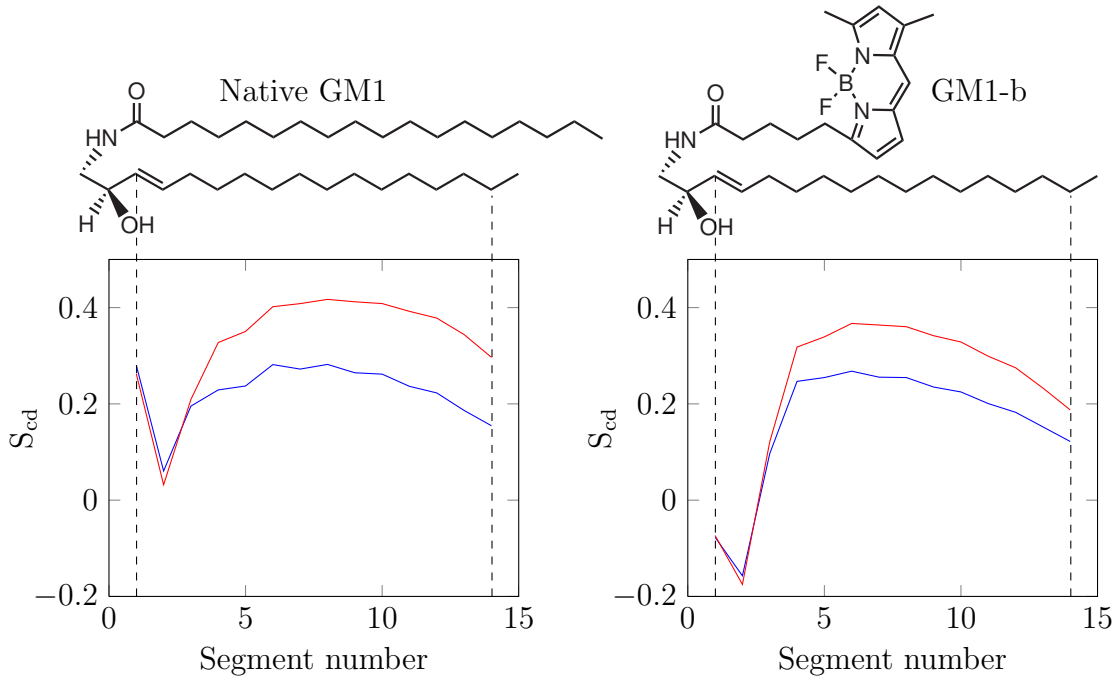

Figure 6.8: On the left is given the deuterium order parameter (S_{cd}) for the tail of GM1, and on the right is shown the S_{cd} for GM1-b. The same tail of GM1 and GM1-b was used in calculations to ease the comparison. Different colours represent different lipid phases as: ——: l_o, ——: l_d

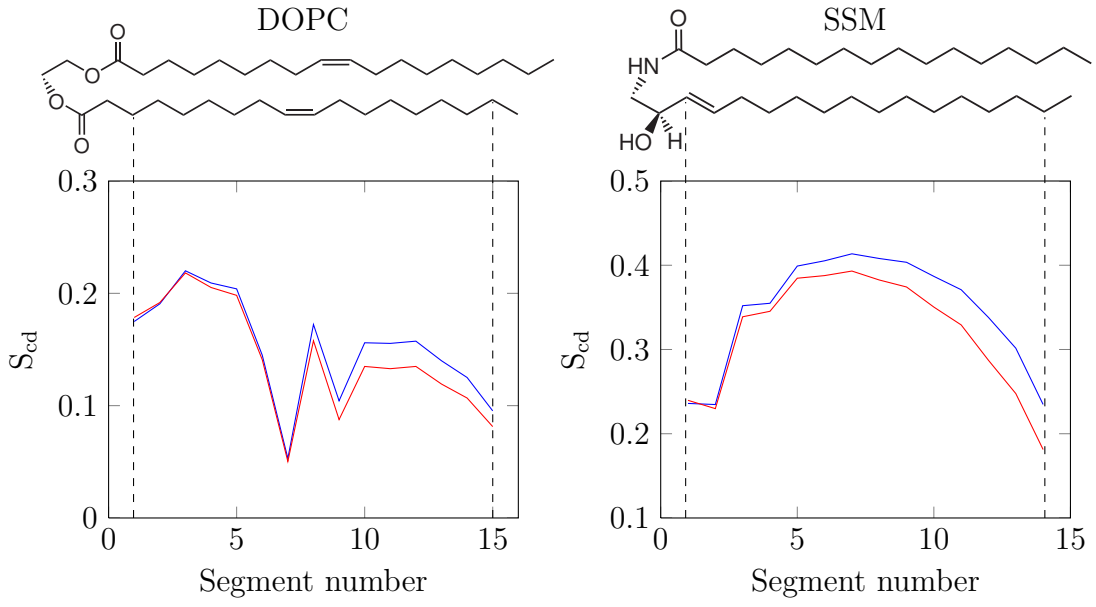

Figure 6.9: On the left is given the deuterium order parameter for the tail of DOPC, and on the right is shown the S_{cd} for the tail of SSM. Different colours represent the systems with different modifications of GM1 as: ——: native GM1, and ——: GM1-b.

cholesterol molecules have a very small head group, which gives more space for the other lipids in the head group area to move.

Table 6.4: Area per lipid during the 300–500 ns interval in each system.

Simulated system	Area per lipid (nm^2)
Ld/GM1	0.621 ± 0.005
Ld/GM1-b	0.626 ± 0.007
Lo/GM1	0.424 ± 0.002
Lo/GM1-b	0.436 ± 0.002

6.4.3 Density Profiles

In addition to the order parameter and the area per lipid, the thickness of the membrane is also a commonly used quantity to analyse membrane properties. For this purpose, the GROMACS tool `g_density` was used. The density profiles were calculated for the phosphate group in the headgroup of either DOPC or SSM in the l_d and l_o phases, respectively, and for the two residues in the head group of GM1: the galactose group in the tip of the forefinger and the other galactose group. In the calculations, the number of bins was selected to be 50.

As can be seen from Fig. 6.10, the addition of the BODIPY fluorophore into the tail of GM1 causes thinning of the membrane. This partly goes hand in hand with the order parameter: if the order of the tail is higher, the tail is more ordered and therefore the thickness of the membrane increases. Because BODIPY makes the tails more disordered, the effect on membrane thickness is also more significant in the l_o phase.

6.4.4 Electrostatic Potential of the Membranes

In addition to the density profiles of the lipids, the distribution of ions in water was calculated. A remarkable difference in the head group region of bilayers can be noticed when the l_d and l_o phases are compared with each other. By looking at the graphs, sodium ions are located deeper within the membrane in the liquid-ordered phase. If we take into account the fact that the membrane is also thicker in the liquid-ordered phase, this highlights the difference even more in this sense. In the case of the liquid-ordered phase, two different peaks of sodium ions can be seen at around 2.2 nm and 3.5 nm from the bilayer center. These peaks show that the membranes attract the sodium ions. In contrast, in the liquid-disordered phase the ions are more likely in the water phase and they are not so attracted by the membrane.

To get a better understanding of the effect of ions, the electrostatic potential

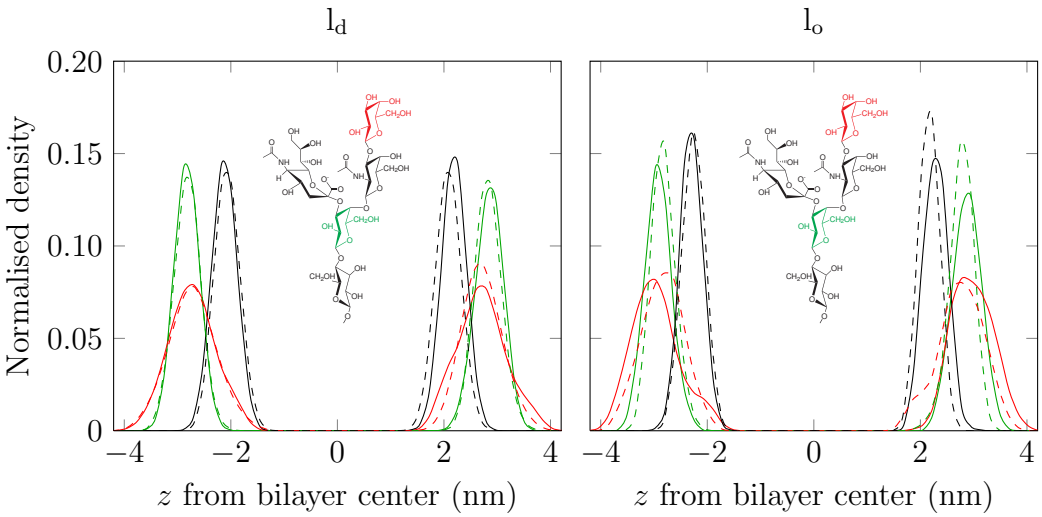

Figure 6.10: Left: normalised density profiles of two galactose residues of GM1 head group and a phosphate group of DOPC lipid in the l_d phase. Right: the same galactose groups from the GM1 head group and a phosphate group from SSM are shown for the systems in the l_o phase. The galactose group in the tip of the forefinger is coloured as —— and the other galactose group as ——. Phosphate groups are coloured as ——. The head groups of GM1 and GM1-b are shown in both pictures with the colors corresponding to the density profiles of GM1 and GM1-b.

was calculated with the GROMACS tool `g_potential` along the membrane normal. As can be seen from Fig. 6.11, the potential is rather different in the head group area when comparing the systems with different lipid packing. As was in the case of density of sodium ions, two different peaks can also be seen in the electrostatic potential of the liquid-ordered phase. Most of the CTB residues which were noticed to form hydrogen bonds with GM1 molecules have positively charged side chains. By following the Coulomb interaction, the positively charged amino acid has a repulsive interaction with the surface of the membrane if there are lots of positively charged sodium ions. Therefore, these changes can have a large effect on the accessibility of CT to the GM1 head group.

6.5 Liquid-disordered and Liquid-ordered Phases

This thesis does not include any experimental data although this is an ongoing project done in collaboration with an experimental group. They have observed that the lipid packing changes continuously instead of changing rapidly, for example from the liquid-disordered phase to the liquid-ordered phase (unpublished data). Moreover, it was previously noticed that the CTB binds more likely into the lipid bilayer in the liquid-disordered phase [210]. One of our challenges was to unravel the question of why the binding is different when the lipid packing changes.

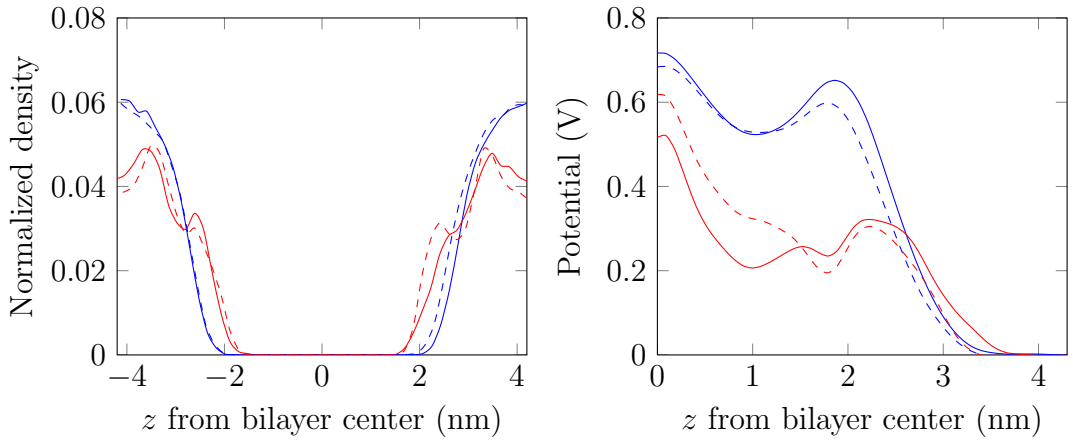

Figure 6.11: Left, density profiles for sodium ions in each system. Right, the electrostatic potential of each membrane. Different colours represent different membrane as: ——: l_d with GM1, ——: l_o with GM1, - - -: l_d with GM1-b and - - -: l_o with GM1-b.

By following the results presented in this chapter, we can present a few explanations for the differences in binding. First, we noticed that our model membranes follow the basic idea of liquid-disordered and liquid-ordered phases: the membrane consisting of DOPC was noticed to be much more disordered than the membrane consisting of a 1:1 mixture of cholesterol and SSM. The membrane thickness was also noticed to change. Secondly, the GM1 lipids in the liquid-ordered phase were noticed to have more restricted structures, which may affect binding: if the geometry of the GM1 head group is favorable for the binding in one of the most probable positions (see Fig. 6.6), then the binding may occur. On the contrary, if the needed orientation for the binding is not one of the noticed orientations, then the probability for the binding decreases. Finally, the membrane in the liquid-ordered phase was noticed to attract more sodium ions into the head group area comparing to the membrane in liquid-disordered phase, even though the head groups of lipids were the same (PC) in all the membranes. Due to the difference in the amount of ions, the electrostatic potential of the membrane was noticed to change dramatically. If we take into account that most of the residues in CTB, which form hydrogen bonds with GM1 molecules, involve positively charged side chains, the long-range interaction between these residues and the surface of the membrane is not as attractive as in the case of the liquid-disordered phase, where the sodium ions are more likely in the water phase.

6.6 Effect of BODIPY Fluorophore

The same experimental team has used not only the native GM1 molecules, but also the BODIPY labelled GM1 molecules in their studies [210]. In order to understand the different behaviour of the native and the modified GM1 molecule, it was relevant to understand how the fluorescent probe affects the membrane properties, and thus the binding of cholera toxin.

As mentioned previously, the BODIPY label was noticed to change the properties of the membrane into the liquid-disordered phase: the order of the lipid tails was noticed to decrease, and therefore the membrane thickness was noticed to be smaller. Although the binding of CT was speculated to be more favorable into the liquid-disordered membrane, the affinity of the binding of CT was not noticed to be better for the GM1-b lipids, although they disorder the membrane.

When changing from l_d to l_o, the average of the calculated angles were noticed to remain approximately the same. Instead, when GM1 was labelled, its thumb was observed to change its orientation. As the binding was proposed to mimic GM1 taking a grip of CTB by pinching it, the change in the orientation of one of the fingers may play a major role in the binding. The electrostatic potential of the membrane was found to remain approximately the same when GM1 was labelled. Thus, it most likely does not affect the binding via changing electrostatic potential of the membrane. Therefore, labelling of GM1 with the BODIPY probe influences strictly the geometrical properties of the GM1 head group and thus affects the specific receptor–ligand fit.

7. CONCLUSIONS

The aim of this Thesis was to use atomistic molecular dynamics simulations to study how modifications in lipid composition of a protein-free membrane affect the binding of cholera toxin with a membrane. The idea for this study originate from experimental studies, which have shown that lipid packing varies continuously instead of being characterized by sharp borders between different phases [211]. Furthermore, by using fluorescence spectroscopy for synthetic Giant Unilamellar Vesicles (GUVs) and cell-derived Giant Plasma Membrane Vesicles (GPMVs) it has been shown that cholera toxin binds intensively into the l_d parts of the vesicles and with a lower affinity to a membrane in the l_o phase [210]. The first goal was to explain why the binding differs when the lipid packing of the membrane is changed.

Two systems were simulated for this purpose: GM1-b in the l_d phase consisting of DOPC, and GM1-b in the l_o phase, consisting of cholesterol and SSM. The results showed that the orientation of the head group of GM1-b changes depending on the lipid environment around the lipid. In the liquid-ordered phase the head group of GM1-b was noticed to have a more rigid structure, which constraints the movements of the head group compared to the same lipids in the l_d phase. The area per lipid calculations showed clearly that there is more space for the head groups to move in the l_d phase, which confirms the result of different orientations of the head group. In addition to geometrical properties of GM1-b, the electrostatic potential of the membrane was observed to change significantly. The membrane in the l_o phase was shown to attract sodium ions, not only deeper into the membrane, but also in the head group region while the head groups of the lipids were the same in both phases. Due to the different distribution of sodium ions in the head group region, the profiles of the electrostatic potential across the membrane differed in the l_d and l_o phases. Based on the calculations of hydrogen bonds between GM1 and all the residues of cholera toxin, the amino acids with positively charged side chains were found to play a major role in the binding process. Due to a change in the electrostatic properties of the membrane, the binding of cholera toxin was found to be the liquid-ordered phase.

Additionally, it has been shown experimentally that there is also a difference in the toxin binding depending on the structure of GM1 [210]. The experiments used not only the BODIPY-labelled GM1, which can be detected by using fluorescence

spectroscopy, but also the native GM1. To elucidate this point, two additional lipid bilayers were created by modifying the two existing lipid bilayers described before in a way that all the GM1-b molecules were transformed into the native GM1. As a result, the thumb moiety of the head group of GM1 bent towards the bulk water while the GM1 was labelled with the BODIPY fluorophore. Due to the fact that CTB is a pentameric protein, a geometrical fit is essential for its interactions with GM1. It seems evident that as the orientation of the head group of GM1 is changed, the specific receptor–ligand fit is interfered, and thus the affinity of CTB towards the GM1-b is not as favored as towards the native GM1.

Further studies could be focused on getting more details of the interactions between cholera toxin and various membranes. So far, only one system for each case has been simulated. To be sure that the most important residues of the CTB in the binding process were correctly identified, and to be certain about the most attractive lipids to the CTB, replicas of these systems are needed. Furthermore, it could be unambiguous to show free energy profiles for the binding process in each simulated system, for example by using the umbrella sampling method [212]. However, this approach has some problems in this case. First of all, the initial structure for proper binding is needed which may require much longer simulation times than those used in this study. Secondly, the umbrella sampling windows itself are heavy to calculate for systems of this size — if it could be done for one system, they would still have to be repeated for four different systems to compare the binding into different lipid bilayers. A more realistic approach to compare free energy profiles of the toxin binding to different lipid bilayers would be to calculate the free energy profile for just one amino acid at a time. This approach is also a bit problematic though. First, the important amino acids should be known, and secondly, the simulation of just one amino acid is not trivial.

Although some features related to the binding remain unknown, a few striking discoveries were made based on the MD simulations. In particular, appropriate reasons to the observed differences in toxin binding to various lipid bilayers have been found.

BIBLIOGRAPHY

[1] **Mutreja, A., Kim, D., Thomson, N., Connor, T., Lee, J., Kariuki, S., Croucher, N., Choi, S., Harris, S., Lebens, M., et al.**, Evidence for several waves of global transmission in the seventh cholera pandemic. *Nature*, 477(7365): 462–465. 2011.

[2] **Zuckerman, J.N., Rombo, L., and Fisch, A.**, The true burden and risk of cholera: implications for prevention and control. *Lancet*, 7(8): 521–530. 2007.

[3] **Holmgren, J., Lönnroth, I., and Svennerholm, L.**, Tissue receptor for cholera exotoxin: postulated structure from studies with GM1 ganglioside and related glycolipids. *Infection and Immunity*, 8(2): 208–214. 1973.

[4] **Spangler, B.**, Structure and function of cholera toxin and the related Escherichia coli heat-labile enterotoxin. *Microbiological Reviews*, 56(4): 622–647. 1992.

[5] **Janes, P., Ley, S., and Magee, A.**, Aggregation of lipid rafts accompanies signaling via the T cell antigen receptor. *Journal of Cell Biology*, 147(2): 447–461. 1999.

[6] **Harder, T., Scheiffele, P., Verkade, P., and Simons, K.**, Lipid domain structure of the plasma membrane revealed by patching of membrane components. *Journal of Cell Biology*, 141(4): 929–942. 1998.

[7] **Karolin, J., Johansson, L.B.A., Strandberg, L., and Ny, T.**, Fluorescence and absorption spectroscopic properties of dipyrrometheneboron difluoride (BODIPY) derivatives in liquids, lipid membranes, and proteins. *Journal of the American Chemical Society*, 116(17): 7801–7806. 1994.

[8] **Ramamurthy, T. and Bhattacharya, S.**, *Epidemiological and Molecular Aspects on Cholera*. Infectious Disease, Springer. 2010.

[9] **Aktories, K.**, *Bacterial Toxins*. Laboratory companion, John Wiley & Sons. 2008.

[10] **Chaudhuri, K. and Chatterjee, S.**, *Cholera Toxins*. SpringerLink: Springer e-Books, Springer. 2009.

[11] **Wernick, N., Chinnapen, D., Cho, J., and Lencer, W.**, Cholera toxin: an intracellular journey into the cytosol by way of the endoplasmic reticulum. *Toxins*, 2(3): 310–325. 2010.

[12] **Burrows, W.**, Cholera toxins. *Annual Reviews in Microbiology*, 22(1): 245–268. 1968.

[13] **Macpherson, J.**, *Annals of cholera: from the earliest periods to the year 1817*. HK Lewis. 1884.

[14] **Howard-Jones, N.**, Cholera nomenclature and nosology: a historical note. *Bulletin of the World Health Organization*, 51(3): 317. 1974.

[15] **Wong, K., Wu, L., et al.**, History of Chinese Medicine. Being a Chronicle of Medical Happenings in China from Ancient Times to the Present Period. *History of Chinese Medicine. Being a Chronicle of Medical Happenings in China from Ancient Times to the Present Period.* 1932.

[16] **Barua, D. and Greenough, W.**, *Cholera*. Current Topics in Infectious Disease, Springer. 1992.

[17] **Chin, C.S., Sorenson, J., Harris, J.B., Robins, W.P., Charles, R.C., Jean-Charles, R.R., Bullard, J., Webster, D.R., Kasarskis, A., Peluso, P., et al.**, The origin of the Haitian cholera outbreak strain. *New England Journal of Medicine*, 364(1): 33–42. 2011.

[18] **Koch, R.**, An address on cholera and its bacillus. *British Medical Journal*, 2(1235): 403–407. 1884.

[19] **Cash, R., Forrest, J., Nalin, D., and Abrutyn, E.**, Rapid correction of acidosis and dehydration of cholera with oral electrolyte and glucose solution. *Lancet*, 296(7672): 549–550. 1970.

[20] **Sack, R., Cassells, J., Mitra, R., Merritt, C., Butler, T., Thomas, J., Jacobs, B., Chaudhuri, A., and Mondal, A.**, The use of oral replacement solutions in the treatment of cholera and other severe diarrhoeal disorders. *Bulletin of the World Health Organization*, 43(3): 351. 1970.

[21] **J. B. Kaper, J.G.M.J. and Levine, M.M.**, Cholera. *Clinical Microbiology Reviews*, 8(1): 48–86. 1995.

[22] **Ryan, K., Ray, C., Ahmad, N., Drew, W., and Plorde, J.**, *Sherris Medical Microbiology, Fifth Edition*. McGraw-Hill Companies, Incorporated. 2010.

[23] **Graphics, E.**, ScienceArt - Image: Cholera Bacterium showing Nucleoid. [WWW]. Referred on January 1st. 2013. Available at `http://www.scienceart.co.uk/page.php?p=image&img=4494306873&gid=All%20Images`. Accessed on December 20th, 2012.

[24] **Kaper, J., Bradford, H., Roberts, N., and Falkow, S.**, Molecular epidemiology of Vibrio cholerae in the US Gulf Coast. *Journal of Clinical Microbiology*, 16(1): 129–134. 1982.

[25] **Kaper, J., Nataro, J., Roberts, N., Siebeling, R., and Bradford, H.**, Molecular epidemiology of non-O1 Vibrio cholerae and Vibrio mimicus in the US Gulf Coast region. *Journal of Clinical Microbiology*, 23(3): 652–654. 1986.

[26] **Koblavi, S., Grimont, F., and Grimont, P.**, Clonal diversity of *Vibrio cholerae* 01 evidenced by rRNA gene restriction patterns. *Research in Microbiology*, 141(6): 645–657. 1990.

[27] **Minami, A., Hashimoto, S., Abe, H., Arita, M., Taniguchi, T., Honda, T., Miwatani, T., and Nishibuchi, M.**, Cholera enterotoxin production in Vibrio cholerae O1 strains isolated from the environment and from humans in Japan. *Applied and Environmental Microbiology*, 57(8): 2152–2157. 1991.

[28] **Selander, R., Caugant, D., Ochman, H., Musser, J., Gilmour, M., and Whittam, T.**, Methods of multilocus enzyme electrophoresis for bacterial population genetics and systematics. *Applied and Environmental Microbiology*, 51(5): 873. 1986.

[29] **Chatterjee, S. and Chaudhuri, K.**, Lipopolysaccharides of Vibrio cholerae: I. Physical and chemical characterization. *Biochimica et Biophysica Acta (BBA)-Molecular Basis of Disease*, 1639(2): 65–79. 2003.

[30] **Yoon, S. and Mekalanos, J.**, Decreased potency of the Vibrio cholerae sheathed flagellum to trigger host innate immunity. *Infection and Immunity*, 76(3): 1282–1288. 2008.

[31] **Lubran, M.**, Bacterial toxins. *Annals of Clinical & Laboratory Science*, 18(1): 58–71. 1988.

[32] **Schaechter, M.**, *Desk Encyclopedia of Microbiology*. Academic Press, Elsevier Science. 2009.

[33] **De, S.**, Enterotoxicity of bacteria-free culture-filtrate of Vibrio cholerae. *Nature*, 183: 1533–1534. 1959.

[34] **Dutta, N., Panse, M., and Kulkarni, D.**, Role of cholera toxin in experimental cholera. *Journal of Bacteriology*, 78(4): 594. 1959.

[35] **Falnes, P. and Sandvig, K.**, Penetration of protein toxins into cells. *Current Opinion in Cell Biology*, 12(4): 407–413. 2000.

[36] **Finkelstein, R. and LoSpalluto, J.**, Pathogenesis of experimental Cholera Preparation and isolation of Choleragen and Choleragenoid. *Journal of Experimental Medicine*, 130(1): 185–202. 1969.

[37] **Finkelstein, R. and LoSpalluto, J.**, Production of highly purified choleragen and choleragenoid. *Journal of Infectious Diseases*, pp. 63–72. 1970.

[38] **Humphrey, W., Dalke, A., Schulten, K., et al.**, VMD: visual molecular dynamics. *Journal of Molecular Graphics*, 14(1): 33–38. 1996.

[39] **Stone, J.**, *An efficient library for parallel ray tracing and animation*. Master's thesis, University of Missouri, Rolla. 1998.

[40] **Berman, H.M., Westbrook, J., Feng, Z., Gilliland, G., Bhat, T.N., Weissig, H., Shindyalov, I.N., and Bourne, P.E.**, The Protein Data Bank. *Nucleic Acids Research*, 28: 235–242. 2000.

[41] **Zhang, R., Scott, D., Westbrook, M., Nance, S., Spangler, B., Shipley, G., Westbrook, E., et al.**, The three-dimensional crystal structure of cholera toxin. *Journal of Molecular Biology*, 251(4): 563. 1995.

[42] **Lencer, W. and Saslowsky, D.**, Raft trafficking of AB_5 subunit bacterial toxins. *Biochimica et Biophysica Acta (BBA)-Molecular Cell Research*, 1746(3): 314–321. 2005.

[43] **Gill, D.**, The arrangement of subunits in chlorea toxin. *Biochemistry*, 15(6): 1242–1248. 1976.

[44] **van Heyningen, S.**, The subunits of cholera toxin: structure, stoichiometry, and function. *Journal of Infectious Diseases*, 133(Supplement 1): S5–S13. 1976.

[45] **Kunkel, S. and Robertson, D.**, Factors affecting release of heat-labile enterotoxin by enterotoxigenic Escherichia coli. *Infection and Immunity*, 23(3): 652–659. 1979.

[46] **Kunkel, S. and Robertson, D.**, Purification and chemical characterization of the heat-labile enterotoxin produced by enterotoxigenic Escherichia coli. *Infection and Immunity*, 25(2): 586–596. 1979.

[47] **Gill, D., Clements, J., Robertson, D., and Finkelstein, R.**, Subunit number and arrangement in Escherichia coli heat-labile enterotoxin. *Infection and Immunity*, 33(3): 677–682. 1981.

[48] **Spangler, B. and Westbrook, E.**, Crystallization of isoelectrically homogeneous cholera toxin. *Biochemistry*, 28(3): 1333–1340. 1989.

[49] **Zhang, R., Westbrook, M., Westbrook, E., Scott, D., Otwinowski, Z., Maulik, P., Reed, R., and Shipley, G.**, The 2.4 Å crystal structure of cholera toxin B subunit pentamer: choleragenoid. *Journal of Molecular Biology*, 251(4): 550–562. 1995.

[50] **Lesieur, C., Cliff, M., Carter, R., James, R., Clarke, A., and Hirst, T.**, A kinetic model of intermediate formation during assembly of cholera toxin B-subunit pentamers. *Journal of Biological Chemistry*, 277(19): 16697–16704. 2002.

[51] **Gill, D. and King, C.**, The mechanism of action of cholera toxin in pigeon erythrocyte lysates. *Journal of Biological Chemistry*, 250(16): 6424–6432. 1975.

[52] **Gill, D. and Coburn, J.**, ADP-ribosylation by cholera toxin: functional analysis of a cellular system that stimulates the enzymic activity of cholera toxin fragment A1. *Biochemistry*, 26(20): 6364–6371. 1987.

[53] **Mekalanos, J.**, Duplication and amplification of toxin genes in Vibrio cholerae. *Cell*, 35(1): 253–263. 1983.

[54] **Dalbey, R. and Chen, M.**, Sec-translocase mediated membrane protein biogenesis. *Biochimica et Biophysica Acta (BBA)-Molecular Cell Research*, 1694(1): 37–53. 2004.

[55] **Luirink, J., Heijne, G., Houben, E., and Gier, J.**, Biogenesis of inner membrane proteins in Escherichia coli. *Annuak Review of Microbiology*, 59: 329–355. 2005.

[56] **Kirn, T., Lafferty, M., Sandoe, C., and Taylor, R.**, Delineation of pilin domains required for bacterial association into microcolonies and intestinal colonization by Vibrio cholerae. *Molecular Microbiology*, 35(4): 896–910. 2002.

[57] **Hirst, T., Hardy, S., and Randall, L.**, Assembly in vivo of enterotoxin from Escherichia coli: formation of the B subunit oligomer. *Journal of Bacteriology*, 153(1): 21–26. 1983.

[58] **Hirst, T., Sanchez, J., Kaper, J., Hardy, S., and Holmgren, J.**, Mechanism of toxin secretion by Vibrio cholerae investigated in strains harboring plasmids that encode heat-labile enterotoxins of Escherichia coli. *Proceedings of the National Academy of Sciences*, 81(24): 7752–7756. 1984.

[59] **Hirst, T. and Holmgren, J.**, Conformation of protein secreted across bacterial outer membranes: a study of enterotoxin translocation from Vibrio cholerae. *Proceedings of the National Academy of Sciences*, 84(21): 7418–7422. 1987.

[60] **Hirst, T. and Holmgren, J.**, Transient entry of enterotoxin subunits into the periplasm occurs during their secretion from Vibrio cholerae. *Journal of Bacteriology*, 169(3): 1037–1045. 1987.

[61] **Hardy, S., Holmgren, J., Johansson, S., Sanchez, J., and Hirst, T.**, Coordinated assembly of multisubunit proteins: oligomerization of bacterial enterotoxins in vivo and in vitro. *Proceedings of the National Academy of Sciences*, 85(19): 7109–7113. 1988.

[62] **Finkelstein, R., Vasil, M., and Holmes, R.**, Studies on toxinogenesis in Vibrio cholerae. I. Isolation of mutants with altered toxinogenicity. *Journal of Infectious Diseases*, 129(2): 117–123. 1974.

[63] **Sandkvist, M.**, Biology of type II secretion. *Molecular Microbiology*, 40(2): 271–283. 2001.

[64] **Sandkvist, M.**, Type II secretion and pathogenesis. *Infection and Immunity*, 69(6): 3523–3535. 2001.

[65] **Sandkvist, M., Michel, L., Hough, L., Morales, V., Bagdasarian, M., Koomey, M., and DiRita, V.**, General secretion pathway (eps) genes required for toxin secretion and outer membrane biogenesis in Vibrio cholerae. *Journal of Bacteriology*, 179(22): 6994–7003. 1997.

[66] **Russel, M. et al.**, Macromolecular assembly and secretion across the bacterial cell envelope: type II protein secretion systems. *Journal of Molecular Biology*, 279(3): 485. 1998.

[67] **Johnson, T., Abendroth, J., Hol, W., and Sandkvist, M.**, Type II secretion: from structure to function. *FEMS Microbiology Letters*, 255(2): 175–186. 2006.

[68] **Craig, L., Pique, M., and Tainer, J.**, Type IV pilus structure and bacterial pathogenicity. *Nature Reviews: Microbiology*, 2(5): 363–378. 2004.

[69] **Hansen, J. and Forest, K.**, Type IV pilin structures: insights on shared architecture, fiber assembly, receptor binding and type II secretion. *Journal of Molecular Microbiology and Biotechnology*, 11(3-5): 192–207. 2006.

[70] **Sixma, T., Pronk, S., Kalk, K., van Zanten, B., Berghuis, A., and Hol, W.**, Lactose binding to heat-labile enterotoxin revealed by X-ray crystallography. *Nature*, 355: 561–564. 1992.

[71] **Korotkov, K., Krumm, B., Bagdasarian, M., and Hol, W.**, Structural and Functional Studies of EpsC, a Crucial Component of the Type 2 Secretion System from *Vibrio cholerae*. *Journal of Molecular Biology*, 363(2): 311–321. 2006.

[72] **Abendroth, J., Rice, A., McLuskey, K., Bagdasarian, M., and Hol, W.**, The Crystal Structure of the Periplasmic Domain of the Type II Secretion System Protein EpsM From *Vibrio cholerae*: The Simplest Version of the Ferredoxin Fold. *Journal of Molecular Biology*, 338(3): 585–596. 2004.

[73] **Abendroth, J., Murphy, P., Sandkvist, M., Bagdasarian, M., and Hol, W.**, The X-ray Structure of the Type II Secretion System Complex Formed by the N-terminal Domain of EpsE and the Cytoplasmic Domain of EpsL of *Vibrio cholerae*. *Journal of Molecular Biology*, 348(4): 845–855. 2005.

[74] **Robien, M., Krumm, B., Sandkvist, M., and Hol, W.**, Crystal Structure of the Extracellular Protein Secretion NTPase EpsE of *Vibrio cholerae*. *Journal of Molecular Biology*, 333(3): 657–674. 2003.

[75] **Yanez, M., Korotkov, K., Abendroth, J., and Hol, W.**, Structure of the Minor Pseudopilin EpsH from the Type 2 Secretion System of *Vibrio cholerae*. *Journal of Molecular Biology*, 377(1): 91–103. 2008.

[76] **Yanez, M., Korotkov, K., Abendroth, J., and Hol, W.**, The Crystal Structure of a Binary Complex of two Pseudopilins: EpsI and EpsJ from the Type 2 Secretion System of *Vibrio vulnificus*. *Journal of Molecular Biology*, 375(2): 471–486. 2008.

[77] **Korotkov, K. and Hol, W.**, Structure of the GspK–GspI–GspJ complex from the enterotoxigenic Escherichia coli type 2 secretion system. *Nature Structural & Molecular Biology*, 15(5): 462–468. 2008.

[78] **Lord, J. and Roberts, L.**, Toxin entry: retrograde transport through the secretory pathway. *Journal of Cell Biology*, 140(4): 733–736. 1998.

[79] **Lencer, W. and Tsai, B.**, The intracellular voyage of cholera toxin: going retro. *Trends in Biochemical Sciences*, 28(12): 639–645. 2003.

[80] **Wolf, A., Jobling, M., Wimer-Mackin, S., Ferguson-Maltzman, M., Madara, J., Holmes, R., and Lencer, W.**, Ganglioside structure dictates signal transduction by cholera toxin and association with caveolae-like membrane domains in polarized epithelia. *Journal of Cell Biology*, 141(4): 917–927. 1998.

[81] **Wolf, A., Fujinaga, Y., and Lencer, W.**, Uncoupling of the cholera toxin-GM1 ganglioside receptor complex from endocytosis, retrograde Golgi trafficking, and downstream signal transduction by depletion of membrane cholesterol. *Journal of Biological Chemistry*, 277(18): 16249–16256. 2002.

[82] **Shogomori, H. and Futerman, A.**, Cholera toxin is found in detergent-insoluble rafts/domains at the cell surface of hippocampal neurons but is internalized via a raft-independent mechanism. *Journal of Biological Chemistry*, 276(12): 9182–9188. 2001.

[83] **Pang, H., Le, P., and Nabi, I.**, Ganglioside GM1 levels are a determinant of the extent of caveolae/raft-dependent endocytosis of cholera toxin to the Golgi apparatus. *Journal of Cell Science*, 117(8): 1421–1430. 2004.

[84] **Orlandi, P. and Fishman, P.**, Filipin-dependent inhibition of cholera toxin: evidence for toxin internalization and activation through caveolae-like domains. *Journal of Cell Biology*, 141(4): 905–915. 1998.

[85] **Torgersen, M., Skretting, G., van Deurs, B., and Sandvig, K.**, Internalization of cholera toxin by different endocytic mechanisms. *Journal of Cell Science*, 114(20): 3737–3747. 2001.

[86] **Hansen, G., Dalskov, S., Rasmussen, C., Immerdal, L., Niels-Christiansen, L., and Danielsen, E.**, Cholera toxin entry into pig enterocytes occurs via a lipid raft-and clathrin-dependent mechanism. *Biochemistry*, 44(3): 873–882. 2005.

[87] **Le, P. and Nabi, I.**, Distinct caveolae-mediated endocytic pathways target the Golgi apparatus and the endoplasmic reticulum. *Journal of Cell Science*, 116(6): 1059–1071. 2003.

[88] **Nichols, B.**, Caveosomes and endocytosis of lipid rafts. *Journal of Cell Science*, 116(23): 4707–4714. 2003.

[89] **Lamaze, C., Dujeancourt, A., Baba, T., Lo, C., Benmerah, A., and Dautry-Varsat, A.**, Interleukin 2 receptors and detergent-resistant membrane domains define a clathrin-independent endocytic pathway. *Molecular Cell*, 7(3): 661–671. 2001.

[90] **Massol, R., Larsen, J., Fujinaga, Y., Lencer, W., and Kirchhausen, T.**, Cholera toxin toxicity does not require functional Arf6-and dynamin-dependent endocytic pathways. *Molecular Biology of the Cell*, 15(8): 3631–3641. 2004.

[91] **Amessou, M., Fradagrada, A., Falguières, T., Lord, J., Smith, D., Roberts, L., Lamaze, C., and Johannes, L.**, Syntaxin 16 and syntaxin 5 are required for efficient retrograde transport of several exogenous and endogenous cargo proteins. *Journal of Cell Science*, 120(8): 1457–1468. 2007.

[92] **Ganley, I., Espinosa, E., and Pfeffer, S.**, A syntaxin 10–SNARE complex distinguishes two distinct transport routes from endosomes to the trans-Golgi in human cells. *Journal of Cell Biology*, 180(1): 159–172. 2008.

[93] **Lu, L., Khan, S., Lencer, W., and Walker, W.**, Endocytosis of cholera toxin by human enterocytes is developmentally regulated. *American Journal of Physiology-Gastrointestinal and Liver Physiology*, 289(2): G332–G341. 2005.

[94] **Badizadegan, K., Wheeler, H., Fujinaga, Y., and Lencer, W.**, Trafficking of cholera toxin-ganglioside GM1 complex into Golgi and induction of toxicity depend on actin cytoskeleton. *American Journal of Physiology-Cell Physiology*, 287(5): C1453–C1462. 2004.

[95] **Nichols, B., Kenworthy, A., Polishchuk, R., Lodge, R., Roberts, T., Hirschberg, K., Phair, R., and Lippincott-Schwartz, J.**, Rapid cycling of lipid raft markers between the cell surface and Golgi complex. *Journal of Cell Biology*, 153(3): 529–542. 2001.

[96] **Richards, A., Stang, E., Pepperkok, R., and Parton, R.**, Inhibitors of COP-mediated transport and cholera toxin action inhibit simian virus 40 infection. *Molecular Biology of the Cell*, 13(5): 1750–1764. 2002.

[97] **Mallard, F., Tang, B., Galli, T., Tenza, D., Saint-Pol, A., Yue, X., Antony, C., Hong, W., Goud, B., and Johannes, L.**, Early/recycling endosomes-to-TGN transport involves two SNARE complexes and a Rab6 isoform. *Journal of Cell Biology*, 156(4): 653–664. 2002.

[98] **Del Nery, E., Miserey-Lenkei, S., Falguieres, T., Nizak, C., Johannes, L., Perez, F., and Goud, B.**, Rab6A and Rab6A (A:n jalkeen ylapilkku) GTPases Play Non-overlapping Roles in Membrane Trafficking. *Traffic*, 7(4): 394–407. 2006.

[99] **Lu, L., Tai, G., and Hong, W.**, Autoantigen Golgin-97, an effector of Arl1 GTPase, participates in traffic from the endosome to the trans-golgi network. *Molecular Biology of the Cell*, 15(10): 4426–4443. 2004.

[100] **Sandvig, K., Spilsberg, B., Lauvrak, S., Torgersen, M., Iversen, T., and van Deurs, B.**, Pathways followed by protein toxins into cells. *International Journal of Medical Microbiology*, 293(7): 483–490. 2004.

[101] **Feng, Y., Jadhav, A., Rodighiero, C., Fujinaga, Y., Kirchhausen, T., and Lencer, W.**, Retrograde transport of cholera toxin from the plasma membrane to the endoplasmic reticulum requires the trans-Golgi network but not the Golgi apparatus in Exo2-treated cells. *EMBO Reports*, 5(6): 596–601. 2004.

[102] **Lodish, H., Berk, A., Kaiser, C., Krieger, M., Scott, M., Bretscher, A., Ploegh, H., and Matsudaira, P.**, *Molecular Cell Biology*. W. H. Freeman. 2007.

[103] **Lencer, W., Constable, C., Moe, S., Jobling, M., Webb, H., Ruston, S., Madara, J., Hirst, T., and Holmes, R.**, Targeting of cholera toxin and Escherichia coli heat labile toxin in polarized epithelia: role of COOH-terminal KDEL. *Journal of Cell Biology*, 131(4): 951–962. 1995.

[104] **Mekalanos, J., Collier, R., and Romig, W.**, Enzymic activity of cholera toxin. II. Relationships to proteolytic processing, disulfide bond reduction, and subunit composition. *Journal of Biological Chemistry*, 254(13): 5855–5861. 1979.

[105] **Tsai, B., Rodighiero, C., Lencer, W., Rapoport, T., et al.**, Protein disulfide isomerase acts as a redox-dependent chaperone to unfold cholera toxin. *Cell*, 104(6): 937–948. 2001.

[106] **Alberts, B.**, *Molecular Biology of the Cell: Reference Edition*. Number nid. 1 in Molecular Biology of the Cell: Reference Edition, Taylor & Francis Group. 2008.

[107] **Forster, M., Sivick, K., Park, Y., Arvan, P., Lencer, W., and Tsai, B.**, Protein disulfide isomerase–like proteins play opposing roles during retrotranslocation. *Journal of Cell Biology*, 173(6): 853–859. 2006.

[108] **Pande, A., Scaglione, P., Taylor, M., Nemec, K., Tuthill, S., Moe, D., Holmes, R., Tatulian, S., and Teter, K.**, Conformational instability of the cholera toxin A1 polypeptide. *Journal of Molecular Biology*, 374(4): 1114–1128. 2007.

[109] **Tsai, B., Ye, Y., Rapoport, T., et al.**, Retro-translocation of proteins from the endoplasmic reticulum into the cytosol. *Nature Reviews: Molecular Cell Biology*, 3(4): 246–255. 2002.

[110] **Tsai, B. and Rapoport, T.**, Unfolded cholera toxin is transferred to the ER membrane and released from protein disulfide isomerase upon oxidation by Ero1. *Journal of Cell Biology*, 159(2): 207–216. 2002.

[111] **Winkeler, A., Gödderz, D., Herzog, V., and Schmitz, A.**, BiP-dependent export of cholera toxin from endoplasmic reticulum-derived microsomes. *FEBS Letters*, 554(3): 439–442. 2003.

[112] **Vembar, S. and Brodsky, J.**, One step at a time: endoplasmic reticulum-associated degradation. *Nature Reviews: Molecular Cell Biology*, 9(12): 944–957. 2008.

[113] **Wiertz, E., Tortorella, D., Bogyo, M., Yu, J., Mothes, W., Jones, T., Rapoport, T., Ploegh, H., et al.**, Sec61-mediated transfer of a membrane protein from the endoplasmic reticulum to the proteasome for destruction. *Nature*, 384(6608): 432–438. 1996.

[114] **Pilon, M., Schekman, R., and Römisch, K.**, Sec61p mediates export of a misfolded secretory protein from the endoplasmic reticulum to the cytosol for degradation. *EMBO Journal*, 16(15): 4540–4548. 1997.

[115] **Schmitz, A., Herrgen, H., Winkeler, A., and Herzog, V.**, Cholera toxin is exported from microsomes by the Sec61p complex. *Journal of Cell Biology*, 148(6): 1203–1212. 2000.

[116] **Dixit, G., Mikoryak, C., Hayslett, T., Bhat, A., and Draper, R.**, Cholera toxin up-regulates endoplasmic reticulum proteins that correlate with sensitivity to the toxin. *Experimental Biology and Medicine*, 233(2): 163–175. 2008.

[117] **Bernardi, K., Forster, M., Lencer, W., and Tsai, B.**, Derlin-1 facilitates the retro-translocation of cholera toxin. *Molecular Biology of the Cell*, 19(3): 877–884. 2008.

[118] **Bernardi, K., Williams, J., Kikkert, M., Van Voorden, S., Wiertz, E., Ye, Y., and Tsai, B.**, The E3 ubiquitin ligases Hrd1 and gp78 bind to and promote cholera toxin retro-translocation. *Molecular Biology of the Cell*, 21(1): 140–151. 2010.

[119] **Ploegh, H.**, A lipid-based model for the creation of an escape hatch from the endoplasmic reticulum. *Nature*, 448(7152): 435–438. 2007.

[120] **Ampapathi, R., Creath, A., Lou, D., Craft Jr, J., Blanke, S., and Legge, G.**, Order–Disorder–Order Transitions Mediate the Activation of Cholera Toxin. *Journal of Molecular Biology*, 377(3): 748–760. 2008.

[121] **Rodighiero, C., Tsai, B., Rapoport, T., and Lencer, W.**, Role of ubiquitination in retro-translocation of cholera toxin and escape of cytosolic degradation. *EMBO Reports*, 3(12): 1222–1227. 2002.

[122] **Hazes, B. and Read, R.**, Accumulating evidence suggests that several AB-toxins subvert the endoplasmic reticulum-associated protein degradation pathway to enter target cells. *Biochemistry*, 36(37): 11051–11054. 1997.

[123] **Wernick, N., De Luca, H., Kam, W., and Lencer, W.**, N-terminal extension of the cholera toxin A1-chain causes rapid degradation after retro-translocation from endoplasmic reticulum to cytosol. *Journal of Biological Chemistry*, 285(9): 6145–6152. 2010.

[124] **Brown, D. and London, E.**, Structure and function of sphingolipid-and cholesterol-rich membrane rafts. *Journal of Biological Chemistry*, 275(23): 17221–17224. 2000.

[125] **Pike, L.**, Lipid rafts bringing order to chaos. *Journal of Lipid Research*, 44(4): 655–667. 2003.

[126] **Simons, K., Ikonen, E., et al.**, Functional rafts in cell membranes. *Nature*, 387(6633): 569. 1997.

[127] **Munro, S.**, Lipid rafts: elusive or illusive? *Cell*, 115(4): 377–388. 2003.

[128] **Sharma, P., Varma, R., Sarasij, R., Gousset, K., Krishnamoorthy, G., Rao, M., Mayor, S., et al.**, Nanoscale organization of multiple GPI-anchored proteins in living cell membranes. *Cell*, 116(4): 577–589. 2004.

[129] **Saffman, P. and Delbrück, M.**, Brownian motion in biological membranes. *Proceedings of the National Academy of Sciences*, 72(8): 3111–3113. 1975.

[130] **Pralle, A., Keller, P., Florin, E., Simons, K., and Horber, J.**, Sphingolipid-cholesterol rafts diffuse as small entities in the plasma membrane of mammalian cells. *Science Signalling*, 148(5): 997. 2000.

[131] **Rodighiero, C., Fujinaga, Y., Hirst, T., and Lencer, W.**, A cholera toxin B-subunit variant that binds ganglioside GM1 but fails to induce toxicity. *Journal of Biological Chemistry*, 276(40): 36939–36945. 2001.

[132] **Kovbasnjuk, O., Edidin, M., and Donowitz, M.**, Role of lipid rafts in Shiga toxin 1 interaction with the apical surface of Caco-2 cells. *Journal of Cell Science*, 114(22): 4025–4031. 2001.

[133] **Spence, M. and Johnson, I.**, *The Molecular Probes Handbook: A Guide to Fluorescent Probes and Labeling Technologies*. Live Technologies Corporation. 2010.

[134] **Fujinaga, Y., Wolf, A., Rodighiero, C., Wheeler, H., Tsai, B., Allen, L., Jobling, M., Rapoport, T., Holmes, R., and Lencer, W.**, Gangliosides that associate with lipid rafts mediate transport of cholera and related toxins from the plasma membrane to endoplasmic reticulm. *Molecular Biology of the Cell*, 14(12): 4783–4793. 2003.

[135] **van Heyningen, W., Carpenter, C., Pierce, N., and Greenough, W.**, Deactivation of cholera toxin by ganglioside. *Journal of Infectious Diseases*, 124(4): 415–418. 1971.

[136] **Angström, J., Teneberg, S., and Karlsson, K.**, Delineation and comparison of ganglioside-binding epitopes for the toxins of Vibrio cholerae, Escherichia coli, and Clostridium tetani: evidence for overlapping epitopes. *Proceedings of the National Academy of Sciences*, 91(25): 11859–11863. 1994.

[137] **Ewers, H., Römer, W., Smith, A., Bacia, K., Dmitrieff, S., Chai, W., Mancini, R., Kartenbeck, J., Chambon, V., Berland, L., et al.**, GM1 structure determines SV40-induced membrane invagination and infection. *Nature Cell Biology*, 12(1): 11–18. 2009.

[138] **Wolf, A., Jobling, M., Saslowsky, D., Kern, E., Drake, K., Kenworthy, A., Holmes, R., and Lencer, W.**, Attenuated endocytosis and toxicity of a mutant cholera toxin with decreased ability to cluster ganglioside GM1 molecules. *Infection and Immunity*, 76(4): 1476–1484. 2008.

[139] **Cuatrecasas, P.**, Gangliosides and membrane receptors for cholera toxin. *Biochemistry*, 12(18): 3558–3566. 1973.

[140] **Cuatrecasas, P.**, Interaction of Vibrio cholerae enterotoxin with cell membranes. *Biochemistry*, 12(18): 3547–3558. 1973.

[141] **Eidels, L., Proia, R., and Hart, D.**, Membrane receptors for bacterial toxins. *Microbiological Reviews*, 47(4): 596. 1983.

[142] **Fishman, P., Moss, J., and Osborne Jr, J.**, Interaction of choleragen with the oligosaccharide of ganglioside GM1: evidence for multiple oligosaccharide binding sites. *Biochemistry*, 17(4): 711–716. 1978.

[143] **Schoen, A. and Freire, E.**, Thermodynamics of intersubunit interactions in cholera toxin upon binding to the oligosaccharide portion of its cell surface receptor, ganglioside GM1. *Biochemistry*, 28(12): 5019–5024. 1989.

[144] **Merritt, E., Sarfaty, S., Akker, F., L'Hoir, C., Martial, J., and Hol, W.**, Crystal structure of cholera toxin B-pentamer bound to receptor GM1 pentasaccharide. *Protein Science*, 3(2): 166–175. 1994.

[145] **Merritt, E., Hol, W., et al.**, AB5 toxins. *Current Opinion in Structural Biology*, 5(2): 165. 1995.

[146] **De Wolf, M., Fridkin, M., Epstein, M., and Kohn, L.**, Structure-function studies of cholera toxin and its A and B protomers. Modification of tryptophan residues. *Journal of Biological Chemistry*, 256(11): 5481–5488. 1981.

[147] **De Wolf, M., Fridkin, M., and Kohn, L.**, Tryptophan residues of cholera toxin and its A and B protomers. Intrinsic fluorescence and solute quenching upon interacting with the ganglioside GM1, oligo-GM1, or dansylated oligo-GM1. *Journal of Biological Chemistry*, 256(11): 5489–5496. 1981.

[148] **Ludwig, D., Holmes, R., and Schoolnik, G.**, Chemical and immunochemical studies on the receptor binding domain of cholera toxin B subunit. *Journal of Biological Chemistry*, 260(23): 12528–12534. 1985.

[149] **Fan, E., O'Neal, C., Mitchell, D., Robien, M., Zhang, Z., Pickens, J., Tan, X., Korotkov, K., Roach, C., Krumm, B., et al.**, Structural biology and structure-based inhibitor design of cholera toxin and heat-labile enterotoxin. *International Journal of Medical Microbiology*, 294(4): 217–223. 2004.

[150] **Demchenko, A.**, *Introduction to Fluorescence Sensing*. Springer. 2009.

[151] **Lakowicz, J.**, *Principles of Fluorescence Spectroscopy*. Springer London, Limited. 2009.

[152] **Albani, J.**, *Structure and Dynamics of Macromolecules: Absorption and Fluorescence Studies: Absorption and Fluorescence Studies*. Elsevier Science. 2011.

[153] **Baumgart, T., Hunt, G., Farkas, E., Webb, W., and Feigenson, G.**, Fluorescence probe partitioning between L_o/L_d phases in lipid membranes. *Biochimica et Biophysica Acta (BBA)-Biomembranes*, 1768(9): 2182–2194. 2007.

[154] **Levental, I., Byfield, F., Chowdhury, P., Gai, F., Baumgart, T., and Janmey, P.**, Cholesterol-dependent phase separation in cell-derived giant plasma-membrane vesicles. *Biochemical Journal*, 424(2): 163. 2009.

[155] **Sengupta, P., Hammond, A., Holowka, D., and Baird, B.**, Structural determinants for partitioning of lipids and proteins between coexisting fluid phases in giant plasma membrane vesicles. *Biochimica et Biophysica Acta (BBA)-Biomembranes*, 1778(1): 20–32. 2008.

[156] **Kuerschner, L., Ejsing, C., Ekroos, K., Shevchenko, A., Anderson, K., and Thiele, C.**, Polyene-lipids: a new tool to image lipids. *Nature Methods*, 2(1): 39–45. 2004.

[157] **Boldyrev, I., Zhai, X., Momsen, M., Brockman, H., Brown, R., and Molotkovsky, J.**, New BODIPY lipid probes for fluorescence studies of membranes. *Journal of Lipid Research*, 48(7): 1518–1532. 2007.

[158] **Hölttä-Vuori, M., Uronen, R., Repakova, J., Salonen, E., Vattulainen, I., Panula, P., Li, Z., Bittman, R., and Ikonen, E.**, BODIPY-Cholesterol: A New Tool to Visualize Sterol Trafficking in Living Cells and Organisms. *Traffic*, 9(11): 1839–1849. 2008.

[159] **Marks, D., Bittman, R., and Pagano, R.**, Use of Bodipy-labeled sphingolipid and cholesterol analogs to examine membrane microdomains in cells. *Histochemistry and Cell Biology*, 130(5): 819–832. 2008.

[160] **Oreopoulos, J. and Yip, C.**, Probing membrane order and topography in supported lipid bilayers by combined polarized total internal reflection fluorescence-atomic force microscopy. *Biophysical Journal*, 96(5): 1970. 2009.

[161] **Eggeling, C., Ringemann, C., Medda, R., Schwarzmann, G., Sandhoff, K., Polyakova, S., Belov, V., Hein, B., Von Middendorff, C., Schönle, A., et al.**, Direct observation of the nanoscale dynamics of membrane lipids in a living cell. *Nature*, 457(7233): 1159–1162. 2008.

[162] **Tyteca, D., D'Auria, L., Der Smissen, P., Medts, T., Carpentier, S., Monbaliu, J., De Diesbach, P., and Courtoy, P.**, Three unrelated sphingomyelin analogs spontaneously cluster into plasma membrane micrometric domains. *Biochimica et Biophysica Acta (BBA)-Biomembranes*, 1798(5): 909–927. 2010.

[163] **Ichikawa, N., Iwabuchi, K., Kurihara, H., Ishii, K., Kobayashi, T., Sasaki, T., Hattori, N., Mizuno, Y., Hozumi, K., Yamada, Y., et al.**,

Binding of laminin-1 to monosialoganglioside GM1 in lipid rafts is crucial for neurite outgrowth. *Journal of Cell Science*, 122(2): 289–299. 2009.

[164] **Coban, O., Burger, M., Laliberte, M., Ianoul, A., and Johnston, L.**, Ganglioside partitioning and aggregation in phase-separated monolayers characterized by bodipy GM1 monomer/dimer emission. *Langmuir*, 23(12): 6704–6711. 2007.

[165] **Mikhalyov, I., Gretskaya, N., and Johansson, L.**, Fluorescent BODIPY-labelled G_{M1} gangliosides designed for exploring lipid membrane properties and specific membrane-target interactions. *Chemistry and Physics of Lipids*, 159(1): 38–44. 2009.

[166] **Polyakova, S., Belov, V., Yan, S., Eggeling, C., Ringemann, C., Schwarzmann, G., de Meijere, A., and Hell, S.**, New GM1 ganglioside derivatives for selective single and double labelling of the natural glycosphingolipid skeleton. *European Journal of Organic Chemistry*, 2009(30): 5162–5177. 2009.

[167] **Shaw, J., Epand, R., Epand, R., Li, Z., Bittman, R., and Yip, C.**, Correlated fluorescence-atomic force microscopy of membrane domains: structure of fluorescence probes determines lipid localization. *Biophysical Journal*, 90(6): 2170. 2006.

[168] **Maier, O., Oberle, V., and Hoekstra, D.**, Fluorescent lipid probes: some properties and applications (a review). *Chemistry and Physics of Lipids*, 116(1): 3–18. 2002.

[169] **Wüstner, D.**, Fluorescent sterols as tools in membrane biophysics and cell biology. *Chemistry and Physics of Lipids*, 146(1): 1–25. 2007.

[170] **Wang, T. and Silvius, J.**, Different sphingolipids show differential partitioning into sphingolipid/cholesterol-rich domains in lipid bilayers. *Biophysical Journal*, 79(3): 1478–1489. 2000.

[171] **Valeur, B. and Berberan-Santos, M.**, *Molecular Fluorescence*. Wiley. 2012.

[172] **Ulrich, G., Ziessel, R., and Harriman, A.**, The chemistry of fluorescent bodipy dyes: versatility unsurpassed. *Angewandte Chemie International Edition*, 47(7): 1184–1201. 2007.

[173] **Rapaport, D.**, *The Art of Molecular Dynamics Simulation*. Cambridge University Press. 2004.

[174] **Hess, B., Kutzner, C., Van Der Spoel, D., and Lindahl, E.**, GROMACS 4: Algorithms for highly efficient, load-balanced, and scalable molecular simulation. *Journal of Chemical Theory and Computation*, 4(3): 435–447. 2008.

[175] **Van Der Spoel, D., Lindahl, E., Hess, B., Groenhof, G., Mark, A., and Berendsen, H.**, GROMACS: fast, flexible, and free. *Journal of Computational Chemistry*, 26(16): 1701–1718. 2005.

[176] **van der Spoel, D., Lindahl, E., Hess, B., van Buuren, A.R., Apol, E., Meulenhoff, P.J., Tieleman, D.P., Sijbers, A.L.T.M., Feenstra, K.A., van Drunen, R., and Berendsen, H.J.C.**, Gromacs User Manual version 4.5.4. Retrieved on August 16, 2012.

[177] **Frenkel, D. and Smit, B.**, *Understanding Molecular Simulation: From Algorithms to Applications*, volume 1. Academic Press. 2002.

[178] **Leach, A.R.**, *Molecular modelling: principles and applications*. Addison-Wesley Longman Ltd. 2001.

[179] **Schlick, T.**, *Molecular Modeling and Simulation: An Interdisciplinary Guide*, volume 21. Springer Verlag. 2010.

[180] **Thijssen, J.**, *Computational Physics*. Cambridge Univ Pr. 2007.

[181] **Kaminski, G., Friesner, R., Tirado-Rives, J., and Jorgensen, W.**, Evaluation and reparametrization of the OPLS-AA force field for proteins via comparison with accurate quantum chemical calculations on peptides. *Journal of Physical Chemistry B*, 105(28): 6474–6487. 2001.

[182] **Jorgensen, W. and Tirado-Rives, J.**, Potential energy functions for atomic-level simulations of water and organic and biomolecular systems. *Proceedings of the National Academy of Sciences of the United States of America*, 102(19): 6665. 2005.

[183] **Ewald, P.**, The calculation of optical and electrostatic grid potential. *Annalen der Physik*, 64(3): 253–87. 1921.

[184] **Toukmaji, A. and Board, J.**, Ewald summation techniques in perspective: a survey. *Computer Physics Communications*, 95(2): 73–92. 1996.

[185] **Berendsen, H. and Van Gunsteren, W.**, Practical algorithms for dynamic simulations. *Molecular-Dynamics Simulation of Statistical-Mechanical Systems, North-Holland, Amsterdam*, pp. 43–65. 1986.

[186] **Hockney, R., Goel, S., and Eastwood, J.**, Quiet high-resolution computer models of a plasma. *Journal of Computational Physics*, 14(2): 148–158. 1974.

[187] **Van Gunsteren, W. and Berendsen, H.**, A leap-frog algorithm for stochastic dynamics. *Molecular Simulation*, 1(3): 173–185. 1988.

[188] **Verlet, L.**, Computer" experiments" on classical fluids. I. Thermodynamical properties of Lennard-Jones molecules. *Physical Review*, 159(1): 98. 1967.

[189] **Berendsen, H., Postma, J., Van Gunsteren, W., DiNola, A., and Haak, J.**, Molecular dynamics with coupling to an external bath. *Journal of Chemical Physics*, 81: 3684. 1984.

[190] **Nosé, S.**, A molecular dynamics method for simulations in the canonical ensemble. *Molecular Physics*, 52(2): 255–268. 1984.

[191] **Hoover, W. et al.**, Canonical dynamics: equilibrium phase-space distributions. *Physical Review A*, 31(3): 1695–1697. 1985.

[192] **Bussi, G., Donadio, D., and Parrinello, M.**, Canonical sampling through velocity rescaling. *Journal of Chemical Physics*, 126: 014101. 2007.

[193] **Berendsen, H.**, Transport properties computed by linear response through weak coupling to a bath. *Computer Simulations in Material Science. Meyer, M., Pontikis, V. eds.. Kluwer*, pp. 139–155. 1991.

[194] **Parrinello, M. and Rahman, A.**, Polymorphic transitions in single crystals: A new molecular dynamics method. *Journal of Applied Physics*, 52(12): 7182–7190. 1981.

[195] **Nose, S. and Klein, M.**, Constant pressure molecular dynamics for molecular systems. *Molecular Physics*, 50(5): 1055–1076. 1983.

[196] **Alberts, B.**, Encyclopedia Britannica Online: the cell membrane. [WWW]. Referred on February 15th, 2013. Available at `http://www.britannica.com`. Accessed on February 15th, 2013.

[197] **Korlach, J., Schwille, P., Webb, W., and Feigenson, G.**, Characterization of lipid bilayer phases by confocal microscopy and fluorescence correlation spectroscopy. *Proceedings of the National Academy of Sciences*, 96(15): 8461–8466. 1999.

[198] **Hart, H., Hart, D., Craine, L., and Hadad, C.**, *Organic Chemistry: A Short Course*. Textbooks Available with Cengage YouBook Series, Brooks/Cole. 2011.

[199] **Falck, E., Patra, M., Karttunen, M., Hyvönen, M., and Vattulainen, I.**, Lessons of slicing membranes: interplay of packing, free area, and lateral diffusion in phospholipid/cholesterol bilayers. *Biophysical Journal*, 87(2): 1076–1091. 2004.

[200] *Avanti polar lipids*. [WWW], Availeble at `http://www.avantilipids.com`, Accessed on February 15, 2013.

[201] **Pickens, J., Mitchell, D., Liu, J., Tan, X., Zhang, Z., Verlinde, C., Hol, W., and Fan, E.**, Nonspanning bivalent ligands as improved surface receptor binding inhibitors of the cholera toxin B pentamer. *Chemistry & Biology*, 11(9): 1205–1215. 2004.

[202] **Bussi, G., Donadio, D., and Parrinello, M.**, Canonical sampling through velocity-rescaling. *arXiv preprint arXiv:0803.4060*. 2008.

[203] **Jorgensen, W. and Tirado-Rives, J.**, The OPLS [optimized potentials for liquid simulations] potential functions for proteins, energy minimizations for crystals of cyclic peptides and crambin. *Journal of the American Chemical Society*, 110(6): 1657–1666. 1988.

[204] **Jorgensen, W., Chandrasekhar, J., Madura, J., Impey, R., and Klein, M.**, Comparison of simple potential functions for simulating liquid water. *Journal of Chemical Physics*, 79: 926. 1983.

[205] **Hess, B., Bekker, H., Berendsen, H., Fraaije, J., et al.**, LINCS: a linear constraint solver for molecular simulations. *Journal of Computational Chemistry*, 18(12): 1463–1472. 1997.

[206] **Essmann, U., Perera, L., Berkowitz, M., Darden, T., Lee, H., and Pedersen, L.**, A smooth particle mesh Ewald method. *Journal of Chemical Physics*, 103: 8577. 1995.

[207] **Maiorov, V. and Crippen, G.**, Significance of root-mean-square deviation in comparing three-dimensional structures of globular proteins. *Journal of Molecular Biology*, 235: 625–634. 1994.

[208] **Kleman, M., Laverntovich, O., and Friedel, J.**, *Soft Matter Physics: An Introduction*. Partially Ordered Systems, Springer. 2002.

[209] **Schindler, H. and Seelig, J.**, Deuterium order parameters in relation to thermodynamic properties of a phospholipid bilayer. Statistical mechanical interpretation. *Biochemistry*, 14(11): 2283–2287. 1975.

[210] **Sezgin, E., Levental, I., Grzybek, M., Schwarzmann, G., Mueller, V., Honigmann, A., Belov, V.N., Eggeling, C., Coskun, Ü., Simons, K., et al.**, Partitioning, diffusion, and ligand binding of raft lipid analogs in model and cellular plasma membranes. *Biochimica et Biophysica Acta (BBA)-Biomembranes*, 1818(7): 1777–1784. 2012.

[211] **Levental, I., Grzybek, M., and Simons, K.**, Raft domains of variable properties and compositions in plasma membrane vesicles. *Proceedings of the National Academy of Sciences*, 108(28): 11411–11416. 2011.

[212] **Kästner, J.**, Umbrella sampling. *Wiley Interdisciplinary Reviews: Computational Molecular Science*, 1(6): 932–942. 2011.